DETECTION OF TWO-DIMENSIONAL INTERNAL CRACKS IN CONCRETE USING POINT STRAIN SENSORS

A Dissertation
Submitted to the Graduate Faculty
of the
North Dakota State University
of Agriculture and Applied Science

By

Mohanad Natiq Alshandah

In Partial Fulfillment of the Requirements
for the Degree of
DOCTOR OF PHILOSOPHY

Major Department:
Civil and Environmental Engineering

July 2020

Fargo, North Dakota

North Dakota State University
Graduate School

Title

Detecting of Two-Dimensional Internal Cracks in Concrete Using Point Strain Sensor

By

Mohanad Natiq Alshandah

The Supervisory Committee certifies that this ***disquisition*** complies with North Dakota State University's regulations and meets the accepted standards for the degree of

DOCTOR OF PHILOSOPHY

SUPERVISORY COMMITTEE:

Dr. Ying Huang
Chair

Dr. Jerry Gao
Co-Chair

Dr. Denish Katti

Dr. Ravi Yellavajjala

Dr. Pan Lu

Approved:

July 10, 2020
Date

Dr. David Steward
Department Chair

ABSTRACT

Tensile cracking in the concrete can destroy the structural frame since it induces water penetration in structure and foundation. For instance, in concrete pavements, cracking increases the potential for pavement distress, the probability of accidents occurring, and the damages for vehicles. Therefore, monitoring techniques to detect hidden internal cracking in concrete such as bottom-up cracks are necessary to ensure the safety of the infrastructure by distinguishing early signs of excessive damage. This study presents an approach to detect internal concrete cracks especially bottom-up cracks using point strain sensors. The stress intensity principle is used in this study to locate and estimate the growth of the cracks. Based on the stress intensity principle, theoretical derivations have been conducted to use the point strain sensors in concrete structures to detect both single and multiple bottom-up cracks. For single crack detection, laboratory experiments showed an average measurement accuracy of 85.76%. For multiple cracks, laboratory tests performed using reinforced concrete beams and the average measurement accuracy was achieved to be over 80%. With the validation in the lab, future efforts are expected to be performed in the field to provide an alternative technique to detect hidden internal cracks in concrete structures, especially pavements.

ACKNOWLEDGEMENTS

Alhamdullilah, first and foremost. I am truly grateful to Allah my God for the countless blessings He has bestowed on me, both generally and in accomplishing this thesis especially. I would like to express my warmest gratitude and deepest appreciation to my academic supervisors, Dr. Ying Huang & Dr. Jerry Gao, for their untiring support, patience, kindness, enthusiasm, calm advice, suggestions with immense knowledge, and guidance throughout my work and during the writing of this thesis. Also, my Advisory committee members: Dr. Dinesh Katti, Dr. Ravi Yellavajjala, and Dr. Pan Lu, and Civil and Environmental Engineering Department & Construction Management and Engineering Department. Special thanks and warm appreciation also go to my beloved wife Aseel Al-Doori. for her patience, love, prayers, standing by me, her kindness, and taking care of our Kids while I was abroad. Thanks to my kids Abdulrahman, Ola, Noor, and Maria. I gratefully acknowledge the financial support from (HCED) The Higher Committee for Education Development in Iraq, and my university (Tikrit University). Finally, many thanks go to my colleagues, friends specially (Dr. Mohanad Abdulazeez), and to everyone who has assisted me, stood by me or contributed to my educational progress in any way.

DEDICATION

To Allah my GOD,

(for giving me the strength to complete this phase of life)

&

To my big family father, mother, brothers and sister

(for believing in my abilities when no one did)

&

To my Wife and my kids

(for coming into my life)

TABLE OF CONTENTS

LIST OF TABLES

LIST OF FIGURES

CHAPTER 1. INTRODUCTION

1.1. Background

Concrete is the most commonly used man-made material on earth. It is an important construction material used extensively in building, bridges, roads and dams. Its uses ranging from structural applications, to pavement, shoulders, pipes and drains [1]. Also, the concrete has several advantageous properties such as strong mechanical properties that can withstand great compressive stresses. This strength is, of course, a function of the material components of the concrete mix. The strength of concrete makes it suitable for constructing foundations, wastewater treatment facilities, super structures, and another establishment [2].

Also, concrete lasts for ages, even under very adverse conditions. Concrete can resist weathering action, chemical action, abrasion, and compressive stress for long periods without compromising its structural integrity. This attribute makes a concrete structure stable and suitable for places with rough conditions. For example, the first instances of human-made concrete date back to 500 BC. The fact that we are still able to see this concrete shows just how durable concrete is. Commercial concrete work requires little maintenance save from a few touch-ups on the finishing. The longevity of concrete makes it a great material for permanent buildings and other structures like bridges, dams, and specially pavements [3]. In addition, concrete is also environmentally friendly as it does not produce toxic fumes in the environment which could lead to air pollution, also, it is energy efficient, fire resistance, waterproof, durable [4].

One of very good examples of concrete application is in the pavement industry. As one of the leading pavements surfacing techniques in addition to asphalt, concrete pavement plays an essential part of road networks worldwide, which directly affects the quality of transportation. When compared to flexible surfacing, concrete pavement is costlier for constriction [5]. However,

when considering less maintenance needs, less delayed time such as loss of work time, less the operation cost such as the cost of gas, the crash cost of vehicles, and driver tension, it still has a lot of benefits regarding economics and environmental effects to use concrete pavements for roads [6]. To be specific, first of all, concrete pavement is durable and safe, which are considerably less prone to wear and tear defects like rutting, cracking, stripping loss of texture, and potholes that can occur with flexible pavement surfaces. This low maintenance requirement is one of the principal advantages of concrete pavements. There are well-designed concrete pavements that have required little or no maintenance well beyond their 40-year design lives. Less maintenance also means fewer traffic delays, a huge advantage on some of our already congested highways. In addition, fuel consumption is a major factor in the economics of road transportation, with the rolling resistance of the pavement being an important contributor to the fuel consumption and the corresponding CO_2 production. Rolling resistance can be attributed in part to a lack of pavement rigidity. In the case of a heavily loaded truck, energy is consumed in deflecting a non-rigid pavement and sub-grade. Using rigid concrete pavement will result in less fuel consumption and a decrease in associated emissions [7, 8].

Another benefit of using concrete as an alternative for flexible pavements is a reduced need for street lighting, due to higher surface reflectivity after dark. Better light reflection on the brighter surface could potentially result in electricity savings of about 30% for lamps, lampposts, and signs. However, the most substantial savings from higher surface reflectivity are to be gained from a reduction in accidents, and the associated loss of life and severe injury [7, 8].

Moreover, roadside noise levels are a public concern, especially when the pavement is in an urban environment. Producers of the various pavement types are investing time and money to develop quieter pavements structures. The Cement Association of Canada (CAC), in conjunction

with the American Concrete Pavement Association (ACPA) is researching to develop smoother concrete pavements to serve the transportation community [9]. This effort involves standardization of tire/pavement noise assessment, the establishment of acoustic performance curves for existing surfaces, development of new surface textures through a laboratory test program, a field validation program, and an implementation phase [10].

1.2. Concrete Cracking

Tensile internal cracks are usually very common in any concrete structures, especially in concrete pavements. This section used concrete pavements as an example to explain how concrete internal tensile cracks or bottom-up cracks formulate and progress. Concrete pavements are typically constructed using a Portland cement bound surface layer over one or more support layers over a prepared natural earth subgrade. The base layer is generally provided to support construction traffic and to ensure uniformity of support to the PCC surface. The base layer may consist of unbound aggregate, bitumen-, or cement-bound aggregate. The bound layers may be conventional dense-graded asphalt, lean concrete, or cement-treated, or open-graded asphalt or concrete designed to promote lateral drainage within the pavement structure. The subbase layer is typically used to protect the pavement from the effects of frost heave and used to improve the constructability of the pavement layers above the subbase [11, 12]. The pavement designer should have a thorough understanding of the parameters and their reflection of actual site conditions prior to using them to select a pavement thickness. Projects that have traffic or site conditions that differ significantly from the values assumed herein should be evaluated with a site-specific pavement design [13,14]. Concrete pavement deformation by excess loads or environmental effect leads to cracking, which in turn induces significant pavement damages in addition to increased risk in road accidents and disasters to the automobile.

Cracks are very common in almost any form of concrete pavement, whether the cracking is immediate or occurs years after it was cast. There are two types of cracks, which are either active or inactive. The active cracks are cracks that expand, lengthen, or deepen over time. Dormant cracks do not change unless they were affected by moisture or impact. There are several reasons, such as a combination of repeated loads and shrinkage stress usually, and significant change temperature causes this type of distress.

Pressure cracks are the result of placing too much weight on top of a concrete slab. Excessive weight can put too much stress on the slab or even alter the ground underneath the slab, which can cause cracking. Also, crazing cracks are tiny surface cracks that resemble spider webs caused by premature drying of the slab. If the slab does not have enough moisture or loses moisture too quickly, crazing cracks are likely to form. Since these cracks are minor and only visible on the surface, they do not pose a threat to repair.

Shrinkage Cracks, the earliest crack that will form, is because of a process known as plastic shrinkage. Plastic shrinkage can occur if the mixture of water and cement is too watery. Too much water will take up space, causing the solid ingredients of the mix to separate. When the water evaporates, the areas in the combination remain, leaving cracks sometimes, only a hair-thin Heaving refers to concrete that is raised by either movement underneath or by excessive freeze and thaw cycles. Sidewalks or any pavement that lies over a tree root can result in cracks caused by heaving. In addition, types of cracks in concrete pavement depend on the crack's direction, including longitudinal, transverse, diagonal cracks, top-bottom, and bottom-up.

The bottom-up cracking develops as a zone where micro-cracks localized. These cracks formed are resulting from the frequent loads on the surface, poor construction, and the decrease in pavement load-supporting characteristics such as poor drainage or thaw ice and an increase in

loading. Fatigue cracking is predicted to initiate at the bottom of the concrete pavement layer, and it assumed that these fatigue cracks propagate upwards with many cracks that observed in practice spreading through the entire concrete thickness following. Furthermore, the cracks that have spread through the whole pavement thickness are mostly related to reflective cracking to bottom-up fatigue, which means that the weakening of the material takes place over a specific area. The material will lose its stiffness due to the development of these micro and small isolated macro cracks. Loss of stiffness can be measured through strain measurements and the measurement of surface deflections. Both will show an increase in the measured value as a result of the deterioration that develops. Also, it is characterized by cracks that divide the slab into two or three pieces.

Consequently, bottom-up cracks are considered as the most severe case regarding detection because bottom-up cracks happened under pavement, and we do not know when the crack is starting and where the location is. Therefore, a bottom-up crack detection system to diagnose early cracking in pavements would save agencies cost and labor for maintenance, but yet is available [15].

1.3. Literature Review

1.3.1. Crack Detection in Concrete

Cracking is a concern for concrete structures if it has the potential to deteriorate and pose serviceability or structural problem, or both. The impact of cracking depends on cracking, climate, traffic, and pavement design. To determine bottom-up cracks in concrete cracks in field is very challenging. There are several non-destructive detection (NDE) techniques and methods investigated by researchers to detect internal cracks in concrete structures, including ground penetrating radar (GPR) [16, 17], ultrasonic technology [18, 19]. In addition, for concrete

pavements as an example, cracking assessment was also performed through either full-scale field test section construction, accelerated pavement testing (APT), and Accelerated Loading Facility (ALF) [21, 22].

GPR emits and measures high-frequency electromagnetic pulse waves to the measured object through the transmitting antenna. Using the difference in the electromagnetic properties of the underground medium, reflections and transmissions of electromagnetic waves are generated at the interfaces of different electrical interfaces [16, 17]. For instance, the dielectric constants of the air and pavement are different, and the receiving antenna receives the reflected echo and records reflection time, which can be used to map the cracks in a highway [18] or the airport pavements [22] and subgrades. The GPR can scan the pavement in three dimensions within a limited depth. Due to the transmission limitation of the electromagnetic waves, however, GPR is hard to get an accurate estimation of cracks when the pavement is very thick or moistures or other interfere.

Ultrasonic technology was also investigated to detect cracks and longitudinal joints in asphalt concrete pavements [23, 24], which measures the ultrasonic reflections. In an ultrasonic system, one transducer sent out a stress-wave pulse and the second transducer received the reflected pulse, the time from the start of the pulse to the arrival of the echo was measured to estimate the crack locations [25, 26]. With multiple arrays of probes, the ultrasonic sensors are possible to detect pavement distresses such as delamination at the mid-depth of concrete pavement slabs, spalling, and map cracking in concrete pavement slabs, and mud balls in a concrete runway. In addition, the recurrence plot quantification analysis (RQA) method can improve the sensitivity to damage in spoiled series, improving the reliability of damage detection with ultrasonic in non-homogeneous materials [27]. However, due to a low transmission capacity of ultrasonic waves

in concrete, the detection limit of this technique limited several conditions such as environment and weather change, different properties of materials could be available during the test.

In some cases, engineers used pavement strength to determine a potential crack initialization in a concrete pavement. Full-scale static step-loads were applied at the free edge of concrete slabs to induce bottom-up and top-down cracks, and then to determine the pavement strength [28]. The full-scale observation of damage and failure mechanisms of pavements due to traffic is quite essential for the improvement of road materials and construction methods, as well as for the development and the validation of modeling tools and pavement design methods.

An alternative to the survey of real roads over long periods to detect pavement cracks consists of performing Accelerated Pavement Tests (APT) test [29]. A wide range of fatigue performance can be performed to calibrate the correlation between crack length and area cracked, surface cracking initiation and cracking rate, crack length variations within the Accelerated Loading Facility (ALF) test site, cracking orientation, and cracking initiation location. Moreover, they found both crack length and percent area cracked were used to measure the cracking level. The two measurements were found well correlated and the cumulative crack length in the meter is approximately equal to the cumulative percent area cracked. The fatigue performance rankings are identical by both measurements [30]. Advantages and Disadvantages of technologies to detect cracks in a concrete structure in Table 1.

Table 1. Advantages and Disadvantages of NDE Technologies to Detect Cracks in a Concrete structure.

Techniques	Advantages	Disadvantages
Ground Penetrating Radar (GPR)	Accurate Imaging, flexibility, simple operation, accurate location, healthy, and safety.	In the surface, the effect for environmental conditions, traffic closure required during the test
Ultrasonic	High penetrating power, high sensitivity, non-hazardous to operations, results are immediate.	In the surface, the effect for environmental conditions,
Laser Imaging Techniques	Record a high-res 3D profile of the road surface, Analyze the 3D profiles with algorithms to identify surface defects.	In the surface, the effect for environmental conditions, traffic closure required during the test
Field Test	It helps control the load, the number of traffic passes, temperature, tire pressure, etc. for a more accurate and consistent assessment of road performance, long-term pavement performance monitoring.	costly, In the surface, the effect for environmental conditions, traffic closure required during the test
Embedded Electrical Resistance-Based	Operate over a wide range of temperatures, Suitable for dynamic Loads, Available in a wide variety of gauge lengths, Long-term reliability, Easy installation, Low cost.	dynamic measurement only, some crystals are water-soluble and dissolve, limited numbers of the sensor can place

1.3.2. Structural Health Monitoring

Other than the NDE technologies, structural health monitoring (SHM) refers to monitoring technologies that aims to gain knowledges of the integrity of in-service structures on a continuous real-time basis. They use the changes in measurements at the same locations at two different times to identify the condition of the structure. SHM also refers to sensor networks that monitor the behavior of structures while they are in service. In the literature, different words refer to SHM, such as local health monitoring or global health monitoring. The definition and goals of SHM have been changing as technologies evolve. If the monitoring design is performed carefully, it ensures monitoring with a lot of profits on the structures. Though, it is good to keep in mind that there are a lot of obstacles in the way to the ideal monitoring as the field is new and associated technologies

are still under development. Nevertheless, some benefits of monitoring are mentioned, including real-time monitoring with alarms, downtime reduction, assessing and understanding the actual behavior of the structure, and decreased maintenance costs.

Modern civil structures may need a continuous assessment of their structural integrity to avoid catastrophic failures that can lead to economic and potential human loses. In this regard, the knowledge of SHM schemes, in particular of sensors and signal processing algorithms, has become a necessity for civil and structural engineers to monitor and detect the performances of the civil infrastructure [31, 32]. SHM network can also measure crack widening which increases the overall resilience of the structure by indicating the areas where maintenance work should focus [33]. The availability of a continuous, real-time, and automatic structural health monitoring system is considered a useful tool for early detection of a potentially dangerous situation for the structure and its occupants [34].

1.3.3. Single Crack Detection in Concrete

In order to detect a single crack in concrete, embedded sensors can be used to form a SHM system. One of the most popular embedded sensors used is the electrical resistance-based strain gauge [35, 36]. When a strain gauge is tightly bonded to a measuring object, the mechanical elongation or contraction of the bonded structure will change the electric resistance of the metal sensing element of the strain gauge, which can be measured. Strain gauges installed in asphalt pavement in airport runways successfully detected strain changes with airplane take-off and landing and potential damages over time, especially in the gauges nearest to the taxiway [37].

In addition to electrical resistance-based strain gauges, optic fiber strain gauges were also investigated for crack detections such as fiber Bragg grating sensors and distributed fiber optic sensors [38, 39]. These fiber optic strain gauges can detect strain changes in pavements, which can

be related to crack initiation in pavements [40]. By using two fiber optic sensor nodes, information of bridge performance had been collected [41]. Also, Fiber Bragg grating (FBG) sensors can be used to monitor pavement performances in a harsh environment [42]. However, most embedded sensors to detect pavement cracks were still installed near the pavement surface, preventing them to detect cracking from bottom to up with different weather conditions, traffic, and the environmental effect [43].

1.3.4. Multiple Cracks Detection in Concrete

The multi-crack identification is important in many practical application fields such as concrete pavement structures and design. To detect the multiple cracks in concrete, there are several techniques which can be used such as simulation, distributed fiber optics sensing (DFOS) techniques, piezo-electrical transducers (PZT) sensors, acoustic emission (AE), and modal analysis [44-42].

Machines and structural components require continuous monitoring for the detection of cracks and crack growth for ensuring an uninterrupted service [44]. The difficulty of identifying multiple cracks without a priori knowledge of the number of cracks is overcome by comparing the residual sum of squares of each solution with an assumed number of cracks [45]. Simulations to identify multiple cracks in concrete beams using an evolutionary algorithm were developed by researchers by considering the crack detection procedure as an optimization problem with some strain energy parameters and stress intensity. The depths of the cracks were also attempted to be detected using simulation using inverse analysis. Inverse analysis for the calibration of materials or structural models consists of data collection from experimental tests in laboratory or in situ, computer simulation of the tests by employing the model to calibrate minimization, with respect to the sought parameters, of a suitable norm which quantifies the discrepancy between

experimental data and the corresponding values provided by the simulation. Several aspects of the inverse problem theory and its applications are treated systematically [46, 47, 48].

Since simulation is not a field technique for crack detection, distributed fiber optics sensing (DFOS) techniques were developed recently for the detection of damages in a laboratory size reinforced concrete beam [49]. The sensitivity of this technique to micro-cracks was compared to standard traditional sensors. Moreover, the capacity of a DFOS technique to localize cracks and quantify crack openings was also assessed. The results showed that the implementation of DFOS techniques allow the detection of early subtle changes in reinforced concrete structures until crack formation. The DFOS techniques cover larger areas since it is a distributed technique. However, the DFOS has a low detection frequency and high cost, which limited its widespread.

To save cost, point sensors such as piezo-electrical transducers (PZT) sensors [50] and acoustic emission (AE) sensors [51] can also be used to detect multi-cracks in concrete. A smart rebar network based on the PZT sensors were tested which showed possibility of detecting crack damages. It was found that as the crack numbers increases, the times of stress wave's reflection and refraction increases, leading to the rapid decrease of wave strength. The indications increasing crack numbers with the amplitude of the first wave was decreased exponentially. However, this technology has some limitations, such as using for dynamic measurement only, it has high-temperature sensitivity, and some crystals are water-soluble and dissolve in a high humid environment.

Acoustic emission (AE) sensing techniques have the potential for detecting and locating cracking in concrete structures [51]. AE measures the elastic waves produced by crack nucleation and growth with an array of point sensors. The AE instrument system is relatively portable, which

can allow it to be an option for off-site and on-site field application. Laboratory tests demonstrated the possibility of AE in detecting cracks.

In addition, modal and vibration response analysis can be used to detect cracks since the crack propagation, material properties, geometrical dimensions, and boundary conditions affect the modal parameters. For example, the presence of a crack in a structural member alters the local compliance that would affect the vibration response under external loads [52]. For the known material and geometrical dimensions, if modal parameters are known, crack sizes, and their severity may be detected [53, 54]. The vibration-based inspection methods for crack detection in structures may enable the determination of location and size of cracks from the vibration data collected from a signal or, at most, a few points on the component. Also, using an evolutionary algorithm to identify multiple cracks in beams. By considering the crack detection procedure as an optimization problem, an objective function can be constructed based on the change of the eigenfrequencies and some strain energy parameters. The results show that the number of cracks as well as their sizes and locations can be predicted well through this method. [55]. Moreover, the other method to use modal analysis is the differential quadrature method which is a model with linear elastic fracture mechanics and Euler-Bernoulli beam. The cracked beam was modeled as a two-segment beam with the crack simulated as a rotational spring. The crack of the beam was considered as local flexibility, which is a function of the crack depth. However, this method has some limitations, such as the dynamic responses can be obtained by this method only, and crack depth ratio a/h should be less than 0.5 [56, 57].

1.4. Problem Statements

Detections of internal cracks such as bottom-up cracks in concrete structures plays an essential role in damage detection, reliability and performance evaluation of existing

infrastructures. The literatures reviewed above show that currently most of the conventional techniques in the market to detect cracks in concrete, especially, concrete pavements as a potential application, can only detect when crack reaches in surface. Detecting cracks, especially hidden cracks such as bottom-up crack beneath the surface of concrete structures, either for a single crack or multiple cracks, is very challenging to be detected and most of the existing technologies had low detection frequency and high cost.

1.5. Objectives and Organization of the Dissertation

To meet the challenges as mentioned above, this dissertation developed an algorithm to localize and monitor the internal crack initialization and propagation in concrete using minimum numbers of discrete point strain sensors for single crack and multiple cracks. The developed algorithm was based on linear elastic fracture mechanics (LEFM) and was verified by laboratory experiments. Strains inside a concrete structures were measured by minimum numbers of strain sensors embedded, which can be related to stresses or any potential structural performances. In order to achieve this objective, this study identifies two specific tasks which can be summarized as follow:

1) Developing crack detection flowchart using the stress intensity theory with in-point strain sensors in concrete for internal crack detection for both single and multiple cracks;
2) Validating experimentally the proposed system through experimental testing for single and multiple cracks detection.

CHAPTER 2. THEORETICAL ANALYSIS

This chapter presents the theoretical analysis to develop the crack detection algorithms using the stress intensity theory to detect single and multiple cracks in concrete using in-concrete strain sensors followed by the sensitivity study.

2.1. Linear Elastic Fracture Mechanics

Traditionally, strength-of-materials concepts was used to design and analyze of a structural component, in which failure is determined to occur once the applied stress exceeds the material's strength (either yield strength or ultimate strength, depending on the criteria for failure). However, the presence of a crack in a structural component magnifies the stress in the vicinity of the crack and may result in failure prior to that predicted using the traditional strength-of-materials methods. Thus, for the failure of a structural component with an existing crack or flaw, fracture mechanics is used to predict and diagnose the stress/strain distributions inside the component. In fracture mechanics, a stress intensity factor is calculated as a function of applied stress, crack size, and the geometry of the component. Failure occurs once the stress intensity factor exceeds the material's fracture toughness, resulting in rapid and unstable crack growth until fracture [58].

Concrete structures have rigidity and resilience from deformation. These characteristics, however, result in concrete structures lacking the flexibility to move in response to environmental or volume changes. Cracking is usually the first sign of distress in concrete. Failure of concrete structures typically involves stable growth of large cracking zones and the formation of large fractures before the maximum load is reached. Concrete may be referred to as a brittle material. This is because concrete's behavior under loading is completely different from that of ductile materials like steel. But actually, concrete differs from ideal brittle materials in many aspects. In modern fracture mechanics, concrete is considered as a quasi-brittle material. Cracking is an

essential feature of the behavior of concrete structures. Even under service loads, concrete structures are normally full of cracks [59].

This part presents several theories developed in fracture crack relation which have been used in this study. For concrete structures, linear elastic fracture mechanics (LEFM) is an important approach to fracture modeling. LEFM may over-predict the loads at which the crack will propagate. To determine whether LEFM may be used or whether nonlinear fracture mechanics is necessary for a problem. Modifications of LEFM were presented by Hassan et al. (2010) to account for the distributed nature of pre-peak micro-cracking in concrete [60]. These modifications have produced better results in the application of fracture mechanics concepts to brittle failure in reinforced concrete [61]. In concrete, this inelastic zone surrounding the crack tip is being known as the Fracture Process Zone (FPZ) characterized by complex mechanisms. In brittle materials, Fracture Process Zone (FPZ) is defined as the region ahead of the traction free crack tip. A considerable effort has been committed to develop numerical models to simulate the fracture behavior of materials exhibiting tensile softening and FPZ, such as, concrete, used in civil engineering structures [62]. Also, Hillerborg used concept of cohesive zone or cohesive crack to simulate FPZ in discrete cracks [63, 64].

The FPZ region contains lots of distributing microcracks, in which mechanical behavior, such as stress, also, linear elastic fracture mechanics, has the stress to approach infinity at a crack tip. The size of the FPZ can be significant and can be generated from microcracking that occurs in front of the crack tip, and a significant amount of energy is stored in the FPZ. The FPZ may be defined as the area surrounding a crack tip within which inelastic material behavior occurs [65]. The FPZ size grows as load is applied to a crack, until it has developed to the point that the (traction-free) crack begins to propagate. If the size of the FPZ is small compared to other

dimensions in the structure, then the assumptions of LEFM lead to the conclusion that the FPZ will exhibit nonchanging characteristics as the crack propagates [66]. This is called the steady state of the FPZ.

The size of the steady state FPZ depends only upon the material properties. In concrete, as opposed to metals, the FPZ can often be thought of as an interface separation phenomenon, with little accompanying volumetric damage. The characteristics of the steady state FPZ depends upon the aggregate size, shape and strength, and upon microstructural details of the particular concrete under consideration. The FPZ was first studied in detail by Hillerborg et al [64, 65], which considered that the size of the FPZ is dependent on the model used. The growth of the FPZ, until peak load is reached, introduces the effect of structural size on the failure loads [67].

Early attempts to analyze failure in concrete structures caused by crack growth were not successful, even though it was obvious that a fracture mechanics approach would be realistic to model brittle crack propagation type failures. The lack of success in the early attempts to analyze crack propagation failures was due to the use of linear elastic fracture mechanics (LEFM). LEFM assumes that the fracture process is small and can be replaced, and that the rest of the member volume remains elastic. However, research in the last four decades has resulted in modifications to LEFM to account for the distributed nature of pre-peak micro-cracking and the presence of a large FPZ in concrete. These modifications have produced better results in the application of fracture mechanics concepts to brittle failure in reinforced concrete. Theories that allow tensile softening and FPZ of relatively large sizes are classified as nonlinear fracture mechanics models [68].

A considerable effort has been committed to develop numerical models to simulate the fracture behavior of materials exhibiting tensile softening and FPZ, such as mortar, concrete, rock,

or bricks used in civil engineering structures. Two numerical methods to simulate fracture are available, including the smeared crack approach and the discrete crack approach. In the smeared crack approach, introduced by [69], the crack is replaced by a continuous medium with altered mechanical properties. Because the crack is established through stress computations at integration points, a significant number of cracks with small openings are imagined to be continually distributed over the finite element. The constitutive laws, defined by stress-strain relations, are nonlinear and may exhibit strain softening. Strain localization instabilities and spurious mesh sensitivity of finite element calculations are likely when strain-softening are modeled numerically. These difficulties can be overcome by adopting appropriate mathematical techniques [70].

In this study, to simplify the analysis, we assumed that the crack tip in the concrete pavement behaves elastically. Stress and displacement field is developed in crack tip. While in many cases, concrete may be ductile as discussed above, but the size of the plastic zone is very small. Therefore, the plastic zone is ignored. Thus, the LEFM theory is adopted in this study to generate the stress/strain field of the sub-field around the cracks in the concrete structures.

The size effect of structure having geometrically similar properties has been understood in many studies [71, 72] as the effect of the characteristic structure size on the nominal strength. A major deterministic size effect can be caused by stress redistributions caused by stable propagation of fracture or damage and the inherent energy release due to cracks. In general, a size effect that bridges the small-scale power law for nonbrittle (plastic, ductile) behavior and the large-scale power law for brittle behavior signals the presence of a certain nonnegligible characteristic length of the material. The material length, which represents the quintessential property of quasi-brittle materials, characterizes the typical size of material inhomogeneities or the fracture process zone (FPZ). Quasi-brittle behavior can be attained by creating or enhancing material inhomogeneities

in concrete by means of embedded reinforcement. Such behavior is desirable because it endows the structure made from a material incapable of plastic yielding with a significant energy absorption capability [73].

In materials science, an inverse size effect spanning several orders of magnitude must be tackled in passing from normal laboratory tests of material strength to microelectronic components and micro mechanisms. A material that follows linear elastic fracture mechanics (LEFM) on the scale of laboratory specimens cross section of sizes from 152.4*152.4 to 152.4*241.3mm may exhibit quasi-brittle for unreinforced concrete beams or even ductile (plastic) failure for reinforced concrete beams.

In LEFM theory, the stress intensity factor (K) is a significant parameter to describe a crack, and it determines the stress and displacement fields in cracked solids near the crack tip [74]. K predicts the stress state "stress intensity" near the tip of a crack caused by a remote load or residual stresses [75]. It is usually applied to a homogeneous, linear elastic material and is useful for providing a failure criterion for brittle materials, and is a critical technique in the discipline of damage tolerance. The concept can also be applied to materials that exhibit small-scale yielding at a crack tip. In this study, the stress intensity factor is used to derive the strain fields around the cracks. Based on the LEFM theory, if the crack depth (a) in a certain material under loading is known, the magnitude of stress intensity factor can be obtained as:

$$K = \alpha \sigma \sqrt{\pi a} \quad (1)$$

where, σ is applied stress, a is crack length, and α =1.1215, is a parameter dependent on size of the structural component and crack geometry [76,77].

There are three general modes of cracks as shown in Figure 1: Mode I opening, Mode II in-plane shear, and Mode III out-of-plane shear. The bottom-up crack which matters to this paper is in Mode I, opening.

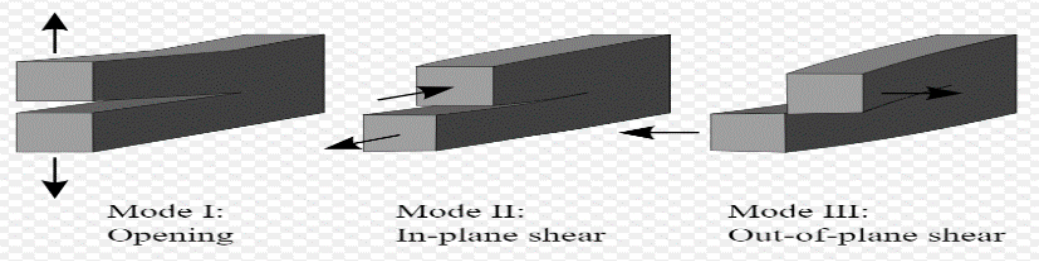

Figure 1. Schematic of the Basic Fracture Modes: Mode I (opening), Mode II (sliding), Mode III (tearing). [78]

For Mode I crack, linear elastic theory predicts that the stress distribution (σ) near the crack tip, in polar coordinates (r, Θ) with origin at the crack tip, has the form also, shown in Figure 2 [79].

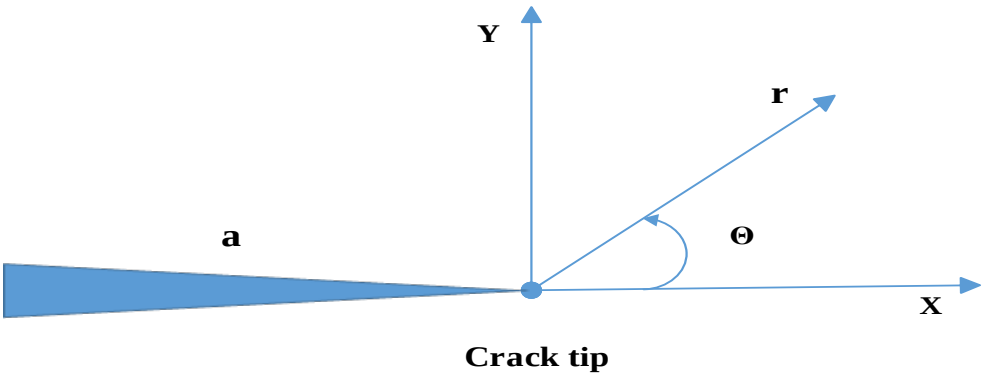

Figure 2. Polar Coordinates at the Crack Tip.

If the stress intensity factor K is calculated based on the crack geometry, the stress in x and y directions at a random location around the crack, (r, Θ), σ_x and σ_y, can be estimated as:

$$\sigma_x = \frac{K}{\sqrt{2\pi r}} \cos\frac{\theta}{2}\left[1 - \sin\frac{\theta}{2}\sin\frac{3\theta}{2}\right] \quad (2)$$

$$\sigma_y = \frac{K}{\sqrt{2\pi r}} \cos\frac{\theta}{2}\left[1 + \sin\frac{\theta}{2}\sin\frac{3\theta}{2}\right] \quad (3)$$

By knowing Young's modulus of concrete materials in advance (E) under the assumption that concrete is a linear elastic material, the strains in x and y directions at the random locations can be estimated as:

$$\varepsilon_x = \frac{\sigma_x}{\mathrm{E}}\ ;\ \ \varepsilon_y = \frac{\sigma_y}{\mathrm{E}} \tag{4}$$

Thus, if several strain sensors are applied at known locations inside the pavements within a sensitive range of the crack tips, it is highly potential to estimate the locations and crack lengths theoretically.

2.2. Single Crack Detection in Concrete Structures

To detect a single crack in concrete pavement, two strain sensors (Sensor #1 and #2) are assumed to be placed in known locations with a certain distance (L) away from each other, which is around a sensitive range of one bottom-up crack with crack width of *a* in concrete pavements with elasticity of E, as shown in Figure 3. Loading is applied on the top of the concrete pavement. The strain sensors measure strains in both x and y directions $(\varepsilon_{x_1},\varepsilon_{y_1})$ and $(\varepsilon_{x_2},\varepsilon_{y_2})$. Thus, in the condition there is a single crack in between the two sensors, the relation between the measured strain increase from the sensors to its physical locations related to the crack based on the semi-inverse method developed by Westergaard can be descried as: [80].

$$\varepsilon_{x1}=\frac{K}{E\sqrt{2\pi r1}}\cos\frac{\theta_1}{2}\left[1-sin\frac{\theta 1}{2}sin\frac{3\theta 1}{2}\right] \tag{5}$$

$$\varepsilon_{y1}=\frac{K}{E\sqrt{2\pi r1}}\cos\frac{\theta 1}{2}\left[1+sin\frac{\theta 1}{2}sin\frac{3\theta 1}{2}\right] \tag{6}$$

$$\varepsilon_{x2}=\frac{K}{E\sqrt{2\pi r2}}\cos\frac{\theta 2}{2}\left[1-sin\frac{\theta 2}{2}sin\frac{3\theta 2}{2}\right] \tag{7}$$

$$\varepsilon_{y2}=\frac{K}{E\sqrt{2\pi r2}}\cos\frac{\theta 2}{2}\left[1+sin\frac{\theta 2}{2}sin\frac{3\theta 2}{2}\right] \tag{8}$$

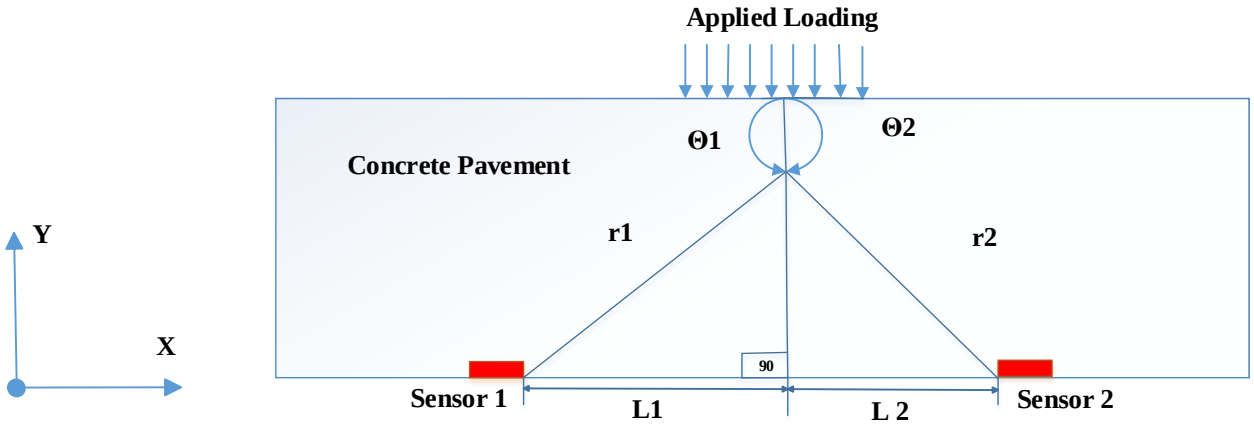

Figure 3. Sensor Locations vs Perpendicular Crack

Based on the assumption that the crack is perpendicular to the bottom of the pavement, then, the geometrical relation between the crack depths (a), the radius distance (r_1), the crack radius angle (θ_1), and the distance between the Sensor 1 and the crack (L_1), can be determined as:

$$\tan(\theta_1 - 90^o) = a/L_1 \quad (9)$$

$$\cos(\theta_1 - 90^o) = L_1/r_1 \quad (10)$$

Thus, the radius distance (r_1) and the crack radius angle (θ_1) can be replaced by the crack depth (a) and the distance between the Sensor 1 and the crack (L_1) as:

$$\theta_1 = \tan^{-1}(a/L_1) + 90^o \quad (11)$$

$$r_1 = \frac{L_1}{\cos(\theta 1 - 90^\circ)} \quad (12)$$

Putting Equations (11, 12) into Equation (5), the measured strain in x direction at Sensor 1 location, ε_1, can be estimated as:

$$\varepsilon_1 = \frac{\sigma\sqrt{a}}{1.4142 * E * \sqrt{\frac{L_1}{\cos\left[\tan^{-1}\left(\frac{a}{L_1}\right)\right]}}} \cos\frac{\tan^{-1}\left[\left(\frac{a}{L_1}\right)+90^\circ\right]}{2}\left[1 - \sin\frac{\tan^{-1}\left[\left(\frac{a}{L_1}\right)+90^\circ\right]}{2}\sin\frac{3\tan^{-1}\left[\left(\frac{a}{L_1}\right)+90^\circ\right]}{2}\right] \quad (13)$$

Following the same procedure as for ε_1, the measured strain in x direction at Sensor 2 location can be estimated based on the crack depth (a) and the distance between the Sensor 2 and the crack (L_2) as below:

$$\boldsymbol{\varepsilon_2} = \frac{\sigma\sqrt{a}}{1.4142 * E * \sqrt{\frac{L_2}{\cos\left[\tan^{-1}\left(\frac{a}{L_2}\right)\right]}}} \cos\frac{\tan^{-1}\left[\left(\frac{a}{L_2}\right)+90°\right]}{2}\left[1 - \sin\frac{\tan^{-1}\left[\left(\frac{a}{L_2}\right)+90°\right]}{2}\sin\frac{3\tan^{-1}\left[\left(\frac{a}{L_2}\right)+90°\right]}{2}\right] \quad (14)$$

Considering that the distance, L, between the two sensors, equals to L_1+ L_2, Equation (14) can be rewritten as:

$$\boldsymbol{\varepsilon_2} = \frac{\sigma\sqrt{a}}{1.4142 * E * \sqrt{\frac{L-L_1}{\cos\left[\tan^{-1}\left(\frac{a}{L-L_1}\right)\right]}}} \cos\frac{\tan^{-1}\left[\left(\frac{a}{L-L_1}\right)+90°\right]}{2}\left[1 - \sin\frac{\tan^{-1}\left[\left(\frac{a}{L-L_1}\right)+90°\right]}{2}\sin\frac{3\tan^{-1}\left[\left(\frac{a}{L-L_1}\right)+90°\right]}{2}\right] \quad (15)$$

Thus, if the strains in X directions at Sensor locations 1 and 2 can be measured, based on Equations (12, 13), the crack location, L_1, and the crack depth, a, can be estimated considering the semi-inverse method [81,82].

As seen from above that Equations (12- 14) were derived based on the assumption that the crack is perpendicular to the bottom surface of the pavement. When the crack is initializing, the assumption of perpendicular crack is a reasonable assumption. Thus, Equations (11-14) can be applicable to estimate the crack initiation location, L_1. However, in practical application, after the crack is initialized and starts to propagate, crack may propagate to random directions, and this assumption may not be true and Equations (12-14) may not be applicable to calculate the crack depth, a. To solve this challenge, based on measured strains from Sensors 1 and 2, Equations (12-14) will be used to calculate the crack initialization location, L1, and noted as L1, t=0. For next time interval, t=i, based on the measured strains and Sensor 1 and 2, the crack location, L1, t=i can

be re-estimated. Thus, the angle of the crack away from the perpendicular direction, ϕ, as shown in Figure. 4, can then be estimated as below:

$$\phi = \sin^{-1}(\Delta L/a) \quad (16)$$

where, ΔL is measured distance difference between $L_{1,\,t=0}$ and $L_{1,\,t=i}$ measurement. Therefore, based on Equations (12, 14, and 15), not only the crack location but also the crack propagation can be estimated based on the real-time measurements of the strains at bottom of the pavement.

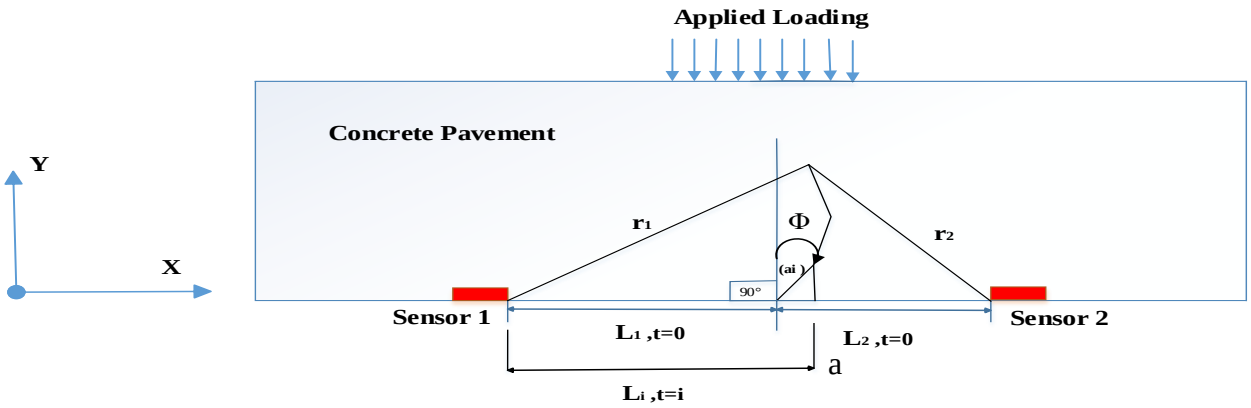

Figure 4. Sensor Locations vs Crack Propagation in Random Directions after Initiation.

As shown in flowchart in Fig. 5, the applied stress on the structure and the detected strains from the strain sensors will be used as input to this algorithm. These inputs will be feed to equations (9,11) to calculate the real-time crack length and the crack locations. As long as the crack length becomes non-zero, the calculated crack location will be noted as the location when crack initiates, $L_{1,\,t=0}$. Equations (13, 15) will be used continuously to estimate the crack location at later time interval, i, which is noted as $L_{1,\,t=i}$ based on the measured strains. The difference between $L_{1,\,t=0}$ and $L_{1,\,t=i}$ will be calculated and input to Equation 12 together with the estimated crack length from Equations (14, 15) from time interval, i. Finally, Equation (16) will be used to estimate the crack directions at time interval, i, which will produce the crack progressing map along the bottom of the pavement.

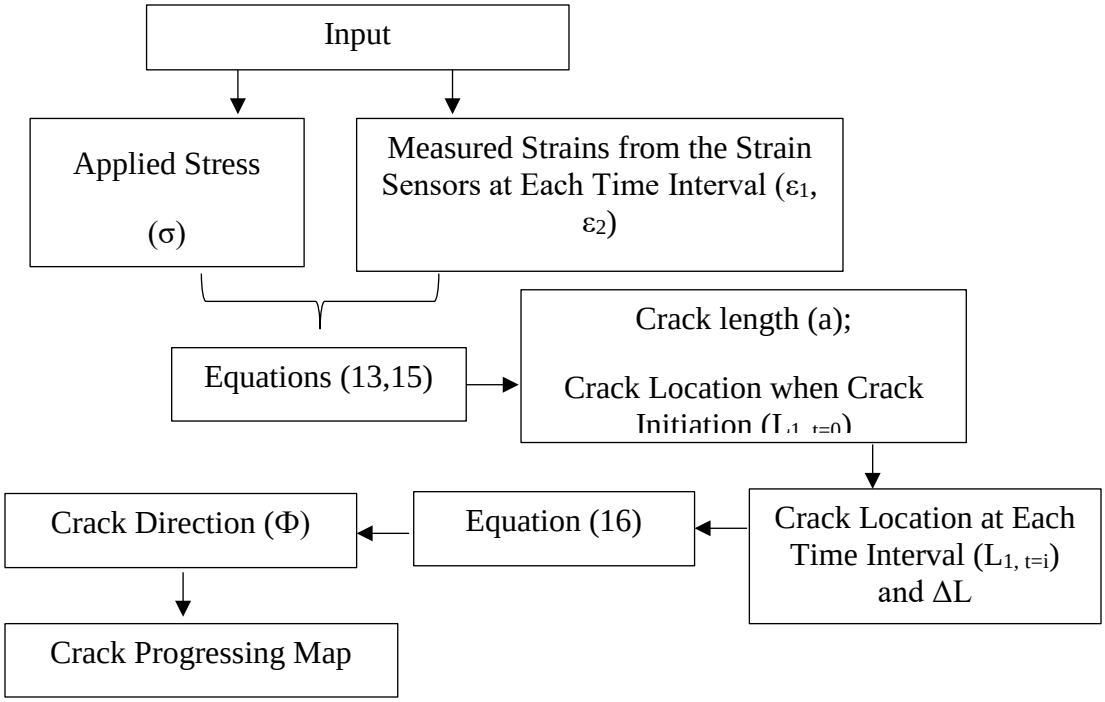

Figure 5. Flowchart for the Developed Crack Detection Algorithm.

2.3. Multiple Cracks Detection in Concrete Structures

The developed algorithms in Section 2.1. can be advanced to detect multiple cracks with a minimum of four strain sensors. In this analysis, four-strain sensors were used to derive the crack distribution along the bottom of the pavements in a case of multiple cracks. To detect multiple cracks using a network of multiple sensors, two assumptions have been made:

1) The cracks start from the bottom of the concrete pavement structure.
2) The cracks (1, 2, …, j, where j is the total number of cracks in between two nearby sensors) are developed in sequences in between two nearby strain sensors.

Based on the assumptions above, before the initiation of two or more cracks, the two strain sensors nearby already detected the initiation location of the first crack, which is $L_{1,\,t=c1}$ away from Sensor 1, and monitor the crack depth and direction development of this single crack, which are $a_{1,t=i}$ and $\Phi_{1,\,t=i}$ following Equations (13, 15, 16). As seen in Fig.6, Sensor 3 is assumed to be placed with a distance of $L_{1\sim3}$ away from Sensor 1, and Sensor 4 is assumed to place with a distance of

$L_{2\sim4}$ away from Sensor 2. Four sensors, including Sensor 1, 2, 3, and 4 form a network for multiple crack detection. The presence of a new crack in between Sensor 1 and Sensor 2, in addition to the first crack, Crack 1, may induce a small sudden change of strain measurements in either Sensor 1 and Sensor 2, depending on the location of the new crack. If the new crack occurs in between Sensor 1 and the first crack, the small sudden strain increase, if any, will be presented by Sensor 1. On the other hand, if the new crack is located in between the first crack and Sensor 2, the small sudden strain increase will be presented by Sensor 2. However, the changes may be too small for Sensor 3 and Sensor 4 to be considered a sudden change. However, the identified crack initiation time from Sensor 1 and Sensor 2 can be used by Sensor 3 and 4 to analyze the crack locations and progress. Either the new cracks occur in between Sensor 1 and Crack 1 or Sensor 2 and Crack 1, only the notation and affected sensor number will change, the analysis progress will be similar for either case. So in this analysis, we use the condition when the other sequences of new cracks occurring in between the first crack and Sensor 1 as shown in Fig. 6 as an example to derive the theoretic solutions of the strain field distribution. The size cracks during the test were reasonable and energy the sensor detects point strain the energy release rate and the rate of energy consumption by fracture by changing strain data. The first one longer than the second one, and it has higher energy that is needed to catch and detect by point strain sensor.

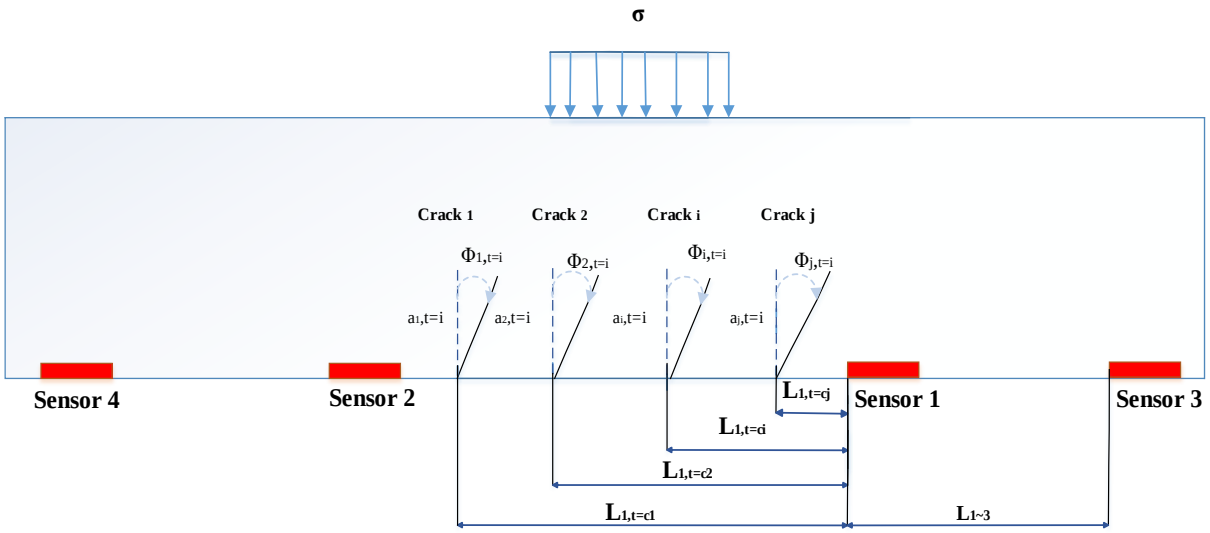

Figure 6. Multiple Bottom-up Cracks in a Pavement Segment

Since the occurance of the new cracks are assumed to occur in between the first crack and Sensor 1, based on Equation 13, it can be seen that Sensor 2 will not be sensitive to this crack since Crack 1 blocked the strains from the new cracks, Cracks 2 and more, on the other side of the Crack 1, till the other new cracks develop their crack depths longer than Crack 1. In another word, when the depths of Crack 2, 3, or more, a_j, is smaller than a_1, ($a_j \leq a_1$), Sensor 2 will be only sensitive to Crack 1 and continue monitor the development (length and direction) of the first crack, Crack 1. In the case of cracks more than two and the depth of all other cracks are smaller than the first crack ($a_j \leq a_1$), Sensor 1 will sense all the cracks in between the longest crack and Sensor 2.

Let's take a look at the problem in the case of two cracks in between the two sensors, which is the simplest case and extend that to multiple cracks more than two. In the case of two cracks, Sensor 1 is expected to sense both Crack 1 and 2 when Crack 2 has a depth smaller than Crack 1. When Crack 2 develops depth larger than Crack 1, Sensor 1 will be only sensitive to Crack 2 and Sensor 2 will be senstitive to both cracks. Thus, Sensor 2 is expected to have a sudden strain increase when Crack 2 develops to be larger than Crack 1. Thus, when $a_j \leq a_1$, the strain measured by Sensor 2 at t=i when i≥C2 and i<C3, can be presented as:

$$\varepsilon_{2,\,t=i} = \varepsilon_2(a=a_{1,\,t=i},\, L_1 = L_{1,\,t=C1}), \qquad C2 \le i < C3 \tag{17}$$

in which the $\varepsilon_2(a=a_{1,\,t=i},\, L_1 = L_{1,\,t=C1})$ is the strain calculated based on Equation 15 in the condition of $a=a_{1,\,t=i},\, L_1 = L_{1,\,t=C1}$. Thus, with measured strain at Sensor 2 in any time instant t=i, $\varepsilon_{2,\,t=i}$, based on Equation 17 and Equation 15, the crack depth $a_{1,\,t=i}$ at any time instant t=i can be obtained. On the other hand, when $a_j \le a_1$, the strain at Sensor 1 can be calculated based on superposition principles which can be represented as:

$$\varepsilon_{1,\,t=i} = \varepsilon_1(a=a_{1,\,t=i},\, L_{1,\,t=C1}) + \varepsilon_1(a_{2,\,t=i},\, L_{1,\,t=C2}), \qquad C2 \le i < C3 \tag{18}$$

in which the $\varepsilon_1(a=a_{1,\,t=i},\, L_1 = L_{1,\,t=C1})$ is the strain at Sensor 1 calculated based on Equation 13 in the condition of $a=a_{1,\,t=i},\, L_1 = L_{1,\,t=C1}$ and $\varepsilon_1(a=a_{2,\,t=i},\, L_1 = L_{1,\,t=C2})$ is the strain at Sensor 1 calculated based on Equation 13 in the condition of $a=a_{2,\,t=i},\, L_1 = L_{1,\,t=C2}$. Similarly, at Sensor 3, the measured strain can be obtained as:

$$\varepsilon_{3,\,t=i} = \varepsilon_3(a_{1,\,t=i},\, L_{1\sim3} + L_{1,\,t=C1}) + \varepsilon_3(a_{2,\,t=i},\, L_{1,\,t=C2}), \qquad C2 \le i < C3 \tag{19}$$

in which the $\varepsilon_3(a=a_{1,\,t=i},\, L_1 = L_{1,\,t=C1})$ is the strain at Sensor 3 calculated based on Equation 13 in the condition of $a=a_{1,\,t=i},\, L_1 = L_{1,\,t=C1}$ and $\varepsilon_3(a=a_{2,\,t=i},\, L_1 = L_{1,\,t=C2})$ is the strain at Sensor 3 calculated based on Equation 13 in the condition of $a=a_{2,\,t=i},\, L_1 = L_{1,\,t=C2}$. With the calculated crack depth $a_{1,\,t=i}$ of the first crack, Crack 1, from Equations 17, the strains at Sensor 1 and Sensor 3 locations from Crack 1, $\varepsilon_1(a=a_{1,\,t=i},\, L_1 = L_{1,\,t=C1})$ and $\varepsilon_3(a=a_{1,\,t=i},\, L_1 = L_{1,\,t=C1})$, can be obtained at any time instant t=i.

Thus, at t=C2, we have the induced strain changes at Sensor 1 and Sensor 3 for a presentence of a new crack, $\Delta\,\varepsilon_{1,\,c2}$, and $\Delta\,\varepsilon_{3,\,c2}$ as

$$\Delta\,\varepsilon_{1,\,c2} = \varepsilon_1(a_{2,\,t=C2},\, L_{1,\,t=C2}) . \tag{20}$$

$$\Delta\,\varepsilon_{3,\,c2} = \varepsilon_3(a_{2,\,t=C2},\, L_{1,\,t=C2}) . \tag{21}$$

At the presence of the second crack, the strain changes at t=C2 from Sensor 1 and 3, $\Delta\,\varepsilon_{1,\,c2}$, and $\Delta\,\varepsilon_{3,\,c2}$, can be measured and $a_{2,\,t=C2,}$ and $L_{1,\,t=C2}$, are the two unknowns. Solving Equations

20 and 21, $a_{2,\ t=C2,}$ and $L_{1,\ t=C2}$ can then be obtained. With $L_{1,\ t=C2}$ calculated, Equations 18 and 19 will be only related to the development of the crack depth, $a=a_{2,\ t=I}$ of the new crack, Crack 2. Thus, to be more accurate, Sensor 1 and Equation 18 will be used to track the continuous development of a depth of Crack 2.

As the continuous development of Crack 2, at a time instant, t= t1, the crack depth of Crack 2, $a_{2,}$ turns to be bigger than a_1, which is $a_j \geq a_1$. Thus, after any time instant $t \geq t1$ when $a_j \geq a_1$ Equations 17 to 19 will be changed to

$$\varepsilon_{1,\ t=i} = \varepsilon_1(a=a_{1,\ t=t1,}\ L_{1,\ t=C1}) + \varepsilon_1(a_{2,\ t=i,}\ L_{1,\ t=C2}), \qquad C2 \leq i < C3 \tag{22}$$

$$\varepsilon_{2,\ t=i} = \varepsilon_2(a=a_{1,\ t=i,}\ L_1 = L_{1,\ t=C1}) + \varepsilon_2(a_{2,\ t=i,}\ L_{1,\ t=C2}), \qquad C2 \leq i < C3 \tag{23}$$

$$\varepsilon_{3,\ t=i} = \varepsilon_3(a_{1,\ t=t1,}\ L_{1\sim3} + L_{1,\ t=C1}) + \varepsilon_3(a_{2,\ t=i,}\ L_{1,\ t=C2}), \qquad C2 \leq i < C3 \tag{24}$$

With measured strains from Sensor 1, 2 and 3, the crack depth of $a_{1,\ t=i}$ and $a_{2,\ t=i}$ can be assessed continuously. As the continuous development of Crack i, the same procedures applies as interaction for the rest of the cracks and more strain sensors may be needed for a more accurate detection since the noises may be too big when too many cracks are developed in between two sensors.

2.4. Sensitivity Study on Single Crack Detection

To demonstrate the feasibility of the developed approach above, parametric study was performed using MATLAB for single crack detection as an example. Table 2 shows the mechanical properties of material (concrete) simulated. The horizontal distance between the two sensors at the bottom of the concrete structure, L, was assumed to be 200 mm, and the crack was assumed to perpendicular to the concrete surface in the analysis. Three cases were analyzed for different crack distance away from Sensor 1, L_1, with 25mm, 50mm, and 100mm as shown in Table 3 for crack locations analyzed for the three cases.

Table 2. Summary of Mechanical Characteristics of Concrete

Parameter	Value
Elastic modulus, E	33.234 GPa
Compressive strength, σ_c	50 MPa
Tensile strength, σ_t	5 MPa

Table 3. Parametric Study Matrix

Case No.	L_1 (mm)	L_2 (mm)
1	25	175
2	50	150
3	100	100

Figures 7(a~c) show the simulated strain changes in the x-direction at Sensor 1 and Sensor 2 locations with different crack depth (a) for the three cases, respectively. When the crack is close to the sensor, for instance, 25mm and 50mm away from Sensor 1, the strain increases as the crack propagating. On the other hand, when the crack is far away from the sensor, larger than 50mm, the strain decreases as the crack propagating. Thus, by tracking the pattern of strain changes measured on strain sensors, it is possible to quickly qualitatively locating the crack's location in respect of the sensor locations.

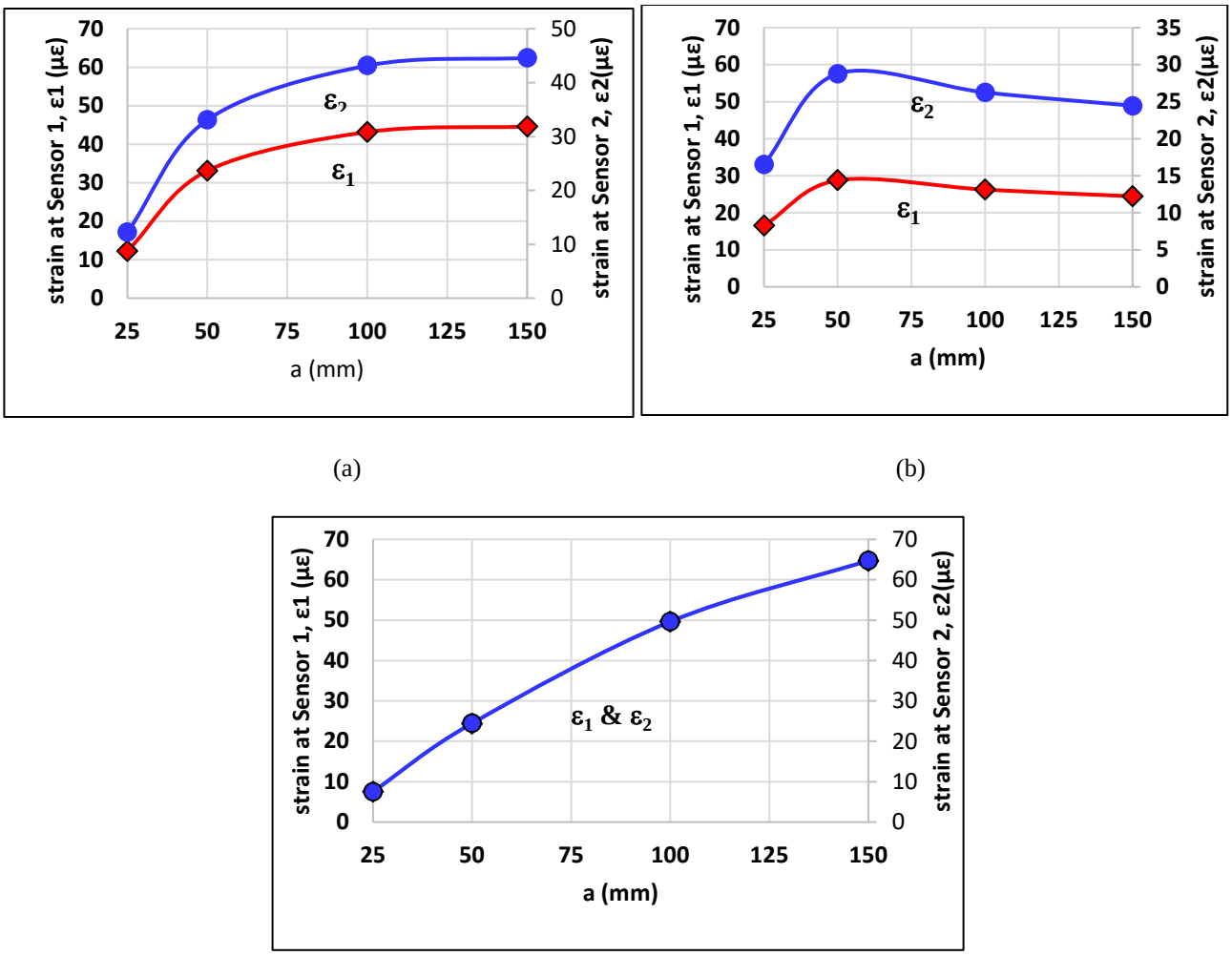

Figure 7. Estimated Strains at Sensor Locations for (a) Case 1, (b) Case 2, and (c) Case 3.

2.5. Summary

This chapter presented the theoretical analysis to develop the crack detection algorithms using the stress intensity theory to detect single and multiple cracks in pavements using point strain sensors embedded inside concrete structures followed by the sensitivity study on single crack detection as an example.

CHAPTER 3. EXPERIMENTAL STUDY FOR SINGLE CRACK DETECTION

This chapter presents the used point strain sensors, the experimental setup, the experimental results, and discussions for single crack detection using the developed algorithm in Chapter 2. The experiments were designed to achieve the objectives of this study, including tests on the compression, flexural, and tensile strength of the concrete samples in addition to the crack detection tests.

3.1. Strain Gauges Used for Single Crack Detection

If attached, strain gauges measure strains on the surface of objects and if embedded strain gauges measure strains inside of an object. The strains are detected by measuring changes in electrical resistances as the strain gauges stretch or contract with the objects they are glued to or embedded in. The resistance change is proportional to the amount of stretching or contracting they experience and is reflected as a change in voltage across designated elements, one being the strain gauge itself, in an electrical circuit [83, 84]. Strain gauges are highly precise with a strain measurement resolution of $\pm 1\mu\varepsilon$ and high accuracy of ±5% if testing is in laboratory as shown in Table 4. Temperature correction is easy to be done for strain gauges with provided temperature influencing curved from the manufacturers. Strain Gauges require easy installation and maintenance with large variety of shapes and sizes. Compared to other point strain sensors such as fiber optic sensors, acoustic sensors, ultrasonic sensors, etc., strain gauges are inexpensive and affordable. Thus, in this study, strain gauges were selected to be the point sensors. Table 4 shows the detailed sensing specifications of the used strain gauges in this study which was provided by the manufacturers. Since the sample size of the unreinforced concrete beam for the single crack detection in this study is small, the strain gauges used for the single crack detection were selected

as the precision strain gages (one axis general purpose) provided by OMEGA Engineering, Inc. This general purpose one-axis strain gauge has a small size of 1.5 mm in grid length and 1.2mm in grid width, which provides strain measurements up to ±2,000με. For unreinforced concrete samples, this measured range is enough to cover the required strain ranges. In addition, due to the fact that the experiments were performed in controlled environments in door and within a few minutes, the influences from the temperature changes were not considered for the strain gauges used in this study.

Table 4. Specifications for Point Strain Sensor in Single Crack Detection

Specifications	**Values**
Accuracy	±5%
Measurement range	±2,000με
Strain resolution	±1με
Operating temperature range	-75 to 200 ºC
Initial resistance	120 Ω
Grid width	1.2 mm
Grid length	1.5 mm

3.2. Concrete Mix Used

A water to cement ratio of 0.35 was used to mix the concrete beam samples and Table 5 shows the detail concrete mix design used in this study. After mixing, the concrete samples for testing were cured for the periods of 28 days [84].

Table 5. Concrete Composition

Materials	**Amount (kg/m^3)**
Cement (Kg)	25
Coarse Aggregate –Gravel pass sieve opening 19 mm (Kg)	10
Coarse Aggregate –Gravel pass sieve opening 16 mm (Kg)	10
Coarse Aggregate –Gravel pass sieve opening 12.5 mm (Kg)	12
Coarse Aggregate –Gravel pass sieve opening 9.5mm (Kg)	16.5
Fine Aggregate-Sand pass sieve opening 4.75 mm (Kg)	12
Fine Aggregate-Sand pass sieve opening 0.075 mm (Kg)	17.5
Water (Kg)	8.7

3.3. Compression and Tension Tests

Before detecting cracks, material characterization tests were conducted on the used concrete, including compression and tensile strength tests. For compression tests, three cylindrical specimens were made with nominal dimensions of 152.4 mm × 304.8 mm. Figure 8 shows the test setup for the compression strength test. Loading was applied continuously until specimen rupture following ASTM C39.

Figure 8. Sample Setup for Compression Tests

The tensile strength tests followed the direct tensile strength test procedure ASTM D2936 − 08. Six prismatic specimens were made for the tensile tests which had nominal dimensions of 50.8 mm × 50.8 mm ×304.8 mm specimens, in which 304.8mm is the length of the specimen, as shown in Figure 9(a). Three samples were prepared with a notch in the middle (in-notch) and three samples were prepared without any notch (out-notch). Figure 9(b) shows the test setup for the tensile strength.

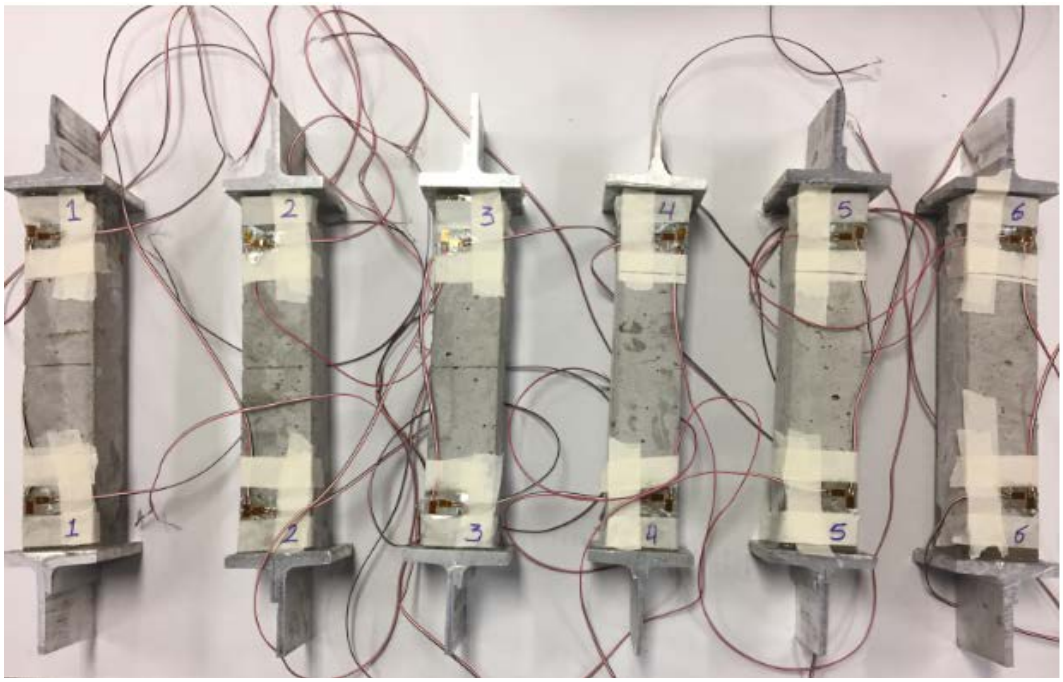

(a) Samples preparation for the test

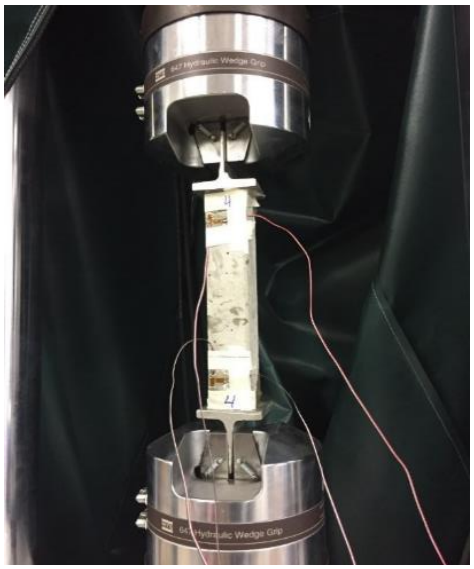

(b) Test Setup

Figure 9. Tensile Strength Test Sample (a) and Test setup (b)

Table 6 shows the tested compression and tensile strengths from the concrete samples. Although six samples were tested for the tensile tests, only the three specimens without notch were used to determine the tensile strength of the used concrete. The average compression strength and

tensile strengths for the used concrete was 45 Mpa and 2.1 Mpa. The cracking strength was tested to be lower than the tensile strength of concrete. Crack propagation is governed by the cracking strength [84].

Table 6**.** Compression and Tentile Test Results

Sample No.	**Compression strength (MPa)**	**Tensile strength (MPa)**
1	45	2.5
2	44	1.8
3	46	2.0
Average	45	2.1

Figure 10 illustrates the differences in failure process from the direct tensile tests for in-notch and out-notch for prismatic tensile strength specimens. It can be noticed remarkably that when comparing the stress–displacement curves obtained during the experiment, the failure crack out-notch for prismatic specimen's concrete almost 40% times higher normal stress and 30% less than for displacement compared to the results measured in in-notch for prismatic specimen's concrete.

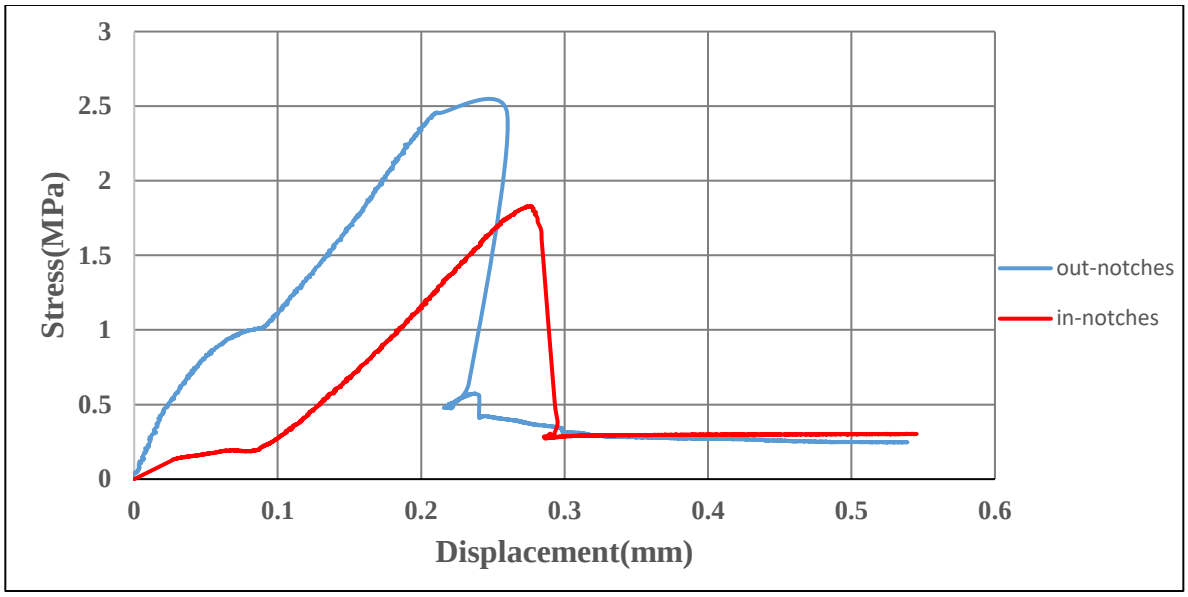

Figure 10. Normal Stress VS Displacement for Both In-notches and Out-notches Failure in Tensile Test

3.4. Flexural Strength Tests

In addition, flexural strength tests were also performed. Unreinforced concrete beams were prepared with dimension of 152.4 mm × 152.4 mm ×508 mm, in which 508mm is the length of the beam as shown in Figure 11 (a). Three test samples were made with notch in the middle of the concrete beam and three samples were made without any notches. The three-point flexible strength tests were following ASTM C78 as shown in Figure 11 (b).

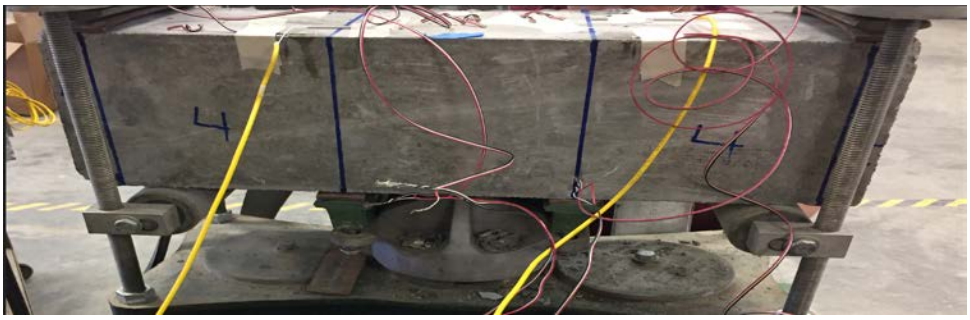

(a)

(b)

Figure 11. Flexural Strength Test Sample (a) and Test Setup (b)

Based on the applied loads and the dimension of the tested specimen, the flexural strength was calculated as [84]:

$$R = \frac{\mathrm{P}l}{\mathrm{b(d-ao)^2}} \tag{33}$$

where, R = modulus of rupture (MPa); P = applied load (N); l = distance between the support bars (mm); b = specimen average width at the rupture section (mm); d = specimen average height at the rupture section (mm); ao=crack length (initial crack).

Rupture occurred at the third average distance between the support's elements in the flexural strength tests, and the flexural strength was calculated by the Eq. (33). Table 7 presents the flexural strength results obtained from the experiments for both the three samples with notch and three samples without notch. The flexural strength for samples with notch had an average of 5.7 Mpa and that for samples without notch had an average of 6.27 Mpa.

Table 7. Flexural Strength Test Results

Sample No.	Flexural Strength (with notch) (MPa)	Flexural Strength (without notch) (MPa)
1	5.3	6.3
2	5.8	6.0
3	6.0	6.5
Average	5.7	6.27

3.5. Sample Preparation for Single Crack Detection

To detect single crack, unreinforced concrete beams were prepared with dimension of 152.4 mm × 152.4 mm ×508 mm, in which 508mm is the length of the beam, following the ASTM testing standard for three-point loads of unreinforced concrete beams [84]. Two types of concrete test samples were made in this study including three samples with initial notches and three samples without notches. Three samples were made with initial notches at various locations on the beam as shown in Figure 12. The three initial notches were all at the center of the beam but had different depth of 25mm, 50 mm, and 75mm, respectively. Figure 12 (a) shows the sample with initial notch of 25 mm in depth, Figure 12 (b) shows the sample with initial notch of 50mm in depth, and Figure 12 (c) illustrates the sample with initial notch of 75mm in depth. For all the samples with notches, each sample had four strain gauges installed on the side of the beam. Two strain gauges installed 154 mm away from the edge of the sample with one in longitudinal direction and the other in the transverse direction and the other two laid out the same way on the symmetric location on the beam. The horizontal distance between the locations of the two sets of sensors were 200 mm. All the detected strains were collected using data acquisition and recorded using a personal computer for post-experiment analysis.

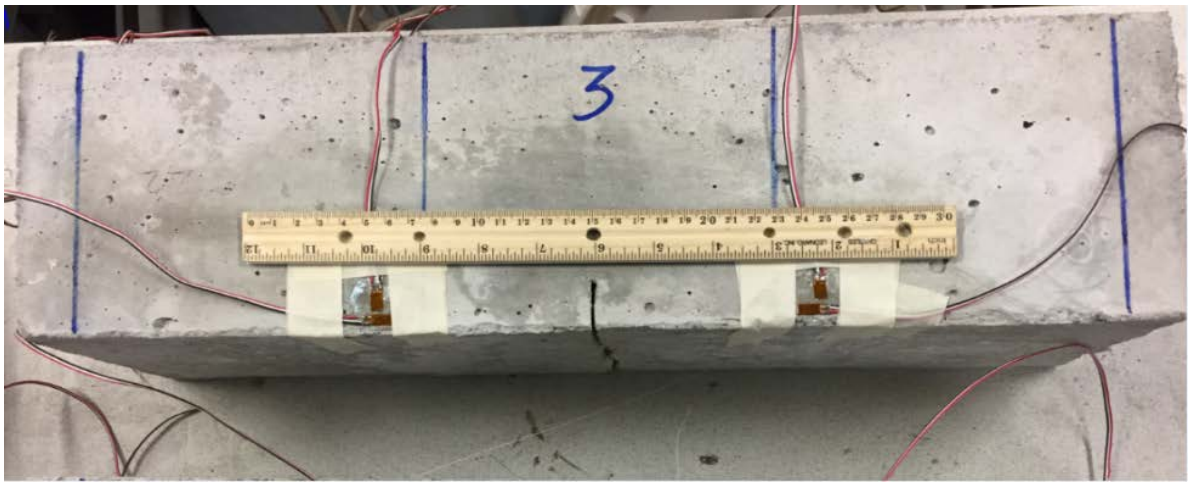

(a) Concrete beam sample with initial notch 75mm

(b) Concrete beam sample with initial notch 50mm

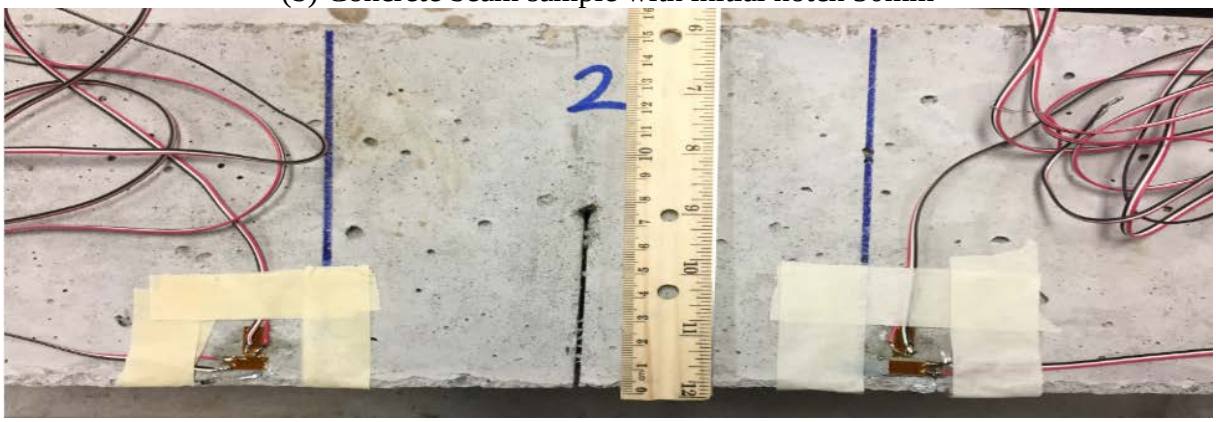

(c) Concrete beam sample with initial crack 25mm

Figure 12. Concrete Beam Samples with Initial Notches

Three samples were made without initial notches as shown in Figure 13 (a). For all the three samples without notches, four strain gauges were installed on the bottom of the sample as seen in Figure 13 (b). Two strain gauges installed 154 mm away from the edge of the sample close

to each side of the beam and the other two laid out the same way on the symmetric location on the beam. The horizontal distance between the locations of the two sets of sensors were 200 mm. All the detected strains were collected using data acquisition and recorded using a personal computer for post-experiment analysis.

(a)

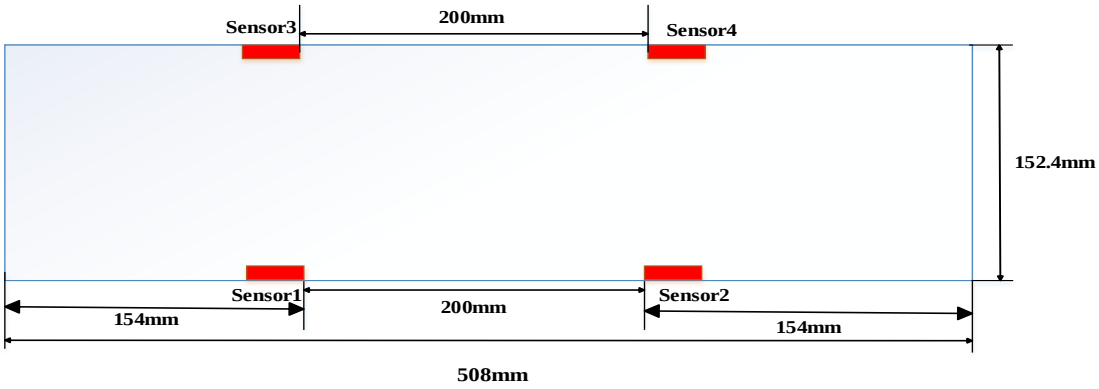

(b)

Figure 13. Photo (a) and Schematic of the Sensor Layout (b)

3.6. Results for Samples with Initial Notches

Figures 14 (a, b) illustrate the measured strains in longitudinal direction from the two strain gauges at the bottom of the beam, Sensor 1 and Sensor 2.

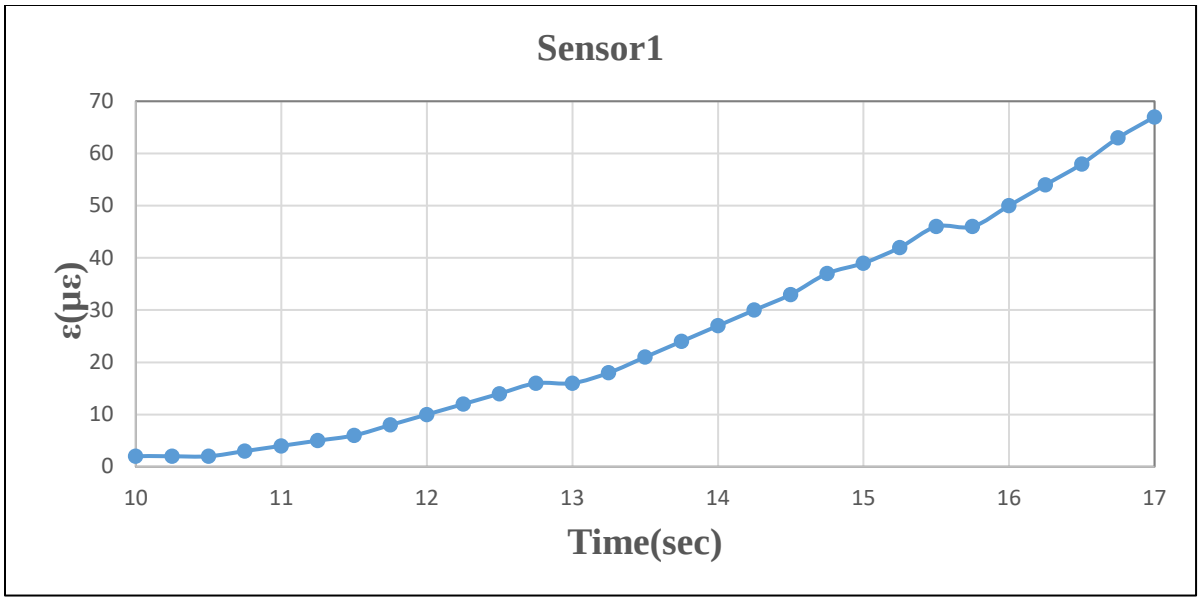

(a) Strain (με) at Sensor 1 Vs Time (Sec)

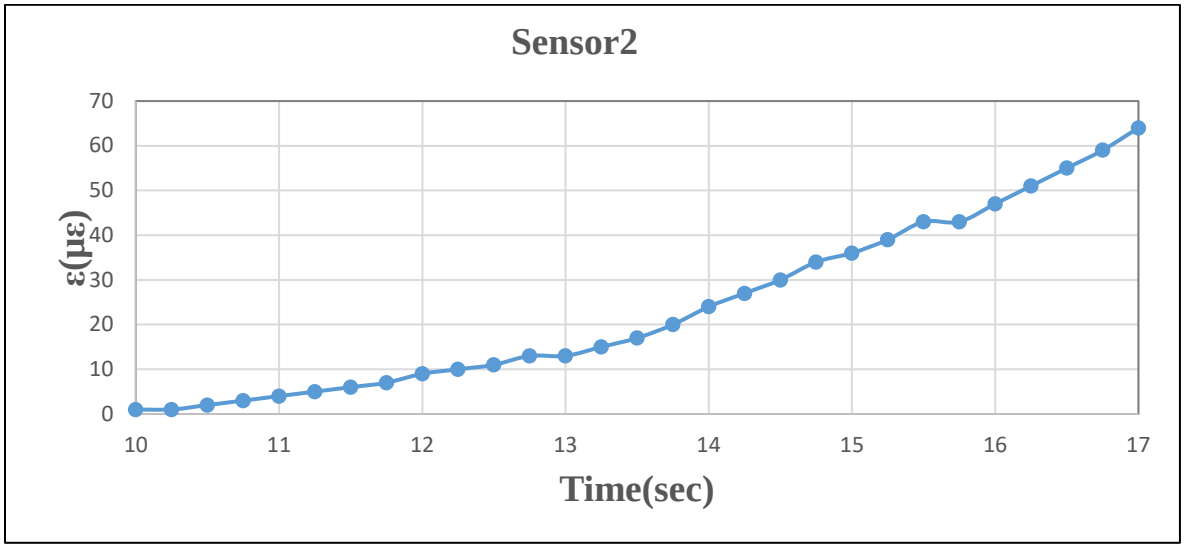

(b) Strain (με) at Sensor 2 Vs. Time (Sec)

Figure 14. Measure Strains for the Sample with an Initial Notch of 50mm

Based on Equation (5) and with the measured strains from Sensor 1 and sensor 2, the crack location away from the sensors (L1, L2) and (r, θ) can be calculated. Figures 15 (a, b) show the calculated crack length progressing as loading increases. The detected final crack length was 115mm based on the sensor measurements. The actual measured crack width using ruler was

102.4mm. The difference between the crack measured by the two-point sensors and the actual crack length was 12.3% for the beam sample with the initial notch of 50mm in depth.

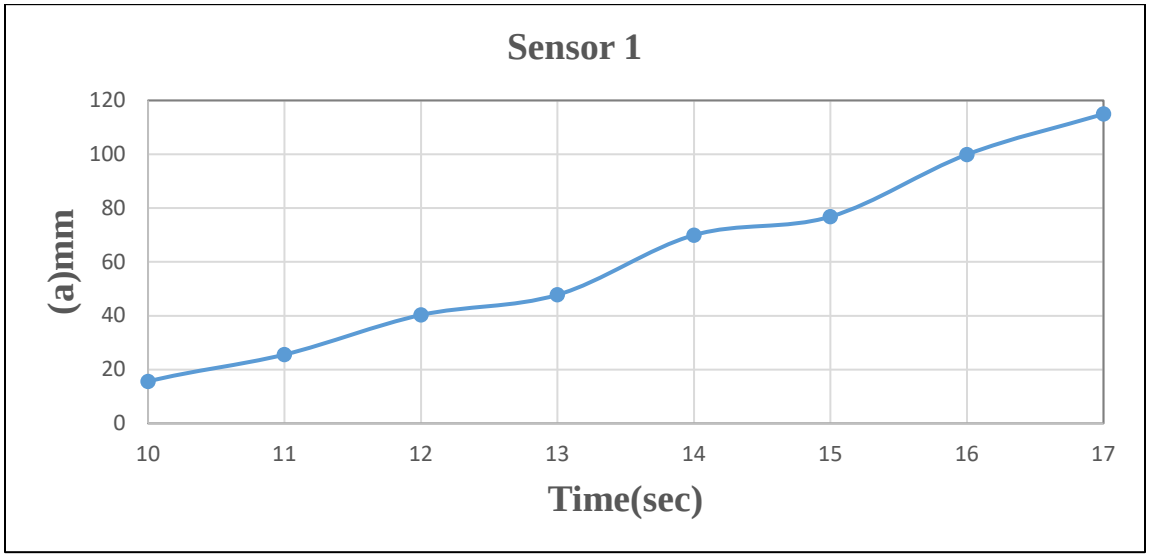

(a) Measured crack length (a) Vs. Time (Sec), from Sensor 1

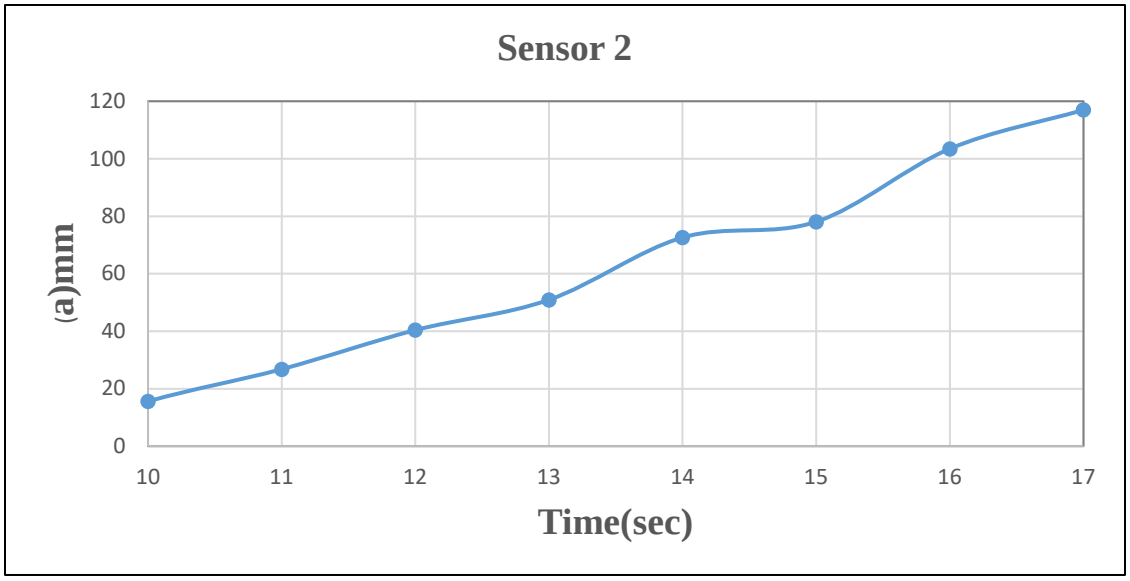

(b) Measured crack length (a) Vs. Time (Sec), from Sensor 2

Figure 15. Crack Detection from Point Sensors for the Concrete Sample with an Initial Notch of 50mm

For the test sample with the initial notch of 25mm in depth, Figure 16 shows the measured crack length propagation from the installed point sensors. The final measured crack length from

the installed sensors was 141.6mm. The actual crack depth was 127.4mm. The measurement difference between the sensors and the actual crack length was 11.15% when the concrete beam sample with the initial notch of 25mm in depth.

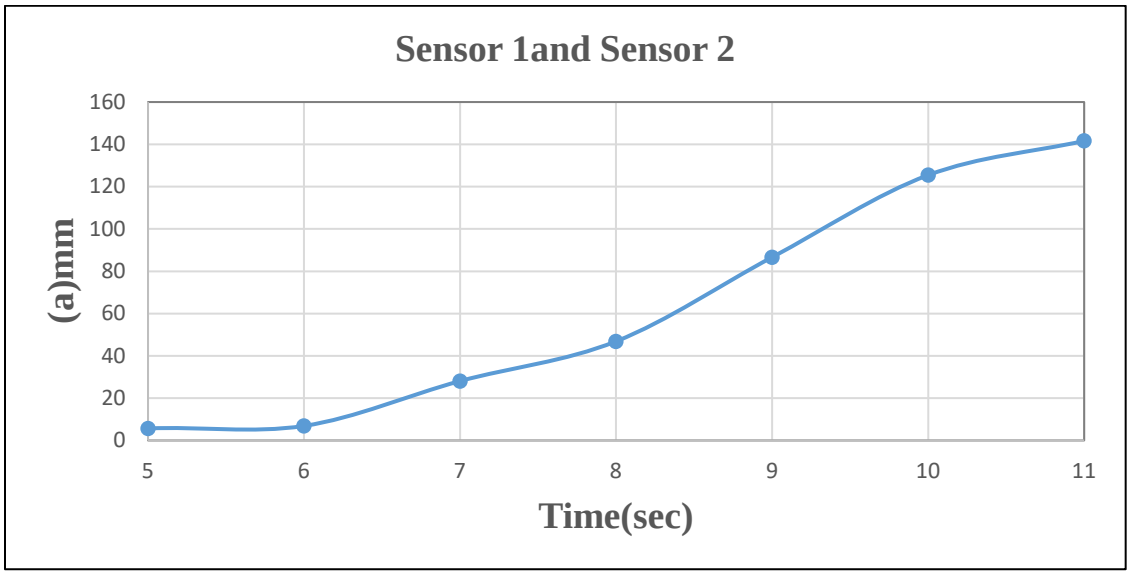

Figure 16. Crack Detection from Point Sensors for the Concrete Sample with an Initial Notch of 25mm

For the test sample with the initial notch of 75mm in depth , Figure 17 shows the measured crack length development from the installed point sensors. The final measured crack length from the installed sensors was 62.76mm. The actual crack depth was 77.4mm. The measurement difference between the sensors and the actual crack length was 18.92% when the concrete beam sample with the initial notch of 75mm in depth. In general, the sensors detected crack length better for the samples with initial notches of 25 mm and 50mm compared to that of 75mm. The reason of this may because the initial 75mm crack was approximately half of the height of sample, and in this case, the sample quickly failed, and the strain had the lowest values so, the crack length measured was small.

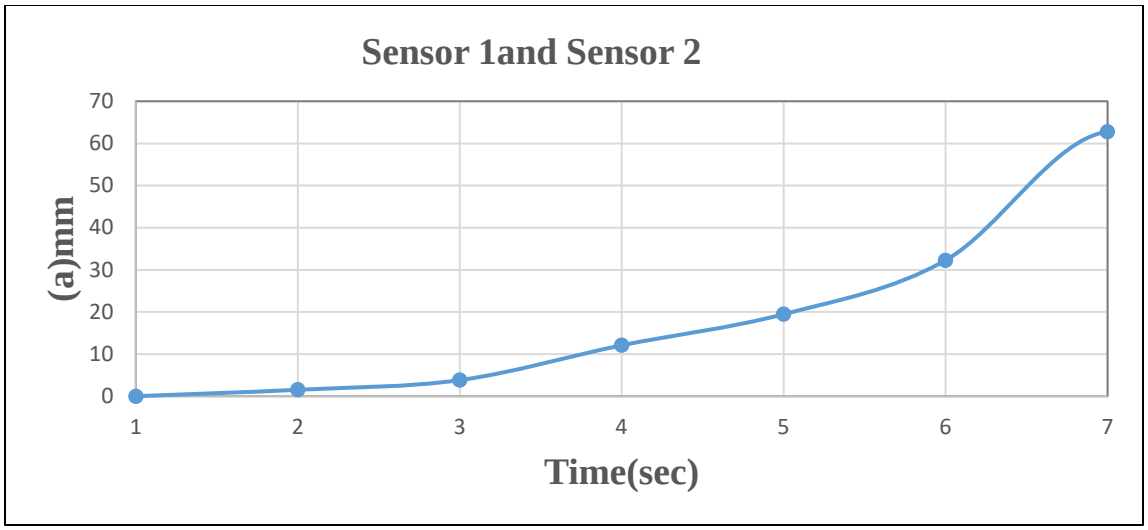

Figure 17. Crack Detection from Point Sensors for the Concrete Sample with an Initial Notch of 75mm

The test results show that for the specimens with initial notches, the average measurement error to detect a single crack using two point strain sensors was 14.12%, yielding an average measurement accuracy of 85.88%.

3.7. Results for Samples without Initial Notch

For samples without initial notches, Figures 18 (a, b) illustrate the measured strains from the strain gauges for Sample 1 during the three-point loading tests. Based on Equations (16, 18, and 20) and with the measured strains from Sensor 1 and 2, the crack location and crack propagation (crack depth) on the front surface of the specimen can be estimated as shown in Figure 19 (a). In Figure 19 (a), X-axis is the distance between the identified crack to Sensor 1 and Y-axis if the crack depth pattern changes in the vertical direction. The actual cracks were also measured from Figure 19 (a) to compare with the estimation of crack patterns based on the sensor readings. Figure 19 (b) also shows the photo of the crack pattern after cracking for Sample 1. For Sample 1, the maximum variance between the crack patterns detected from the sensors is within 8 mm, which is 5 % of crack estimation error.

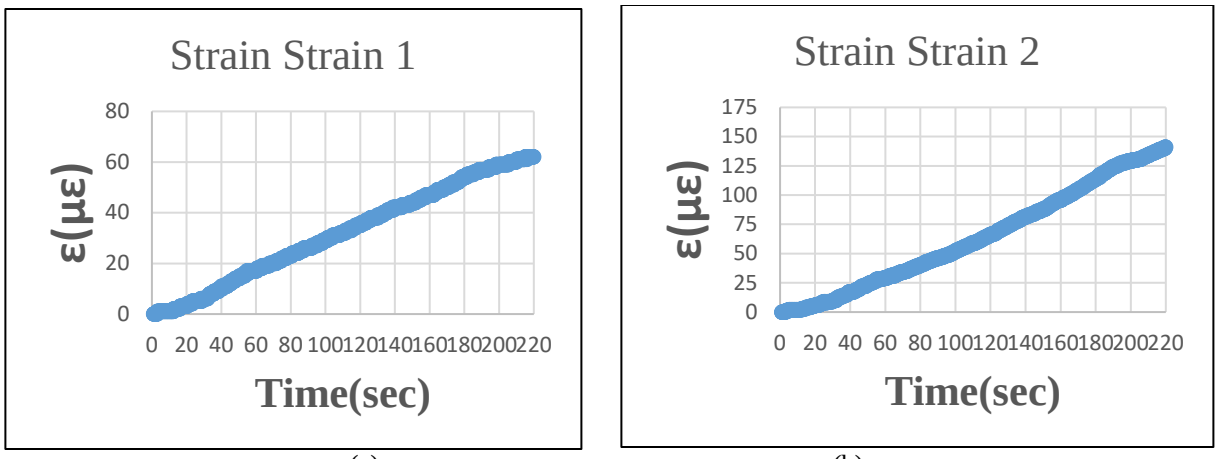

(a) (b)

Figure 18. Measured Strains from the Sensor 1 (a) and Sensor 2 (b) of Sample 1

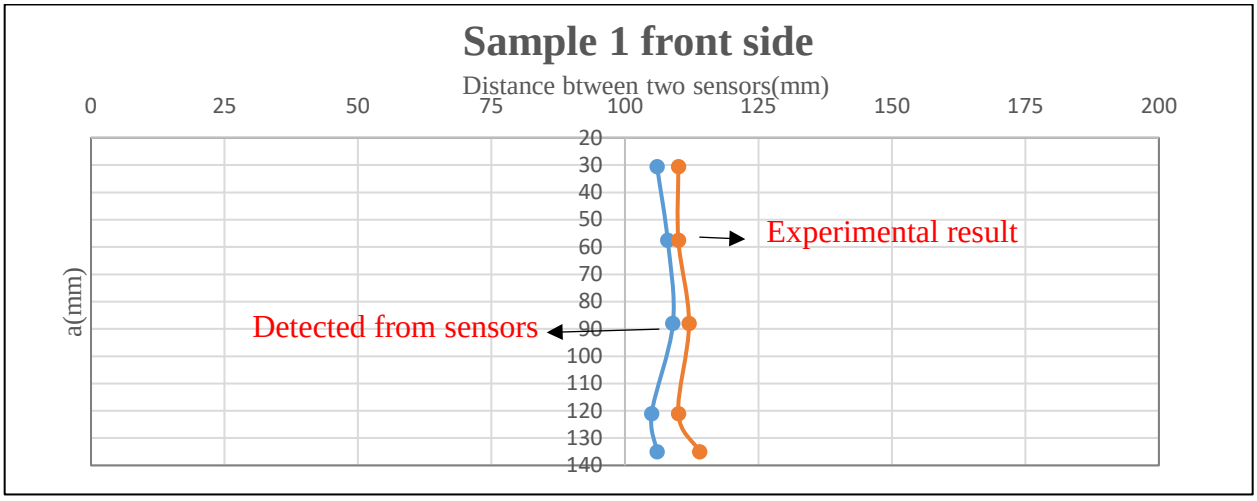

(a)

(b)

Figure 19. Comparison of Detected Crack Compared with Reference Crack (a) and Photo of after Cracking (b) for Sample 1

Figures 20 (a, b) illustrate the measured strains from the strain gauges of the Sample 2 which did not have a notch during the three-point loading tests and Figures 21 (a) is the comparison between crack location and crack propagation (crack depth) in the front surface estimated using sensors and the actual cracks as shown in Fig. 21 (b). For Sample 2, the maximum variance between the crack patterns detected from the sensors is within 46 mm, which is 30.1 % of crack estimation error.

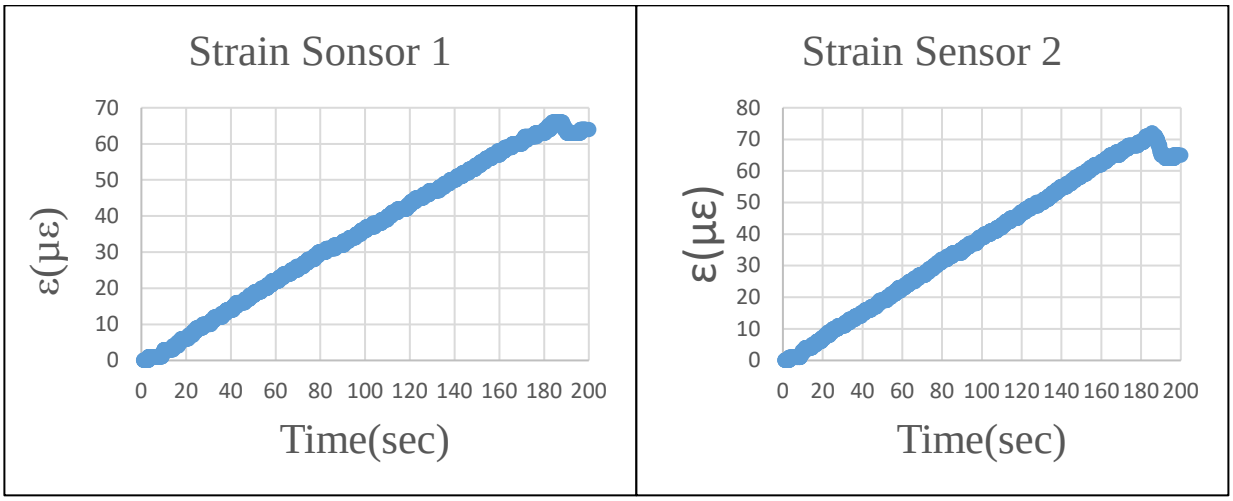

(a) (b)

Figure 20. Measured Strains from the Sensor 1 (a) and Sensor 2 (b) of Sample 2

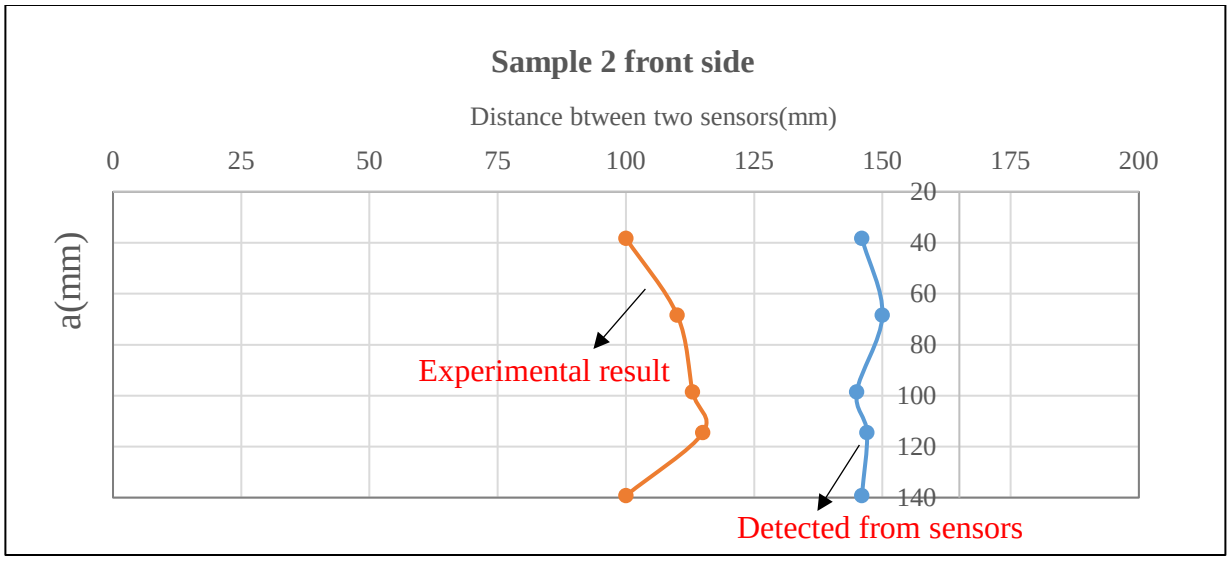

(a)

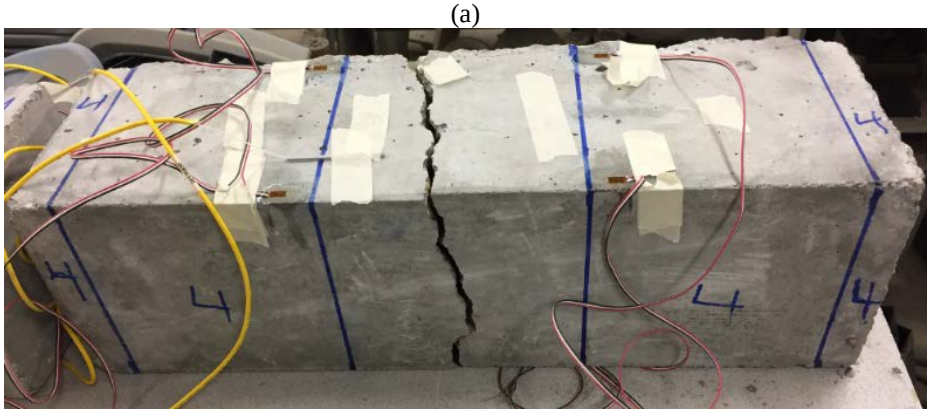

(b)

Figure 21. Comparison of Detected Crack Compared with Reference crack (a) and Photo of after Cracking (b) for Sample 2

Figures 22 (a, b) illustrate the measured strains from the strain gauges of Sample 3 for the samples without notches during the three-point loading tests and Figure 23 (a) is the comparison between crack location and crack propagation (crack depth) in the front surface estimated using sensors and the actual cracks as shown in Figure 23 (b). For Sample 3, the maximum variance between the crack patterns detected from the sensors is within 27 mm, which is 17.71% of crack estimation error.

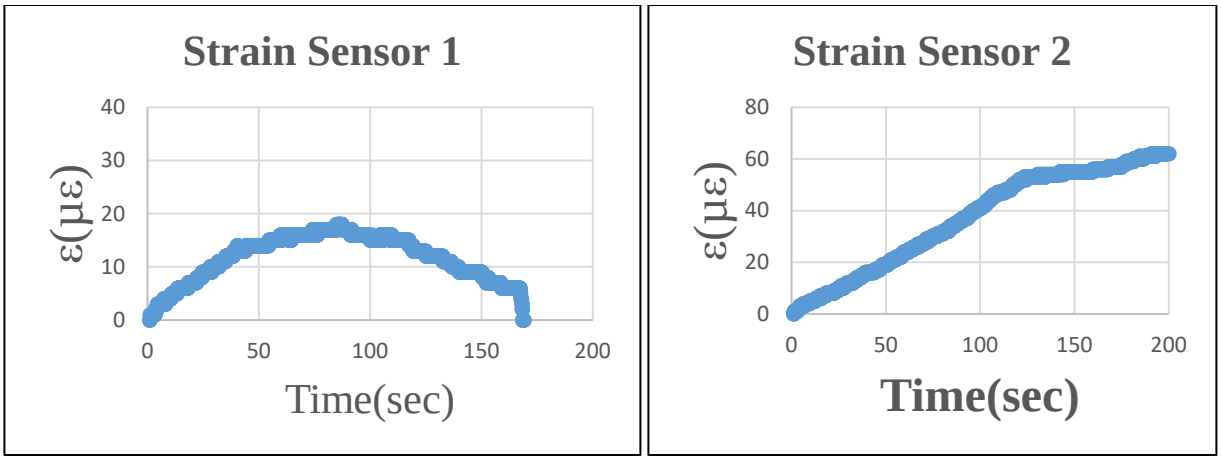

(a) (b)

Figure 22. Measured Strains from the Sensor 1 (a) and Sensor 2 (b) of Sample 2

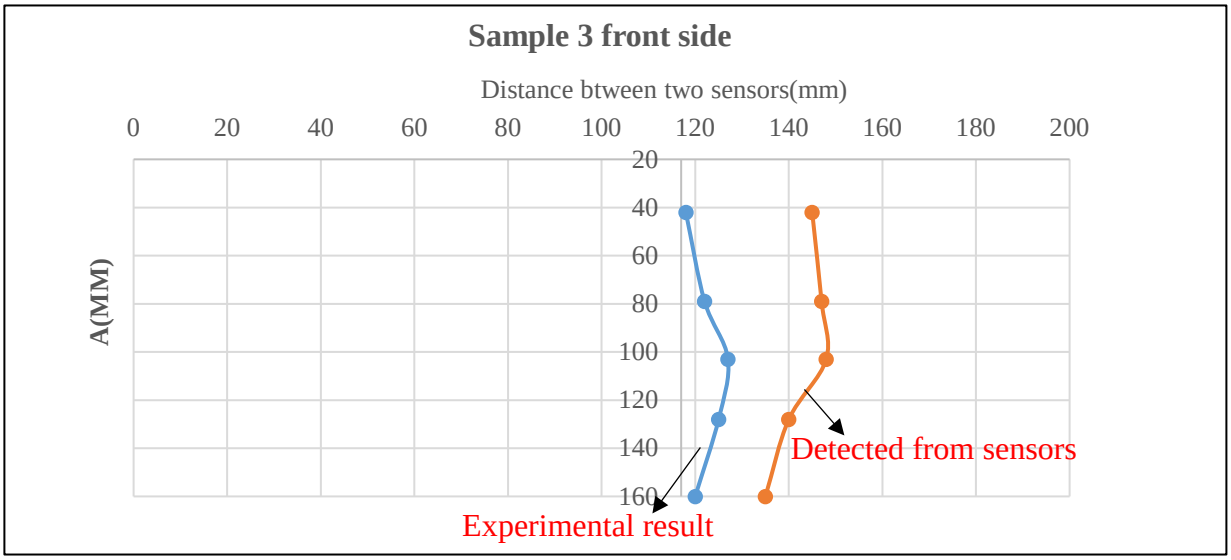

(a)

(b)

Figure 23. Comparison of Detected Crack Compared with Reference Crack (a) and Photo of after Cracking (b) for Sample 3

From Figure 19 (a), 21 (a), and 23 (a), it can be seen that the average variance between the crack pattern detected using the discrete sensors on the bottom of the concrete beam and the actual crack pattern for all three samples is 17.6 %, indicating a promising crack detection approach for internal crack detection.

3.8. Summary

This chapter presented the experimental study for single crack detection. Experimental results with three initial notches of 25, 50, and 75 mm in depth were made on the specimens to control the location for cracks so that comparison between analytical and experimental analysis can be made. An average crack depth detection accuracy yielded 88.85% from the three tested specimens with initial notches. For the samples without notches, the average crack location and depth detection accuracy achieved 82.4%.

CHAPTER 4 EXPERIMENTAL STUDY FOR MULTPULE CRACKS DETECTION

This chapter presents the testing program that was used to investigate detection of multi cracks in concrete using the developed sensing system. To be able to achieve multiple cracks in concrete, reinforced concrete beams were prepared for the laboratory experiments.

4.1. Strain Gauges Used for Multi Crack Detection

Since the sample size of the reinforced concrete beam for the multiple cracks is relatively big, the strain gauges used for the multiple cracks detection were selected as the specific designed strain gages for concrete samples provided by OMEGA Engineering, Inc. Table 7 shows the detailed sensing specifications of the used concrete strain gauges for multiple cracks detection in this study which was provided by the manufacturers. This special purpose one-axis strain gauge has a large size of 30 mm in grid length and 3 mm in grid width, which provides strain measurements up to $\pm 20{,}000\mu\varepsilon$. For reinforced concrete samples, this measured range is enough to cover the required strain ranges. In addition, the influences from the temperature changes were not considered for the strain gauges used in this study since the experiments were performed in controlled environments in door and within a few minutes.

Table 8. Specifications for Point Strain Sensor

Specifications	**Values**
Accuracy	±5%
Measurement range	±20,000με
Strain resolution	±1με
Operating temperature range	-75 to 200 ºC
Initial resistance	350 Ω
Grid width	3mm
Grid length	30 mm

4.2. Samples Preparation and Experimental Setup

The samples used in this experiment were reinforce concrete (RC) beams with dimensions of 152.4 mm × 241.3 mm × 1422.4 mm [85, 86] as shown in Figure 24. The concrete mix followed the same mix design as in Table 5 of Chapter 3. As also shown in Figure 24, ϕ10 and ϕ12 reinforcements were applied in the RC beams as longitudinal reinforcement rebar in the compression and tension regions and ϕ8 at an interval of 152.4mm was used as stirrups for shear reinforcement. The design of the RC followed reference [85, 86]. Table 8 shows the detailed material properties of the used reinforcements. Figure 25 shows the molds for samples with the reinforcements and Figure 26 shows a photo of the casted RC beam sample. Three RC beams were prepared for testing to be statistically valid. On each RC beam, four strain gauges were attached following Figure 6 in Chapter 2. The distance in between each strain gauge is 245mm as also shown in Figure 26.

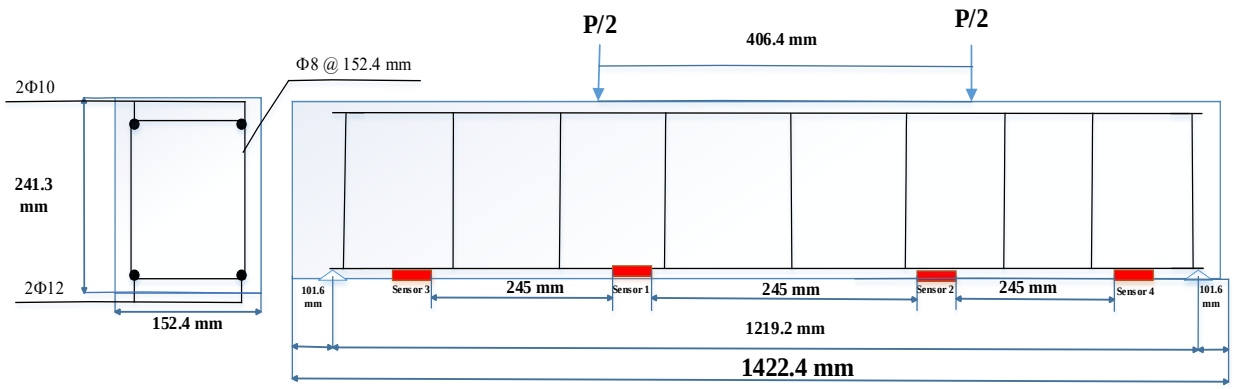

Figure 24. The Schematic of the Reinforced Beam Details and Sensor Layout

Table 9**.** Material Properties of the RC Beams Reported

Reinforcement	**fy Yield strength (N/mm2)**	**ft Tensil strength (N/mm2)**	**E Young's modulus (N/mm2)**
Rebar φ12	468	645	210
Rebar φ10	510	700	210

Figure 25. The Molds for Samples and Rebars before Casting of Concrete.

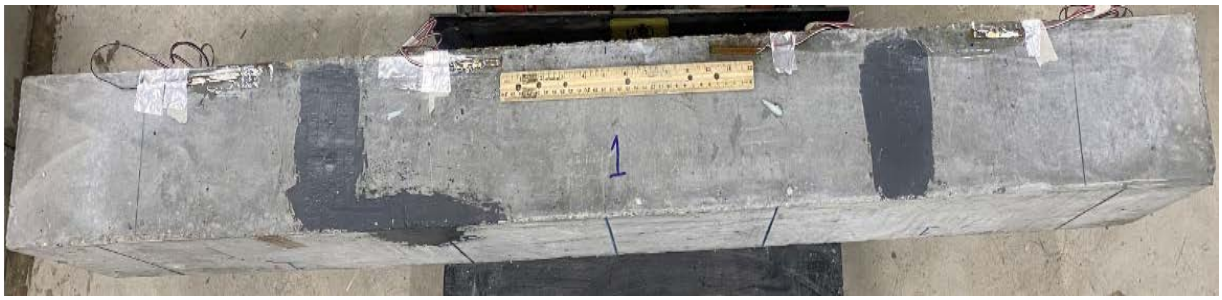

Figure 26. Photo of the RC Sample 1

The three prepared RC beams were tested under continuous four-point loading with a loading speed of 1 kN/min [87, 88] as shown in Figure 27. Figure 28 illustrates the experimental setup for data acquisition and recording using a personal laptop for post-experiment analysis.

Figure 27. Front View of the Loading Arrangement and the RC Beam Instrumented with Sensors

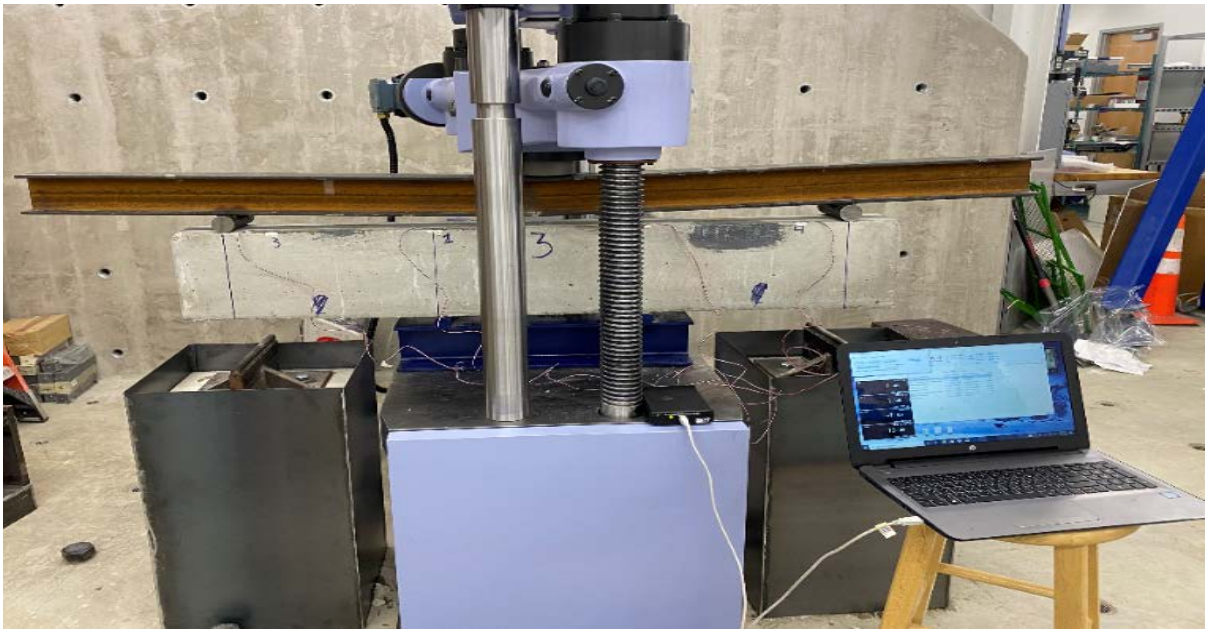

Figure 28. Experimental Setup for Data Acquisition and Recording using a Personal Laptop

4.3. Results and Discussion

Figure 29 shows the measured applied load-displacement curves for RC Sample 1 from the MST machine during the test and Figures 30~32 show the measured load vs time for all the three tested RC samples.

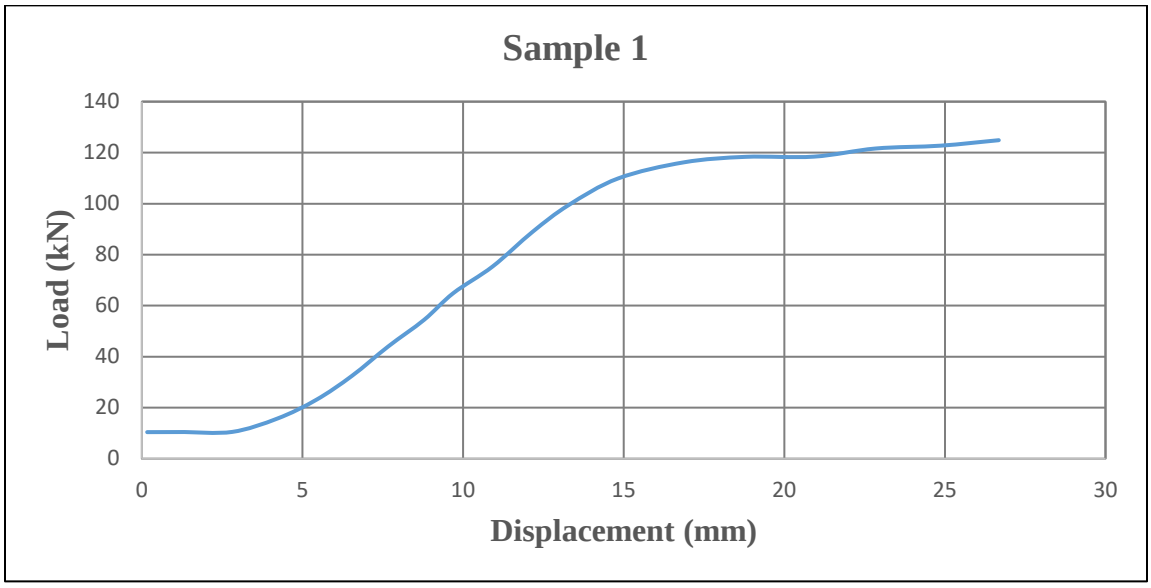

Figure 29. Load Vs Displacement for Sample 1

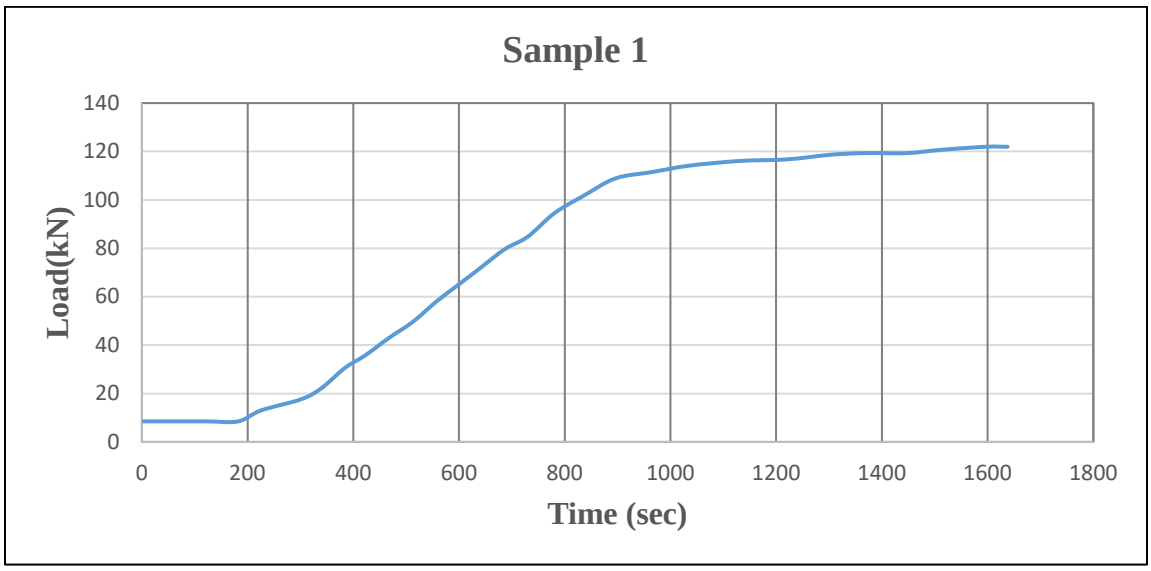

Figure 30. Load VS Time for Sample 1

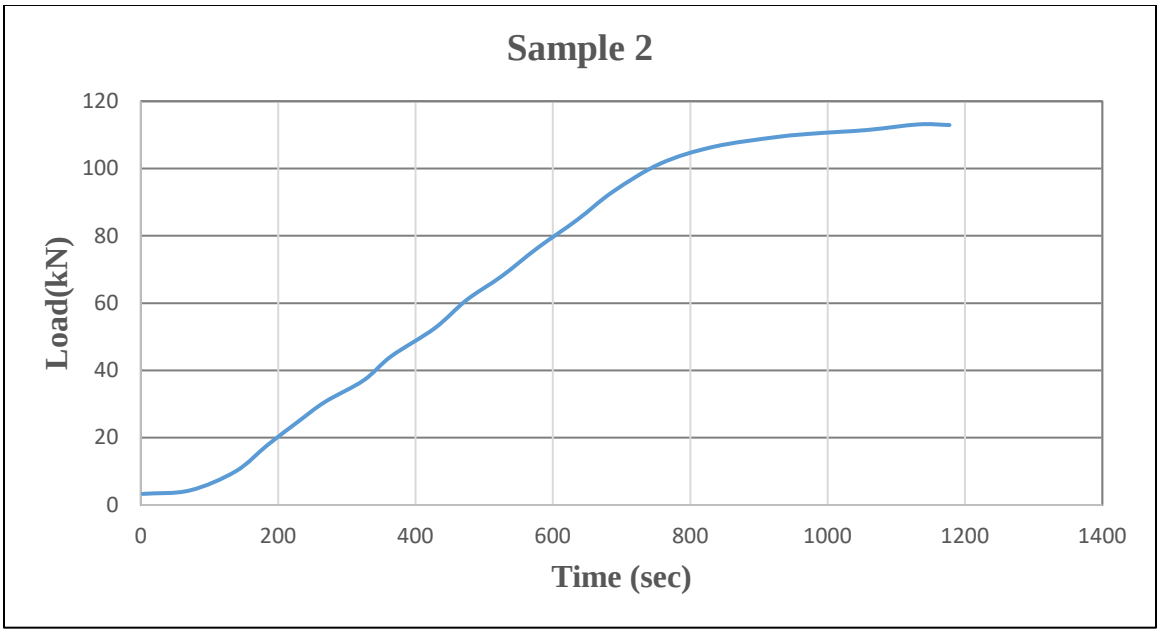

Figure 31. Load VS Time for Sample 2

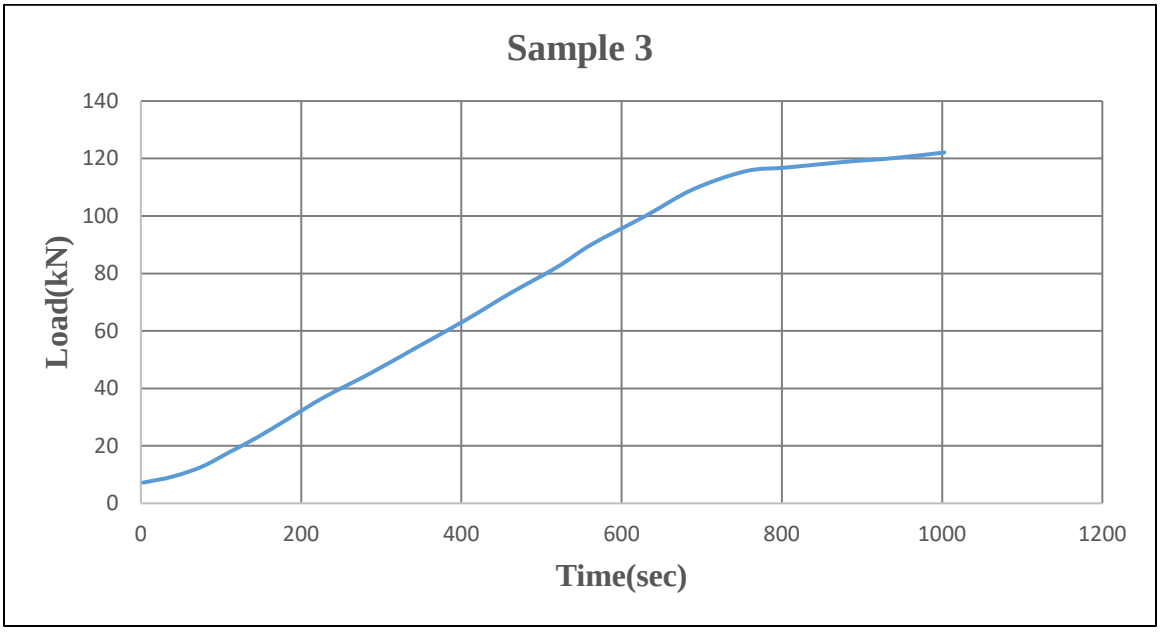

Figure 32. Load VS Time for Sample 3

4.3.1. Experimental Results for RC Sample 1

Figures 33 (a-d) illustrate the measured strains from the strain gauges of Sample 1 during the four-point loading tests. Figure 34 shows the three main cracks for sample 1 after the tests.

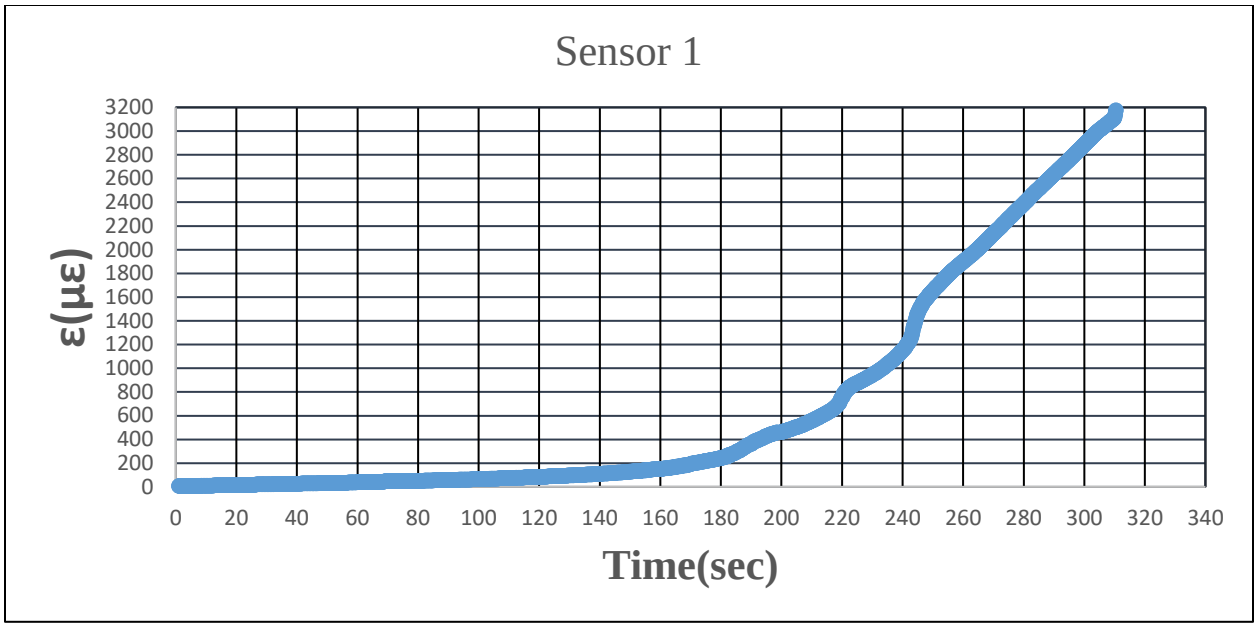

(a) Strain (με) at Sensor 1 Vs. Time (Sec)

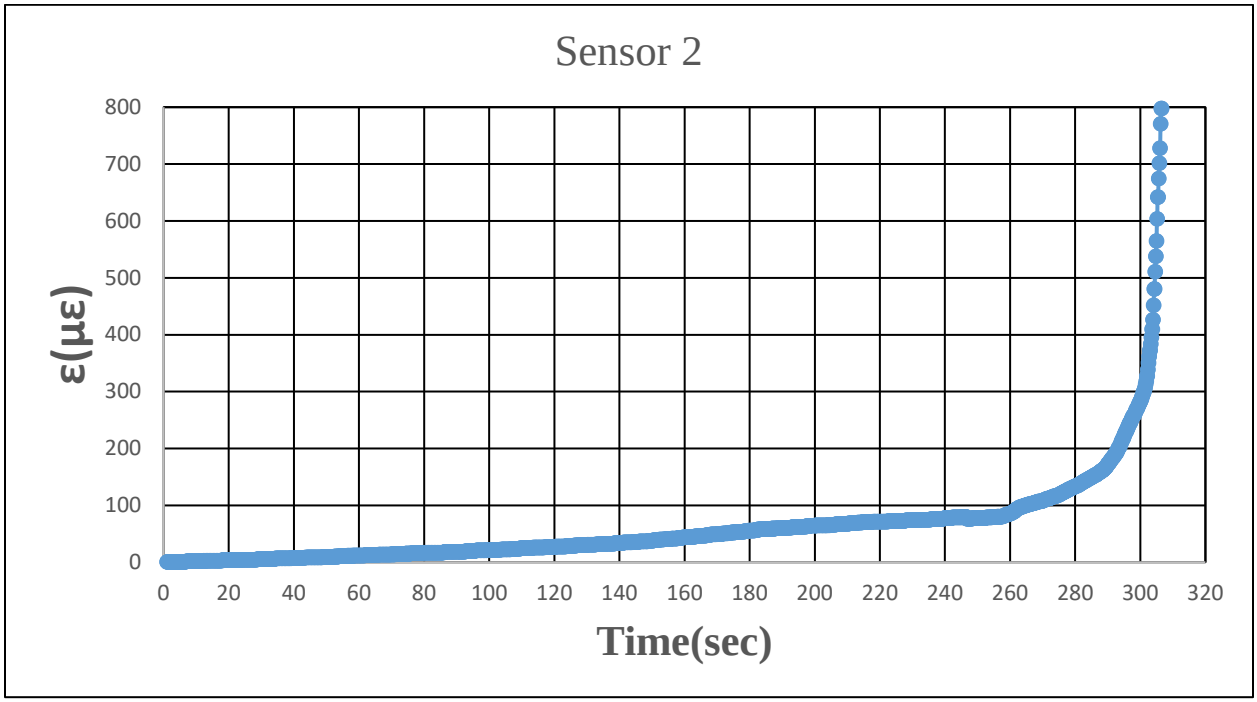

(b) Strain (με) at Sensor 2 Vs. Time (Sec)

Figure 33. Measured Strains from the Sensor 1 (a), Sensor 2 (b), Sensor 3 (c), and Sensor 4 (d) of RC Sample 1

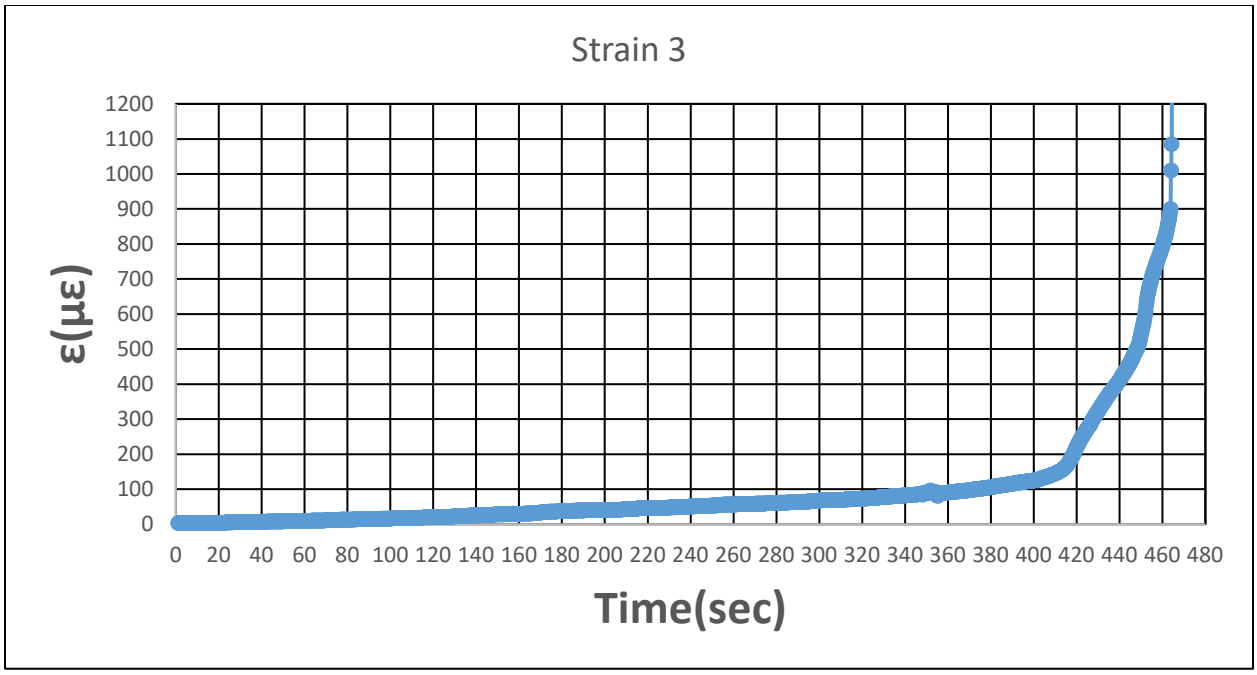

(c) Strain (με) at Sensor 3 Vs. Time (Sec)

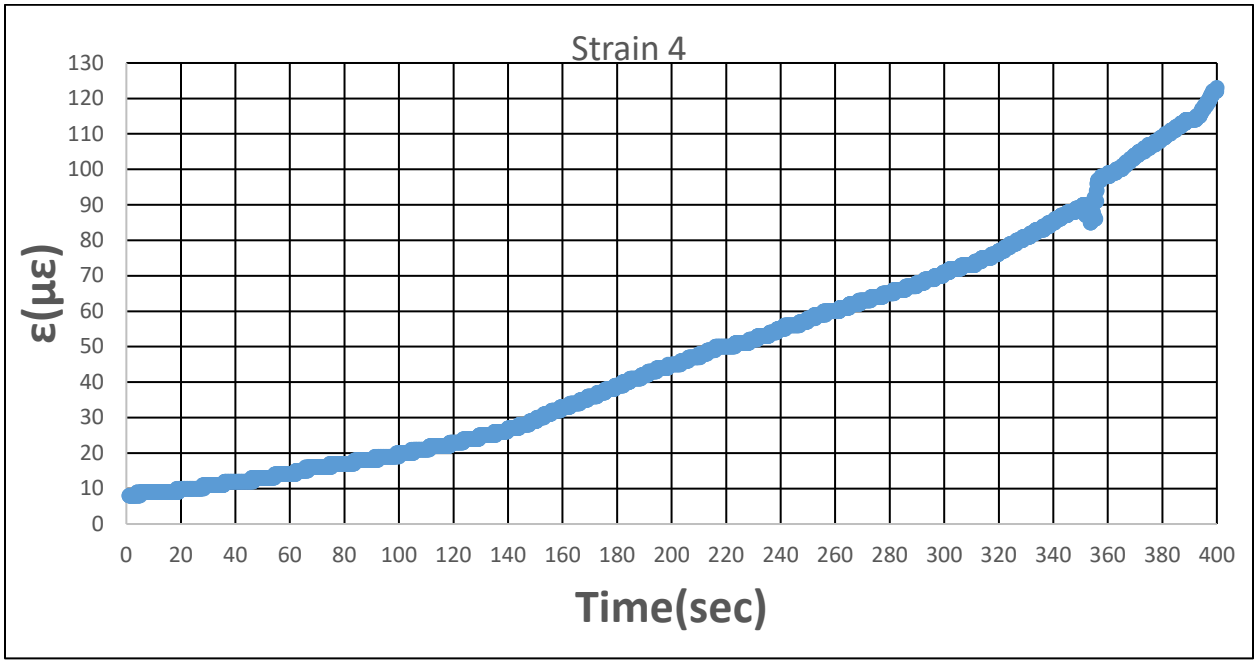

(d) Strain (με) at Sensor 4 Vs. Time (Sec)

Figure 33. Measured Strains from the Sensor 1 (a), Sensor 2 (b), Sensor 3 (c), and Sensor 4 (d) of RC Sample 1 (continued)

Figure 34. Cracks for Sample 1 after the Test

Table 9. summarized the detected cracks from the four strain gauges using the developed algorithm in this study and the comparison with the measured cracks using rulers during the test by video and monitoring the data ($a_1>a_2>a_3$). The first crack happened at 180 sec between sensors 1 and 2. Based on Equations (13, 15, and 16) and with the measured strains from Sensor 1 and 2 for detection initial crack location after that development. The second crack happened at 255 sec between sensor 2 and sensor 4 using equations (17, 18, and 21) for detection initial crack location after that development. Finally, cracks 3 happened between 295 and 320 sec presented by sensor 2. The cracks location and crack propagation (crack depth) on the front surface of the specimen can be estimated as shown in Figure 35 for the comparison of detected cracks compared with reference cracks. Figure 36 shows the cracks length (A) changing with time and Figure 37 illustrates the length of the cracks (A) and locations (L) changing with time for Sample 1. For Sample 1, the sensor network detected locations and length for three main vertical cracks in the meddle (critical zone). From Table 9 and Figures 35-37, it can be seen that the average detection error between the crack pattern detected using the sensor network on the bottom of the concrete beam and the actual crack pattern for all three cracks is 7%.

Table 10. Results Obtained from Sensors Detected for Sample 1.

	Crack 1		Crack 2		Crack 3	
	Location from sensor 1 (mm)	Direction (Φ°)	Location from sensor 1 (mm)	Direction (Φ°)	Location from sensor 1 (mm)	Direction (Φ°)
Initial	**25**		**170**		**350**	
	28	17.5	172	11.5	355	30
	30	17.5	178	13.9	360	30
	32.5	11.5	182	9.2	365	19.5
	35	14.5	185	6.9	370	14.5
	38	17.5				
	40	11.5				
	42	11.5				
Final		**200**		**185**		**190**

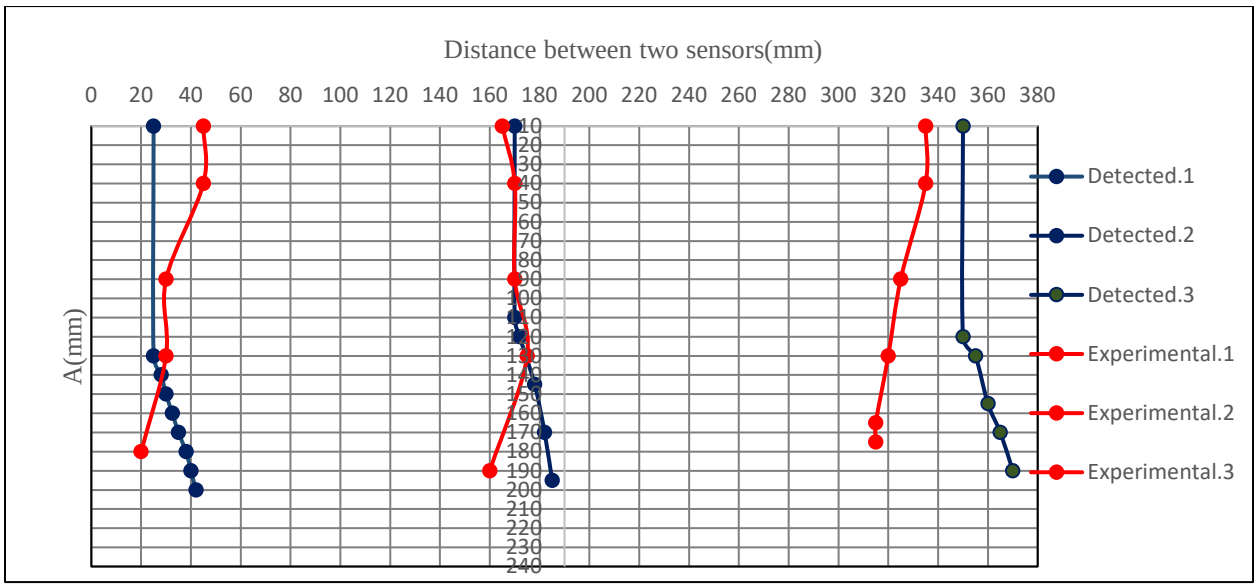

Figure 35. Comparison of Detected Cracks Compared with Reference Cracks for Sample 1

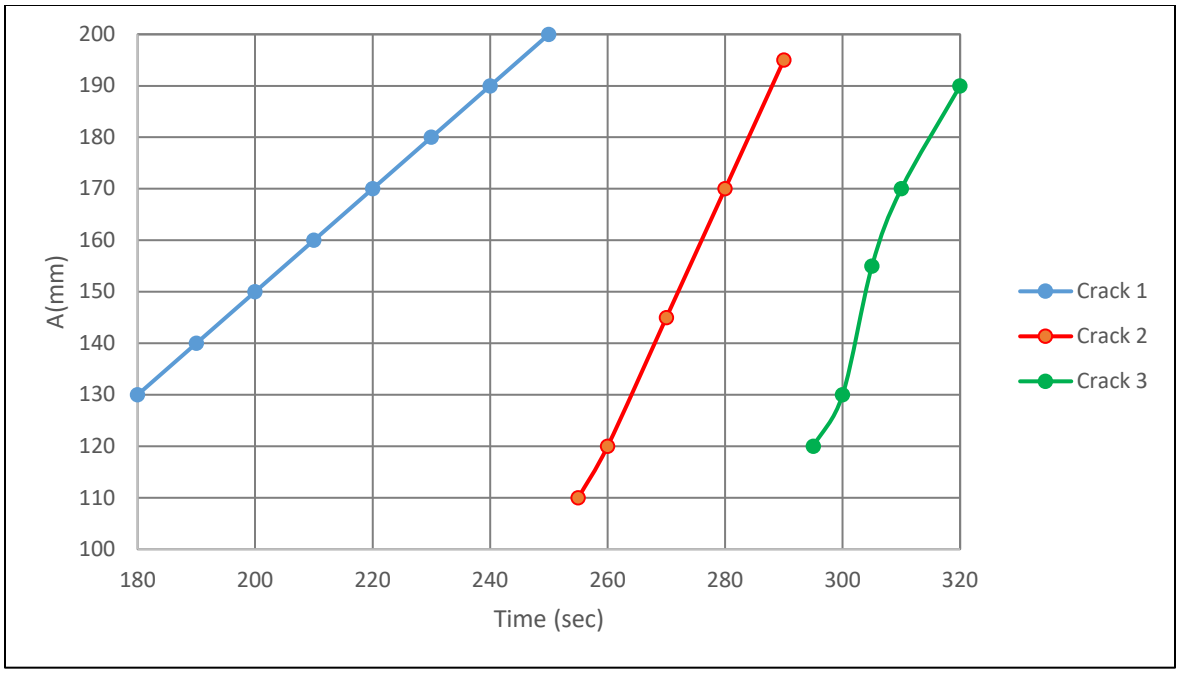

Figure 36. Cracks Length A (mm) with Time (sec) for Sample 1

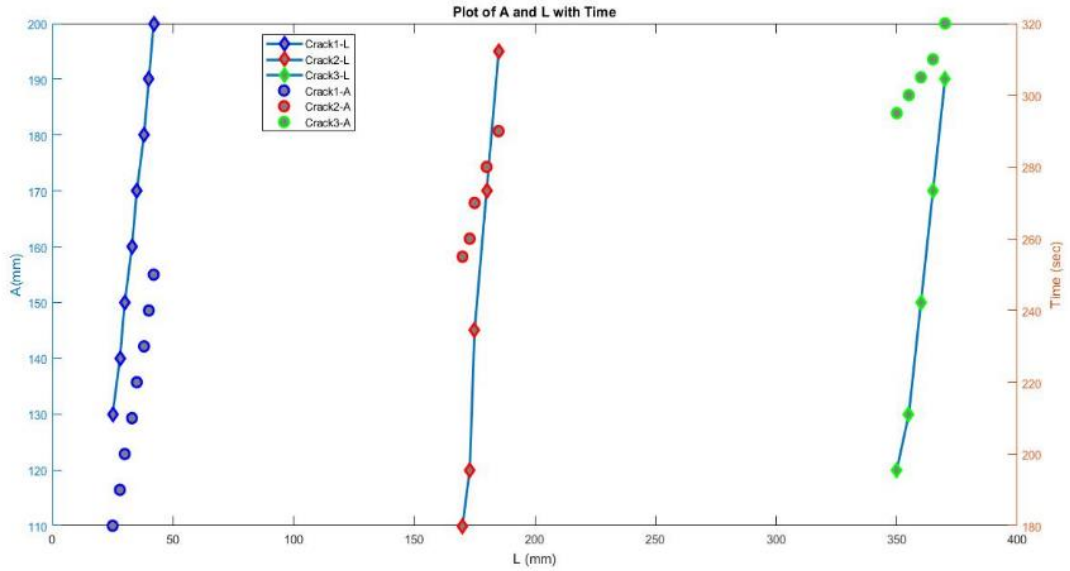

Figure 37. Detected Cracks (A) and Locations (L) with Time for Sample 1

4.3.2. Experimental Results for RC Sample 2

For sample 2, Figure 38 illustrates the photo of Sample 2 with sensors installed at the desired locations. Figures 39 (a~ d) illustrate the measured strains from the strain gauges of Sample

2 during the four-point loading tests. Figure 40 shows the crack pattern after tests. Table 10 summarized the detected cracks from the four strain gauges using the developed algorithm in this study for Sample 2 with Figure 41 comparing the detected cracks with the measured cracks using ruler. Figure 42 shows the cracks length (A) changing with time and Figure 43 illustrates the length of the cracks (A) and locations (L) changing with time for Sample 2. For Sample 2, the sensor network detected locations and length for three main vertical cracks in the meddle (critical zone). From Table 10 and Figures 41~43, it can be seen that the average difference between the crack pattern detected using the sensors on the bottom of the concrete beam and the actual crack pattern for all three cracks for locations is 23.6 % and for crack length is 27 %.

Figure 38. Photo of the Sensor Layout on Sample 2

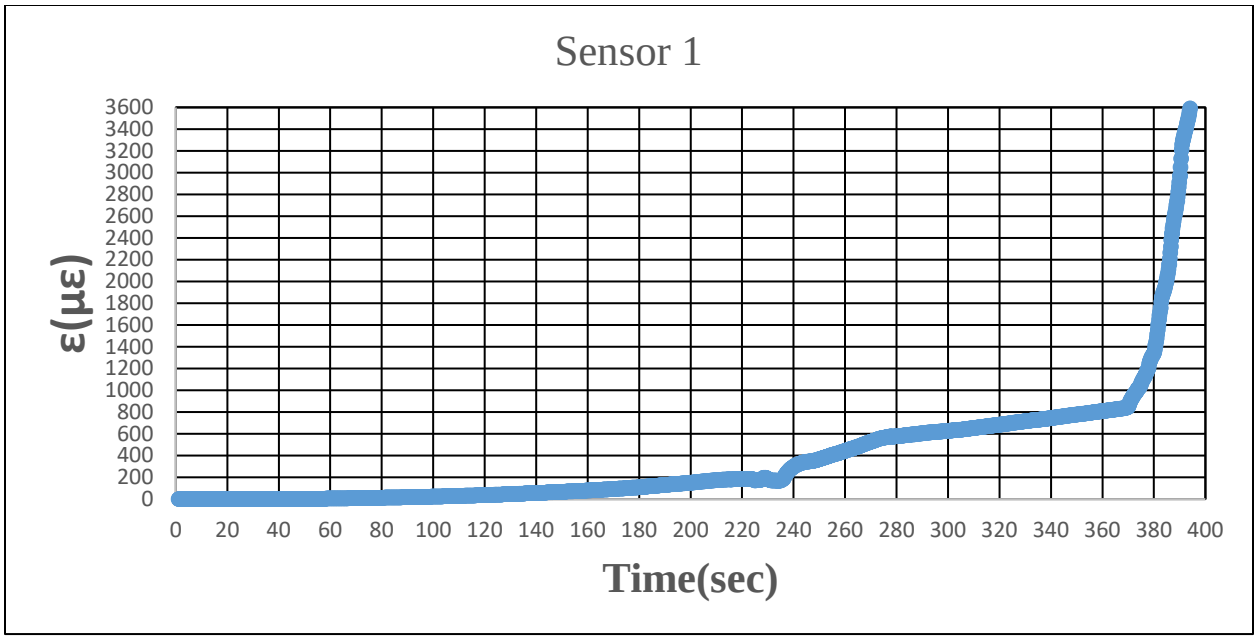

(a) Strain (με) at Sensor 1 Vs. Time (Sec)

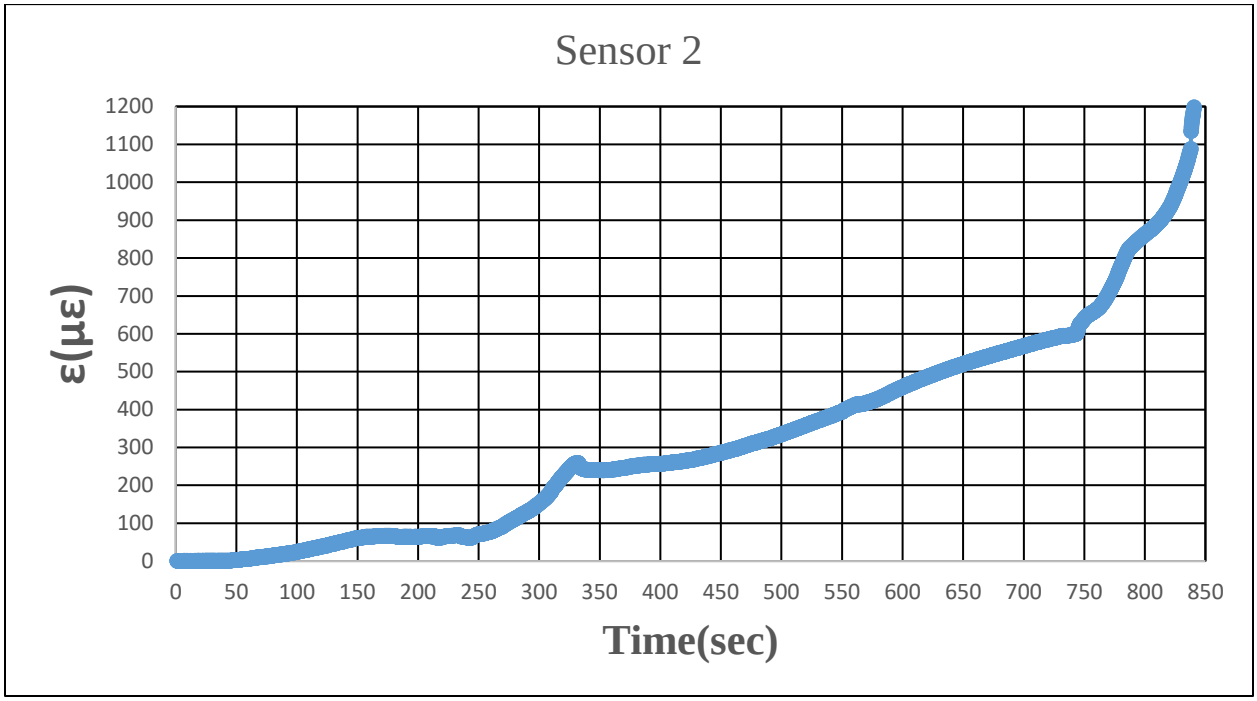

(b) Strain (με) at Sensor 1 Vs. Time (Sec)

Figure 39. Measured Strains from the Sensor 1 (a), Sensor 2 (b) Sensor 3 (c) and Sensor 4 (d) of Sample 2

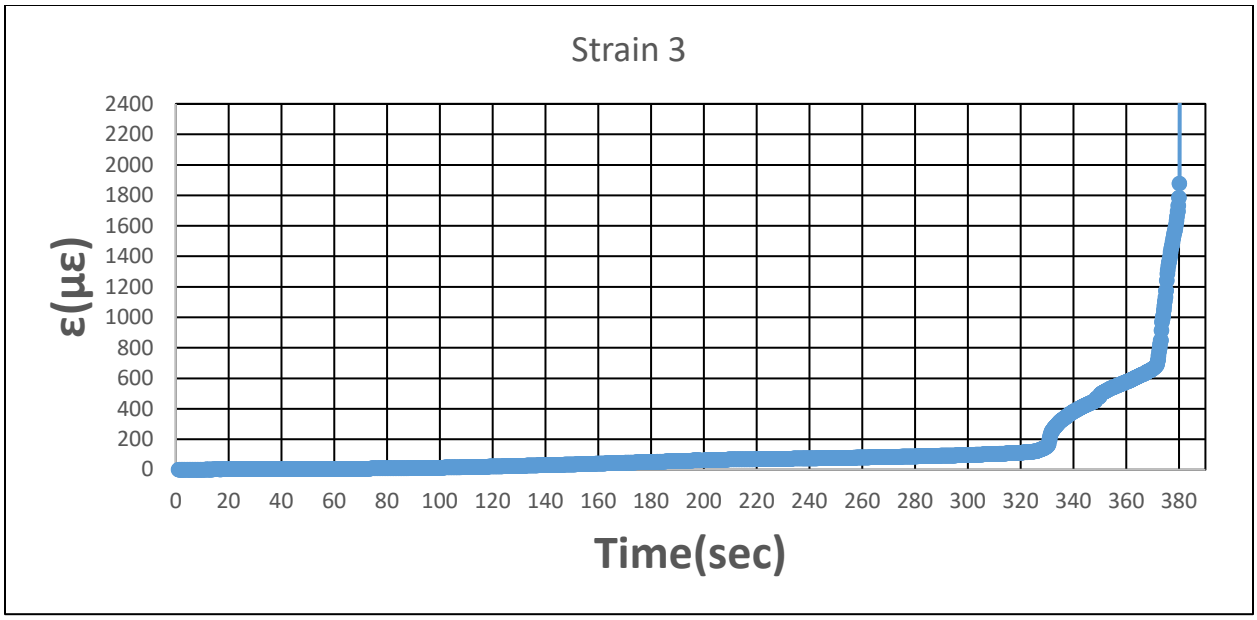

(c) Strain (με) at Sensor 1 Vs. Time (Sec)

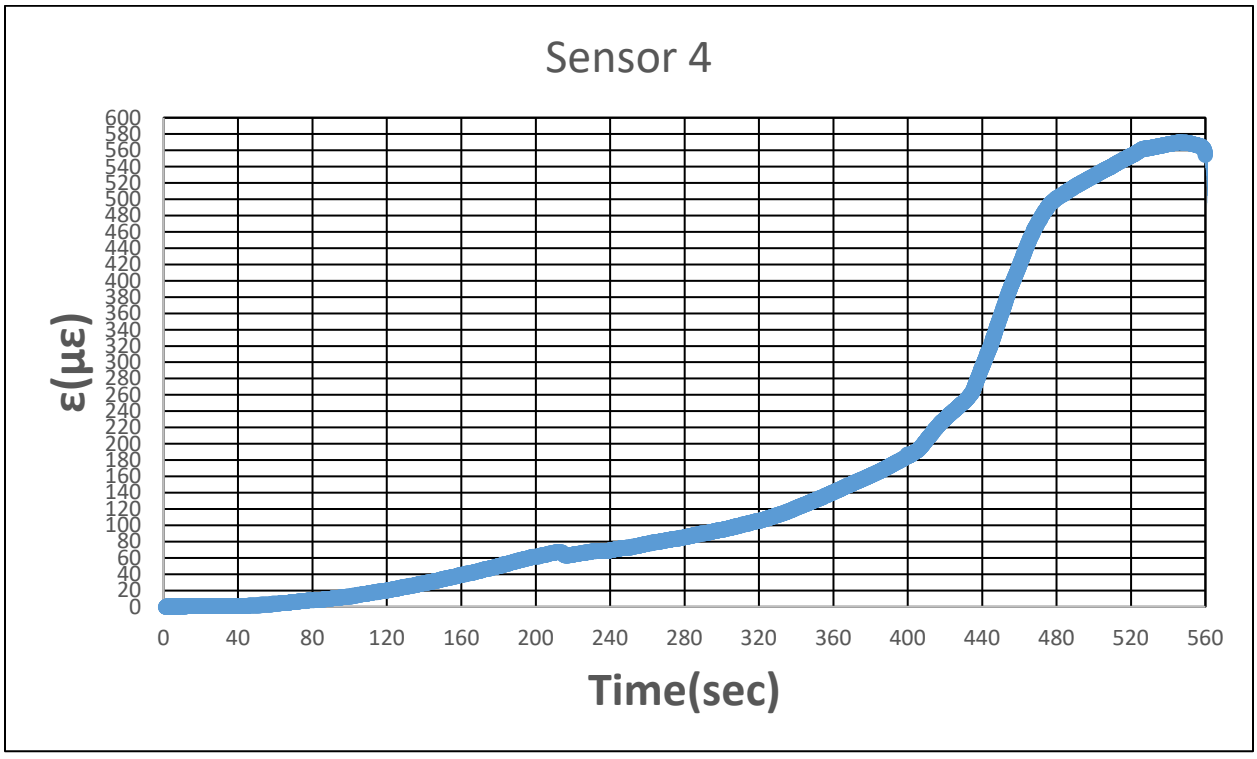

(d) Strain (με) at Sensor 1 Vs. Time (Sec)

Figure 39. Measured Strains from the Sensor 1 (a), Sensor 2 (b) Sensor 3 (c) and Sensor 4 (d) of Sample 2 (continued)

Figure 40. Cracks for Sample 2 after the Test

Table 11. Results Obtained from Sensors Detected for Sample 2.

	Crack 1		Crack 2		Crack 3	
	Location from sensor 1 (mm)	Direction (Φ°)	Location from sensor 1 (mm)	Direction (Φ°)	Location from sensor 1 (mm)	Direction (Φ°)
Initial	**121**		**190**		**290**	
	122.5	5.7	193	36.8	292.5	30
	125	8.6	195	23.6	295	30
	127	14.5	198	36.8	297	23.6
	129.5	14.5	200	11.5	300	36.8
	132	14.5	203	11.5	303	23.5
	134	14.5	205	11.5	305	23.5
	137	11.5	208	17.5	307	36.8
			210	11.5	310	30
					313	30
Final		**150**		**140**		**130**

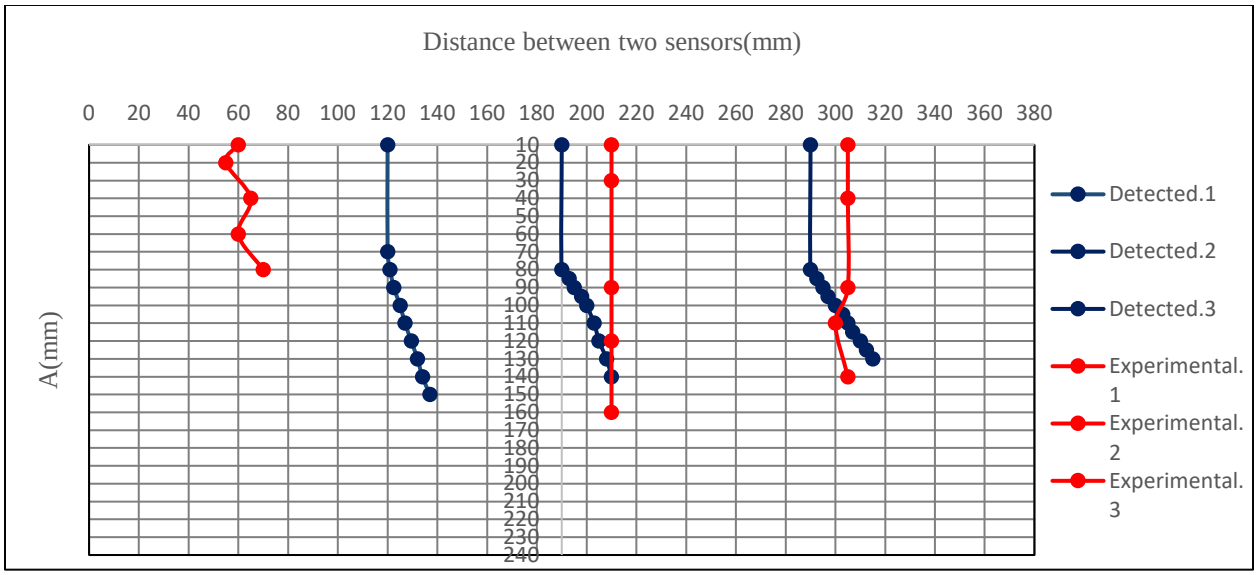

Figure 41. Comparison of Detected Cracks Compared with Reference Cracks for Sample 2

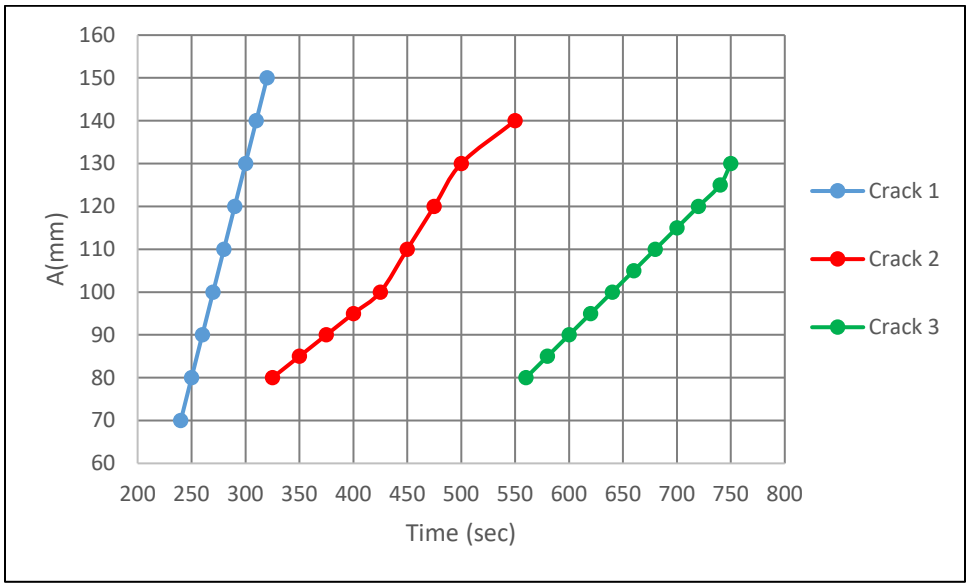

Figure 42. Cracks Length a (mm) with Time (sec) for Sample 2

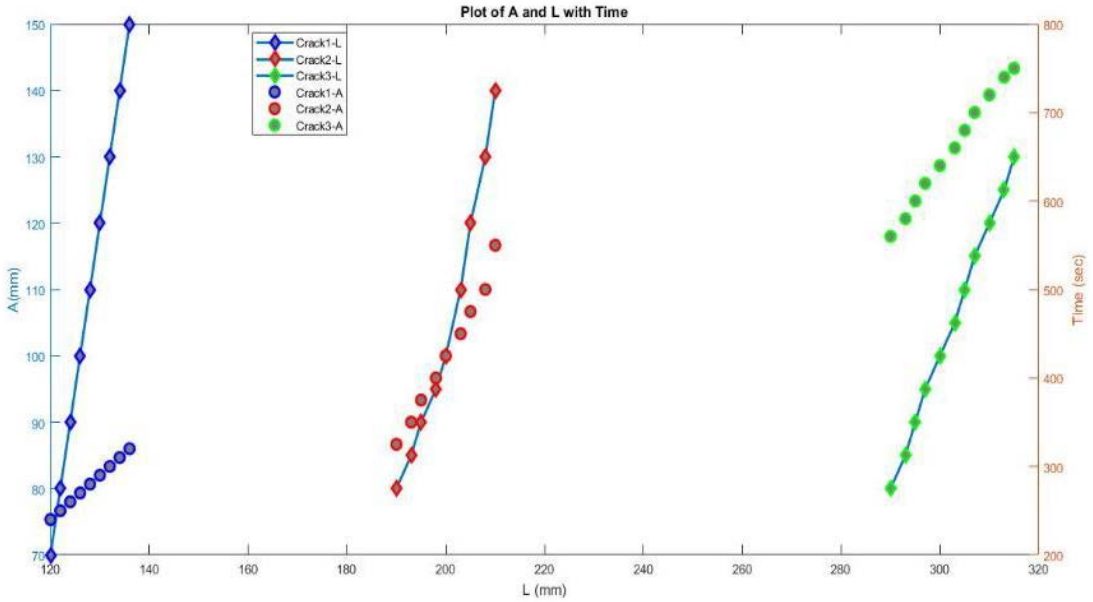

Figure 43. Detected Cracks (a) and Locations (L) with Time for Sample 2

4.3.3. Experimental Results for RC Sample 3

For sample 3, Figure 44 illustrates the photo of the tested Sample 3 with sensors installed at the desired locations. Figures 45 (a~d) show the measured strains from the strain gauges of Sample 3 during the four-point loading tests. Figure 46 shows the crack pattern after tests for Sample 3. Table 11 summarized the detected cracks from the four strain gauges using the developed algorithm in this study for Sample 3 For Sample 3, it had two main cracks ($a_1 > a_2$). The first crack happened at 120sec between sensors 1 and 2. Based on Equations (13, 15, and 16) and with the measured strains from Sensor 1 and 2 for detection initial crack location after that crack. The second crack happened at 180 sec between sensor 1 and sensor 3 using equations (17,18, and 21) for detection initial crack location after that crack. The cracks location and cracks propagation (crack depth) on the front surface of the specimen can be estimated as shown in Figure 47 for comparison of detected cracks compared with reference cracks. Figure 48 shows the cracks length (A) changing with time and Figure 49 illustrates the length of the cracks (A) and locations (L)

changing with time for Sample 2. For sample 3, the sensors detected locations and length for two main vertical cracks in the meddle (critical zone). From Table 11 and Figures 47~49, it can be seen that the average variance between the crack pattern detected using the sensors on the bottom of the concrete beam and the actual crack pattern for all two cracks for locations is 25 %, and for crack lengths is 35 %.

Figure 44. Photo of the Sensor Layout on Sample 3

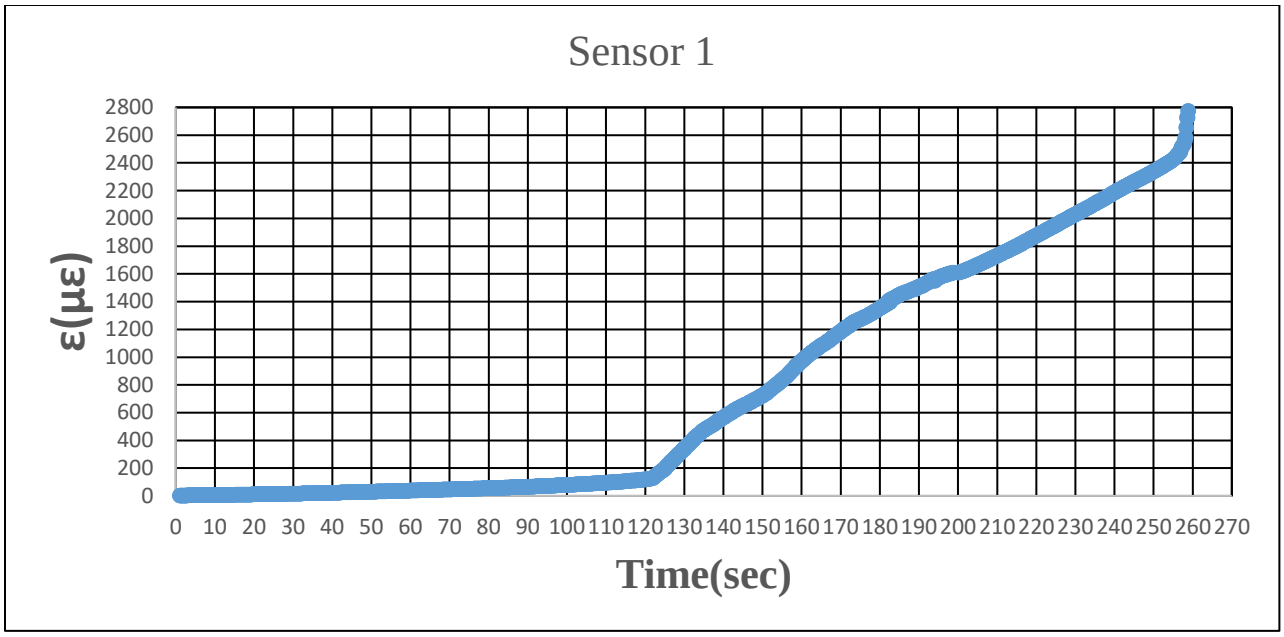

(a) Strain (με) at Sensor 1 Vs. Time (Sec)

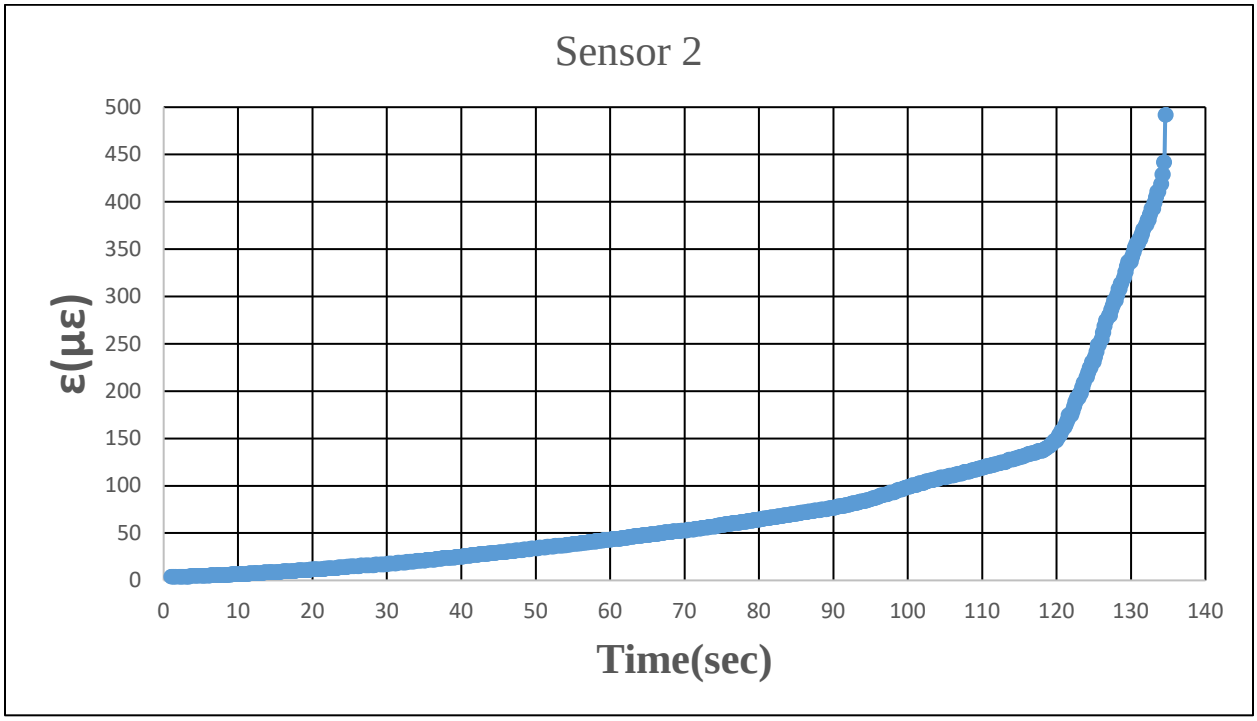

(b) Strain (με) at Sensor 1 Vs. Time (Sec)

Figure 45. Measured Strains from the Sensor 1 (a), Sensor 2 (b) Sensor 3 (c) and Sensor 4 (d) of Sample 3

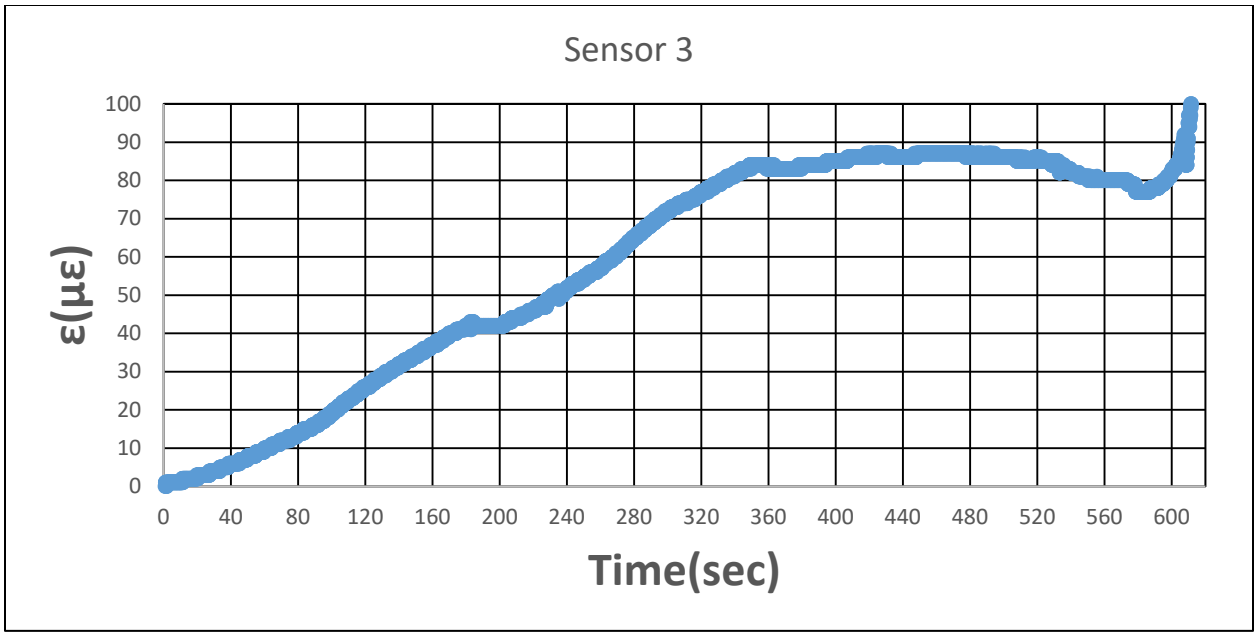

(c) Strain (με) at Sensor 1 Vs. Time (Sec)

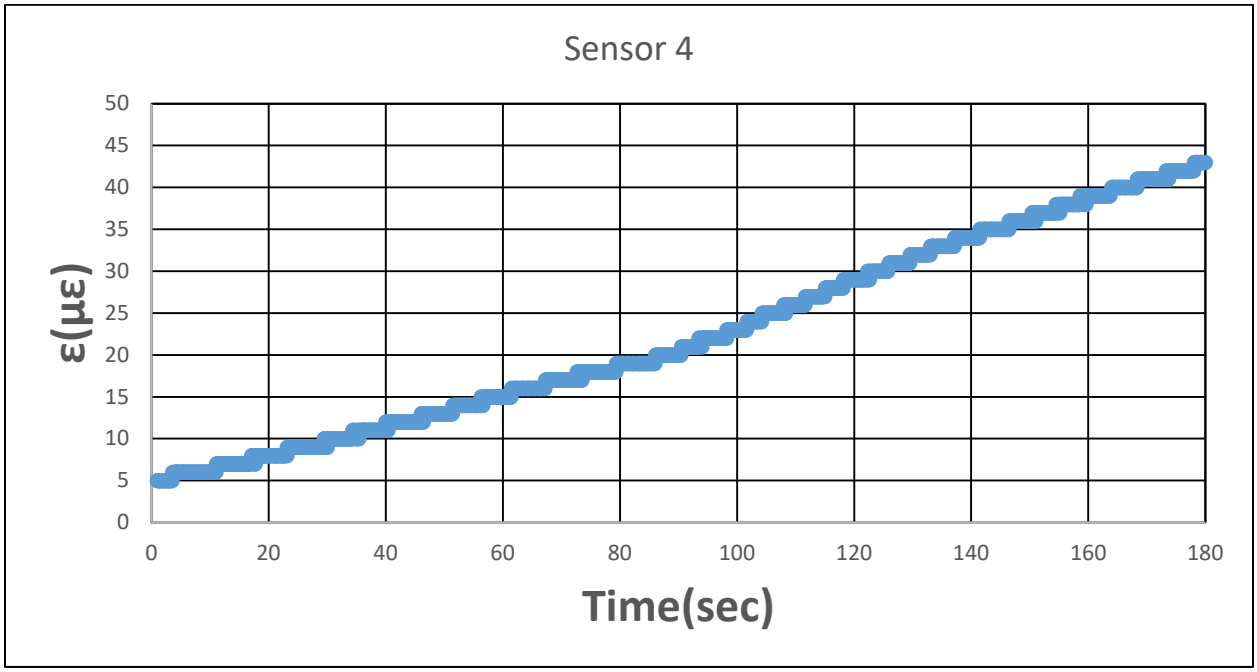

(d) Strain (με) at Sensor 1 Vs. Time (Sec)

Figure 45. Measured Strains from the Sensor 1 (a), Sensor 2 (b) Sensor 3 (c) and Sensor 4 (d) of Sample 3 (continued)

Figure 46. Cracks for Sample 3 after the Test

Table 12. Results Obtained from Sensors Detected for Sample 3.

	Crack 1		Crack 2	
	Location from sensor 1 (mm)	Direction (Φ°)	Location from sensor 1 (mm)	Direction (Φ°)
Initial	**120**		**320**	
	122	11.5	322	11.5
	124	23.5	324	23.5
	127	36.8	326.5	30
	130	36.8	329.5	30
	135	30	332	36
Final		**100**		**90**

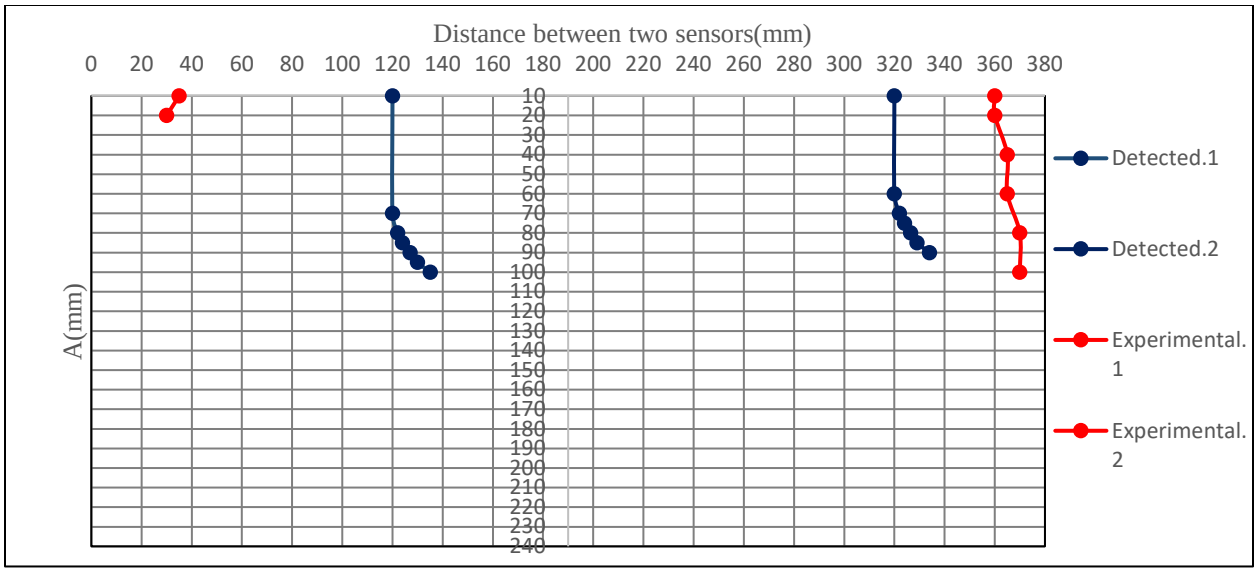

Figure 47. Comparison of Detected Cracks Compared with Reference Cracks for Sample 3

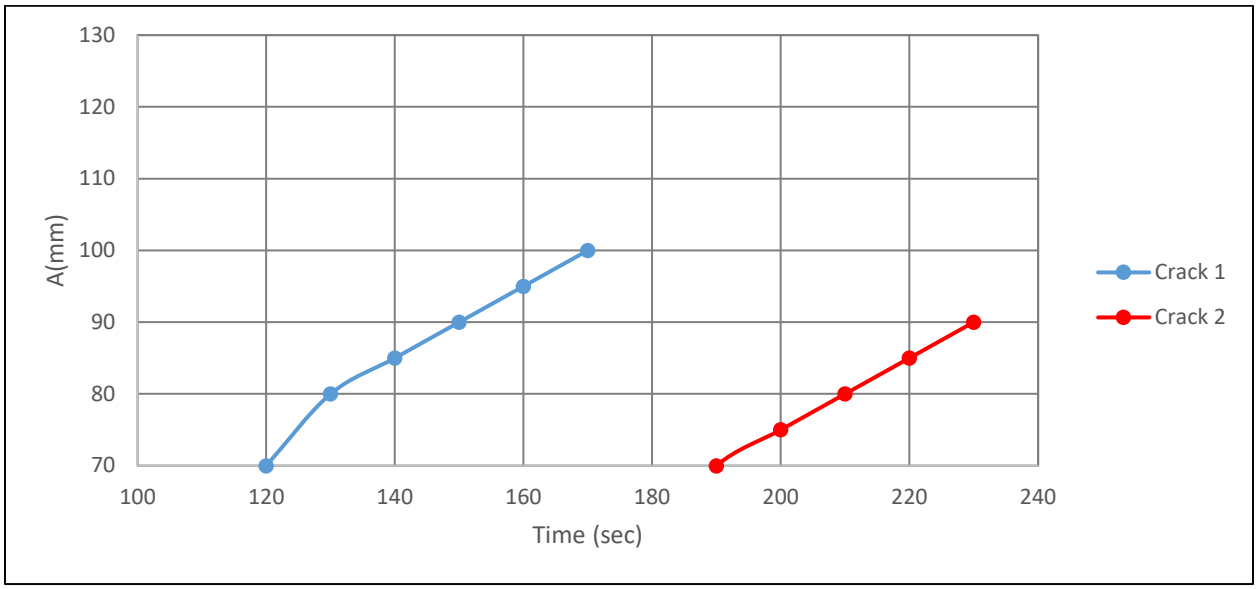

Figure 48. Cracks Length a (mm) with Time (sec)

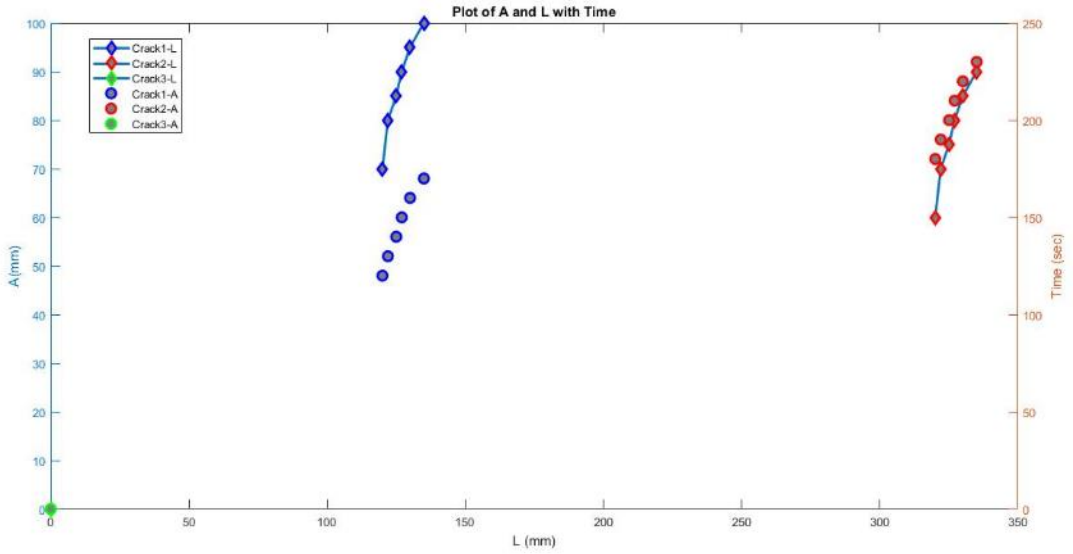

Figure 49. Detected Cracks (A) and Locations(L) with Time for Sample 3

4.4. Behavior Difference between Reinforced and Unreinforced Concrete

Steady state for plastic and fracture process zone (FPZ) extent and morphology is considered an essential principle to understand and predict crack growth in materials. In ductile materials such as metals, the characteristics of the plastic zones vary with thicknesses, texture, and configurations near the crack tip. The FPZ zone progress can be used to quantify the fracture toughness of the material and the conditions for and stability of crack growth. Also, ductile material progresses through three stages, including an initiation stage (I) that is followed by a transition (II) to steady-state crack growth (III) [89]. Moreover, when the maximum crack driving force that may be formed in the structure is equivalent to the material fracture toughness, there is enough energy to drive crack propagation and reach a relatively long distance. One kind of special situation for rapid crack propagation is that the crack grows at a constant speed.

4.4.1. FPZ Progress of Reinforced Concrete

For reinforced concrete, figure 50 illustrates the nominal stress σ, as a function of normalized crack length for the tested RC Sample 1 in Section 4.3.1. It can be seen that reflecting

the three phases of FPZ progress, the crack length with normal stress curve has three crack progress stages including initiation, transition, and steady-state crack as a function of hardening. The hardening phenomenon proceeded by the transition stage, and it was a result of the presence of the reinforcement that causes a further increase in cracking resistance. It is worth mentioning that the bond between concrete and steel bars may influence the stress intensity in the vicinity of reinforcement by slowing down the whole process of the crack formation area.

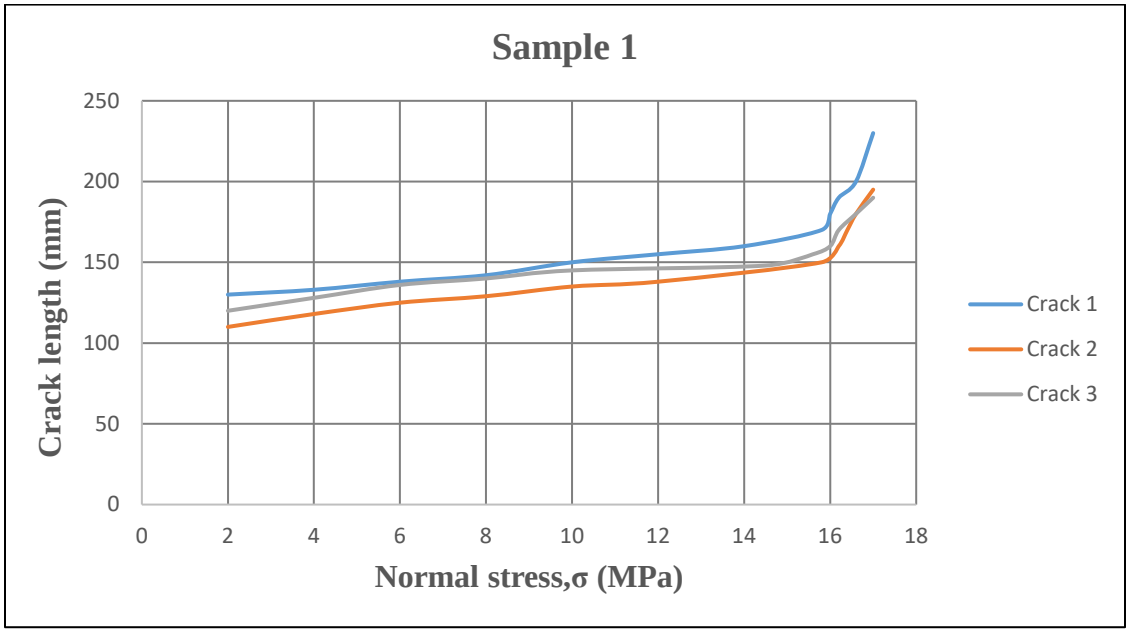

Figure 50. The Nominal Stress σ, VS a Function of Normalized Crack Length for Reinforced Concrete

Figure 51 shows the estimated fracture zone and stress for the development of fracture zone and stress distribution ahead of the initial crack-tip for RC Sample 1 using a/D as longitudinal axis, in which a is the crack length and D is the specimen depth following Reference [90,91]. Figure 52 and 53 illustrate the relation between the stress intensity factor (K) and crack length (a), also, with time in RC Sample 1 for each crack. For RC beams, if crack width is needed, Figure 54 shows the relation between cracks length and cracks width for the crack 1 of RC Sample 1, indicating that

the crack width may be able to be relate to the length of the cracks since an approximate linear relation may occur.

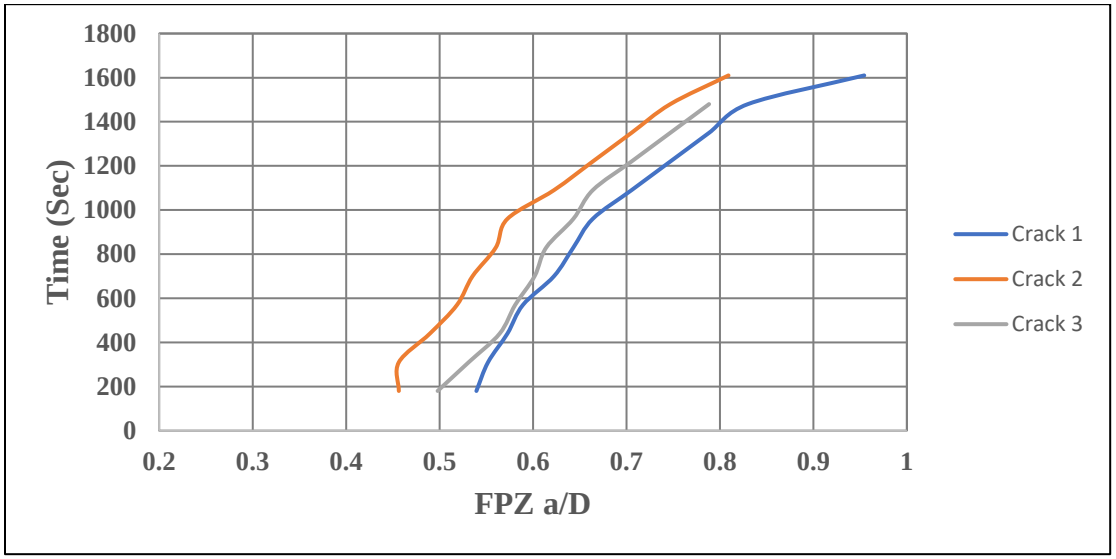

Figure 51. FPZ vs Time (Sec)

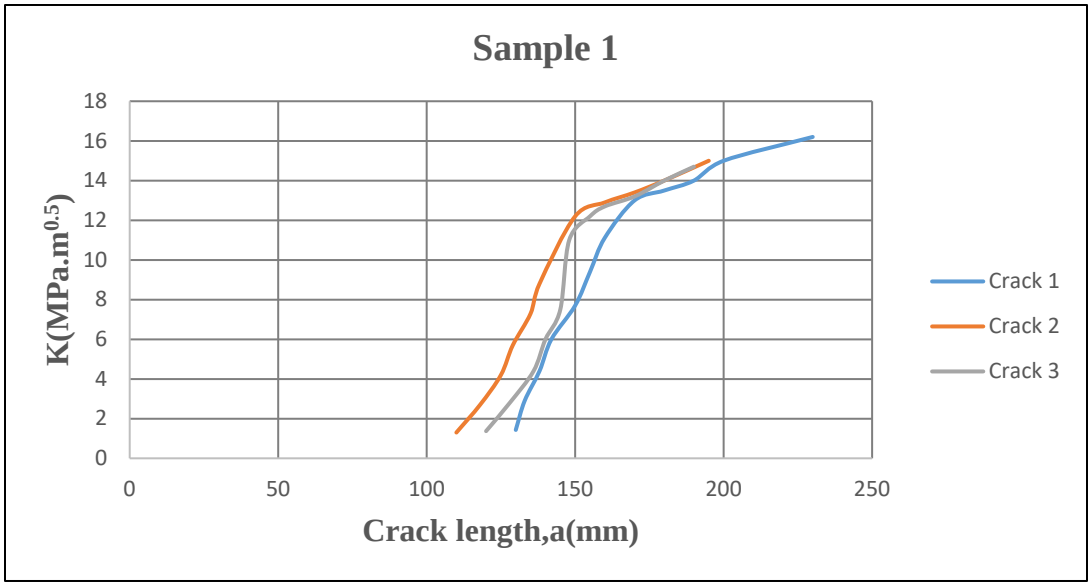

Figure 52. Stress Intensity Factor (K) VS Crack Length for Sample 1

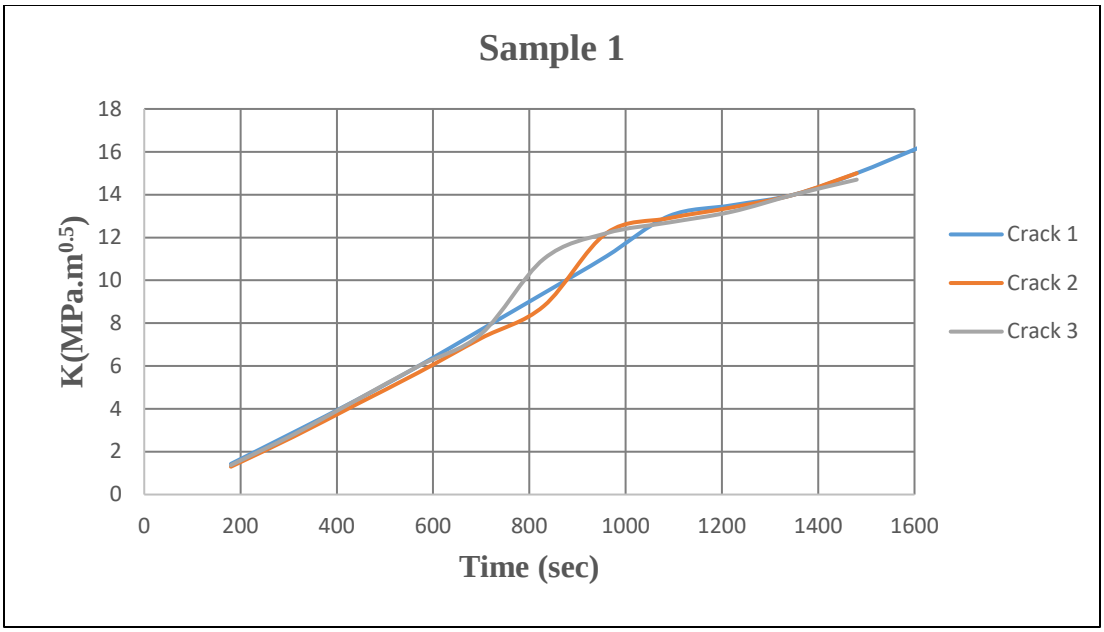

Figure 53. Stress Intensity Factor (K) VS Time for Sample 1

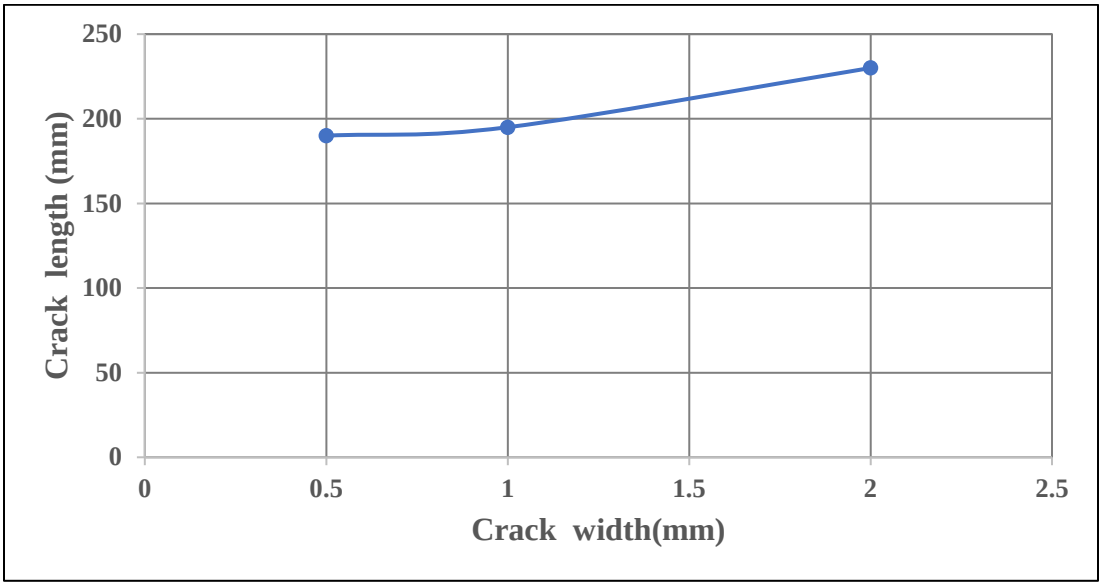

Figure 54. Crack Length vs Crack width

4.4.2. FPZ Progress of Unreinforced Concrete

For unreinforced concrete, Figures 55 (a~c) show the mechanism of crack formation of the three tested concrete beams without reinforcement (without notches) in Chapter 3. The crack length with normal stress curve has the same crack progress for all three stages through initiation,

transition, and steady-state crack as a function of the applied loads. When the normal stress reaches the peak, the failure occurred and the curve exhibit softening passing the localized crack tip zone (initiation stage), as well as descends sharply to reach zero value.

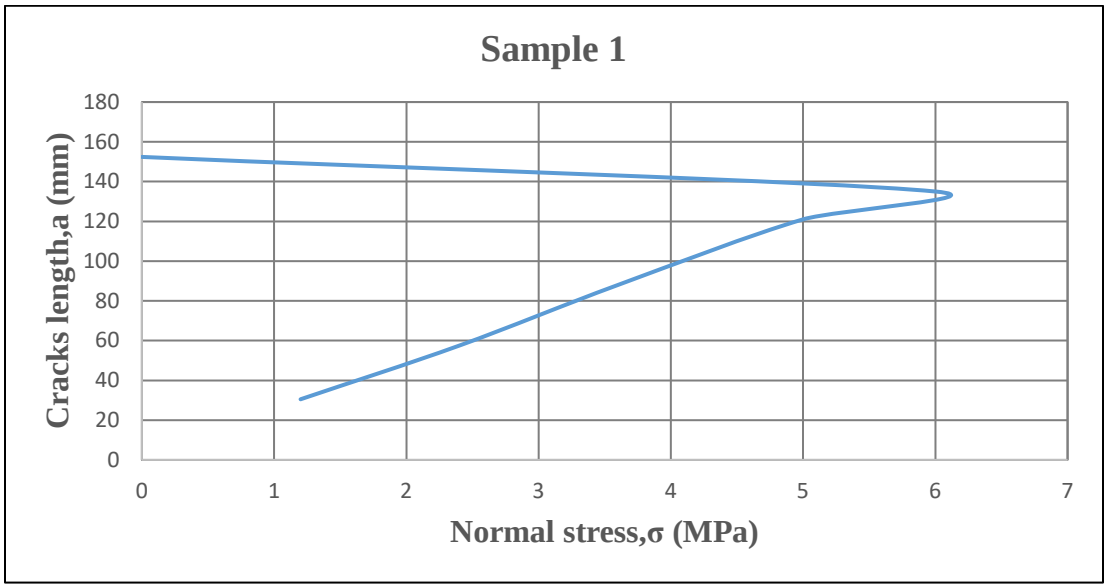

(a) The nominal stress σ, VS a function of normalized crack length for sample 1

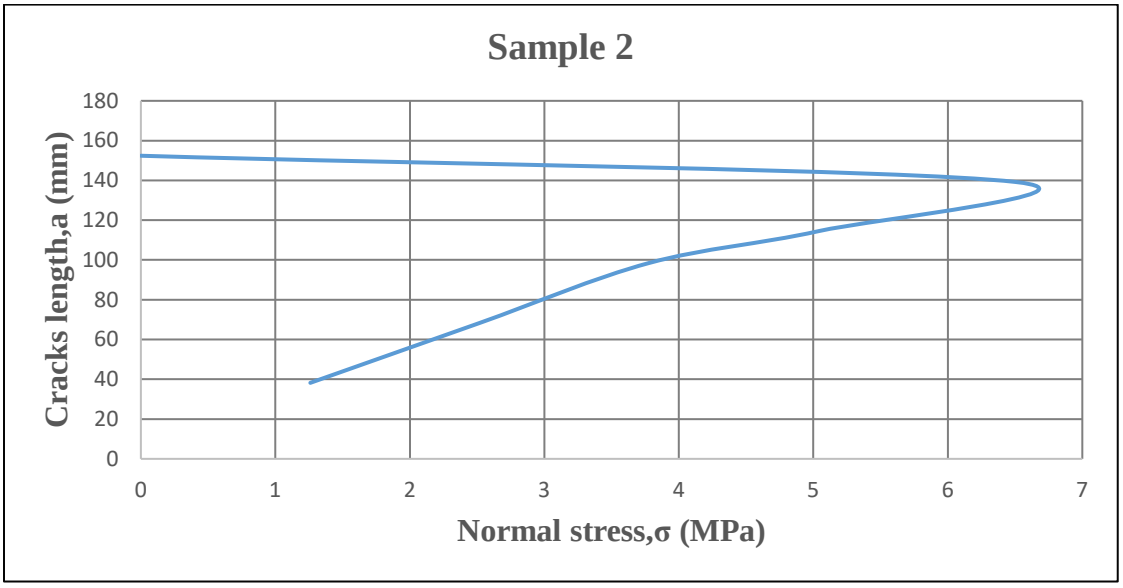

(b) The nominal stress σ, VS a function of normalized crack length for sample 2

Figure 55. The Nominal Stress σ, VS a Function of Normalized Crack Length for Samples in Unreinforced Concrete

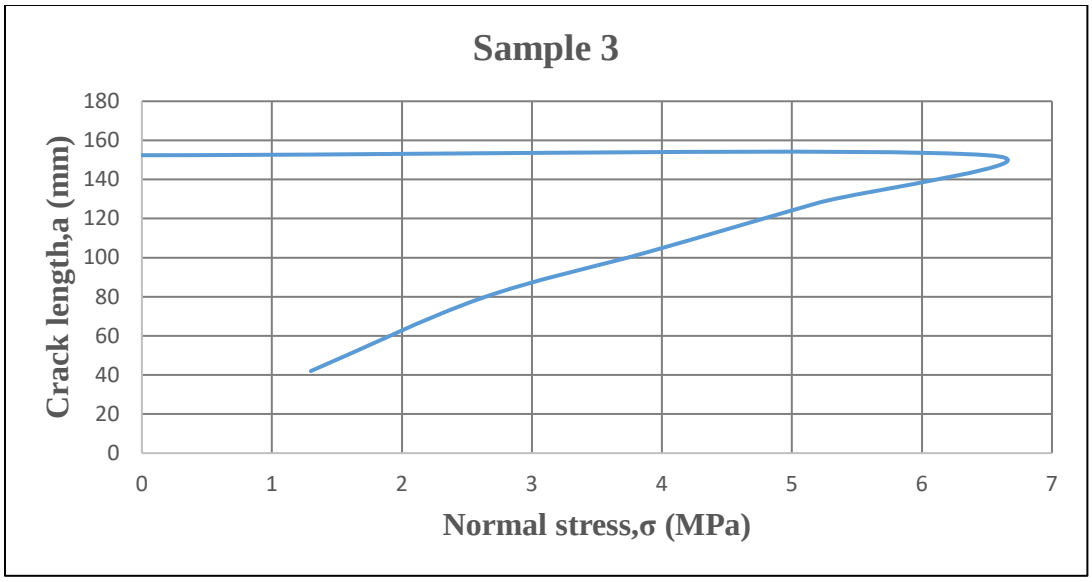

(c) The nominal stress σ, VS a function of normalized crack length for sample 3

Figure 55. The Nominal Stress σ, VS a Function of Normalized Crack Length for Samples in Unreinforced Concrete (continued)

For unreinforced concrete, it is assumed that the material property of the concrete is linear and isotropic material, and the fracture is very small. Figures 56 (a~c) illustrate the relation between the stress intensity factor (K) and crack length (a), also, with time for each unreinforced beam samples tested in Chapter 3. Figures 57 (a~c) show the relation between the stress intensity factor (K) and time (t) for those samples. Approximately linear behavior was noticed for all the three unreinforced beams between the stress intensity and the crack length, indicating no significant FPZ was formed in the unreinforced concrete beams during tests.

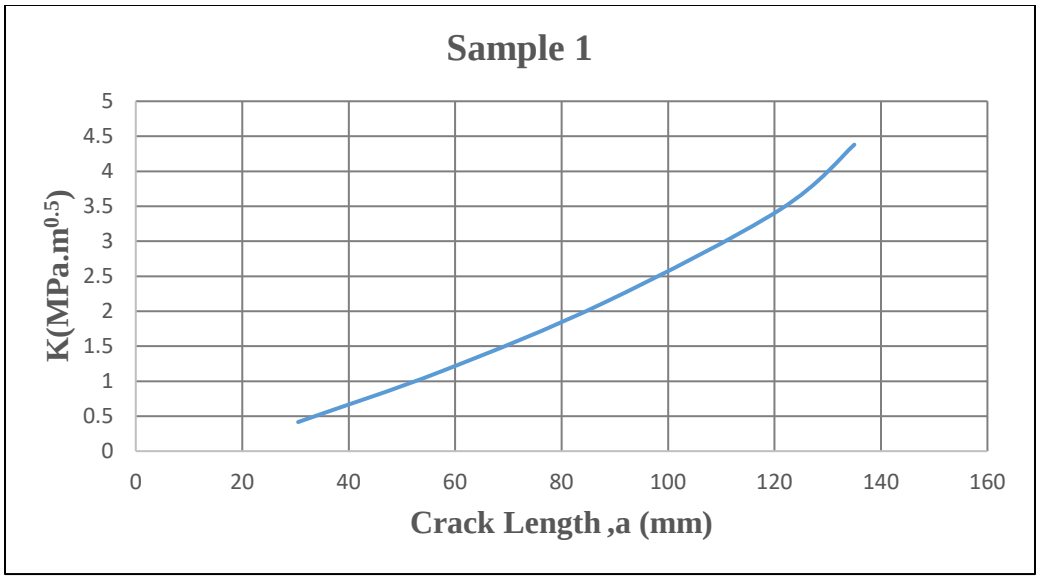

(a) Stress Intensity Factor (K) VS Crack Length for Sample 1

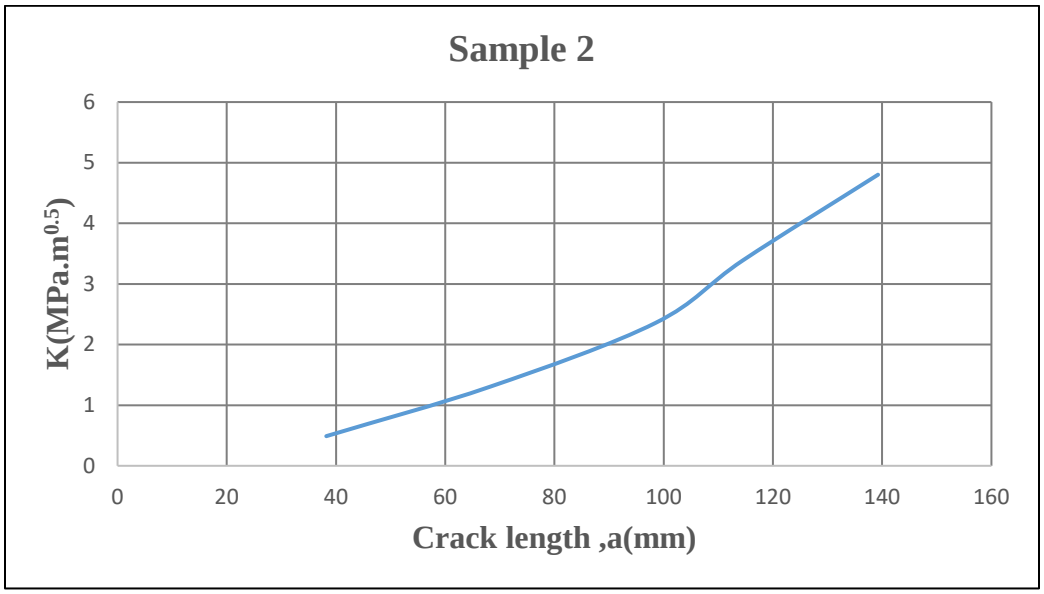

(b) Stress Intensity Factor (K) VS Crack Length for Sample 2

Figure 56. Stress Intensity Factor (K) VS Crack Length for Three Tested Unreinforced Concrete Beams

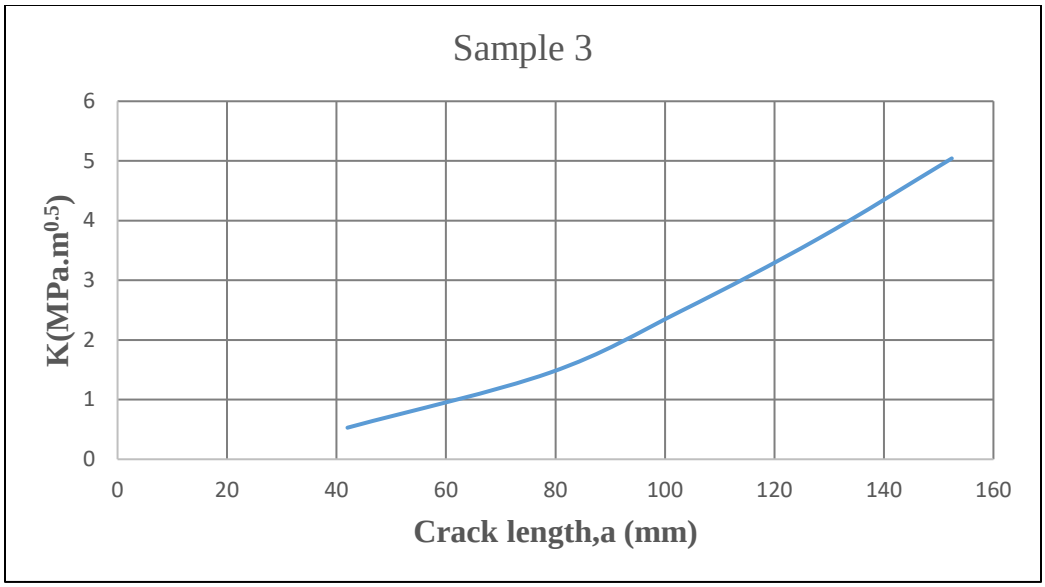

(c) Stress Intensity Factor (K) VS Crack Length for Sample 3

Figure 56. Stress Intensity Factor (K) VS Crack Length for Three Tested Unreinforced Concrete Beams (continued)

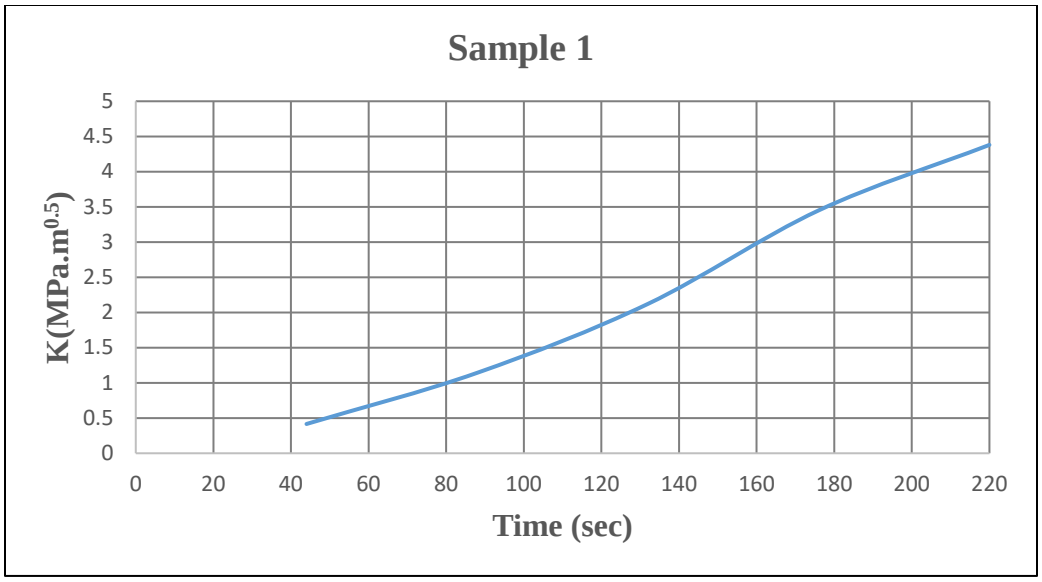

(a) Stress Intensity Factor (K) VS Time for Sample 1

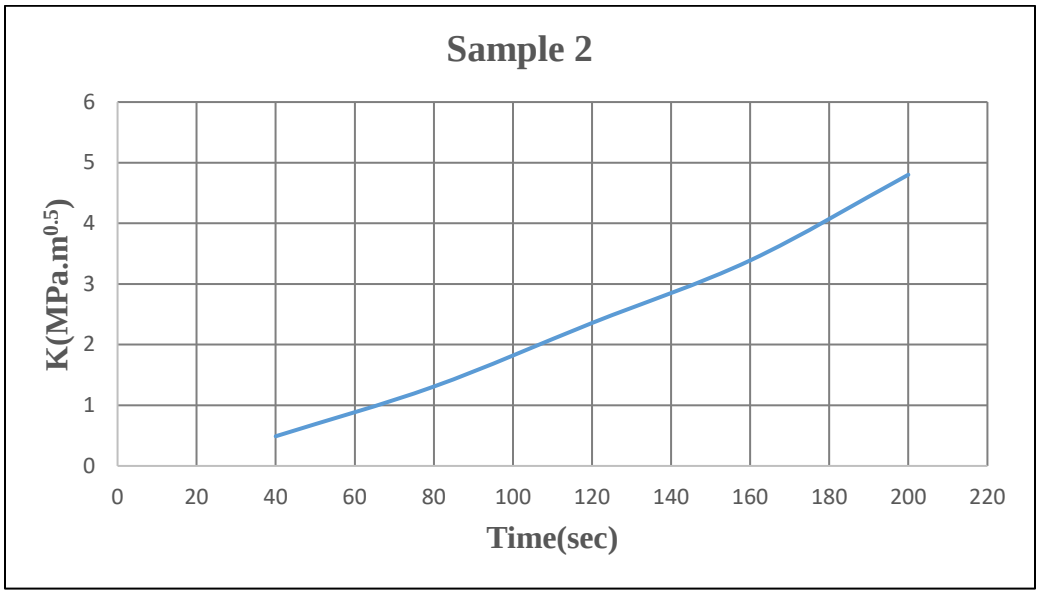

(b) Stress Intensity Factor (K) VS Time for Sample 2

Figure 57. Stress Intensity Factor (K) VS Time for Sample 3

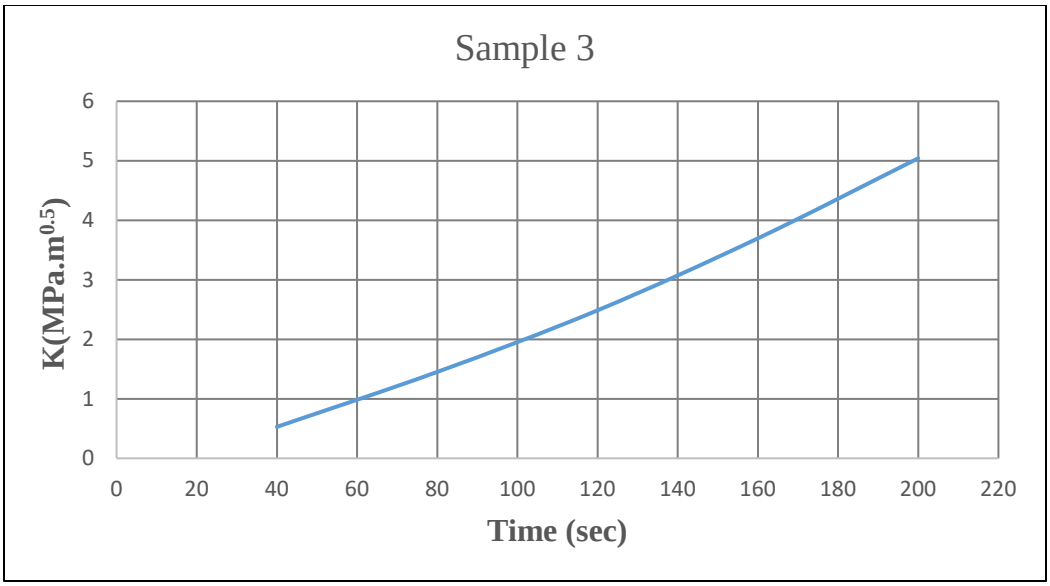

(c) Stress Intensity Factor (K) VS Time for Sample 3

Figure 57. Stress Intensity Factor (K) VS Time for Sample 3 (continued)

The different behavior between reinforced concrete and unreinforced concrete from the tested concrete beams shows that the unreinforced concrete had a brittle failure during the experiment. While the reinforced concrete showed different failure processes presented by higher cracking resistance. The failure crack (flexural crack) did not propagate in the tested reinforced concrete beams as rapidly as in unreinforced concrete beams, and the destructive process in reinforced concrete beams continued progressively even after developing two or three cracks [91]. The difference in failure process connected with developing of flexural cracks in unreinforced and reinforced concrete beams can be noticed remarkably when comparing the normal stress–crack length curves obtained during the experiment when comparing Figures 50 and 55 (c). The significantly slower crack formation after the initiation stage in reinforced concrete beams resulted in almost 62% times higher normal stress compared to the results measured in unreinforced concrete beams.

4.5. Summary

This chapter presented the experimental study for multiple cracks detection. Experimental results showed that the developed algorithm can detect multiple cracks for their locations and length with average measurement accuracy of 79.33% for the three RC samples tested. In addition, the comparsion of detected behaviors between reinforced and unreinforced concrete beams showed that cracks in reinforced concrete would form a significant FPZ but in unreinforced concrete, the FPZ was very small.

CHAPTER 5. CONCLUSIONS AND FUTURE WORK

5.1. Conclusions

In this study, algorithms to detect internal cracks in concrete using minimum numbers of point strain sensors were developed based on the stress intensity principal for both single crack and multiple cracks. Based on this study, following conclusions can be made:

1) The developed algorithms are expected to be able to detect either single of multiple cracks (at least two) in concrete using only a few point sensors at designed locations;
2) Experimental results showed for unreinforced concrete beams with prefabricated notches to control the crack locations, the use of two point strain sensors with the developed algorithm can detect the crack length propagation of a single crack at an average measurement accuracy of 88.85%;
3) For unreinforced concrete beams without prefabricated notches, the use of two point strain sensors with the developed algorithm can simultaneously detect the crack location and crack length propagation of a single crack at an average measurement accuracy of 82.40%;
4) For reinforced concrete beams, four point strain sensors with the developed crack detection algorithm can simultaneously detect the crack locations and lengths propagation of cracks up to three at an average measurement accuracy of 79.3%.

Through the developed crack detection networks from this study, the detected internal crack layout can assist an appropriate future concrete structural maintenance or repair. Besides, these crack layouts can help determine the reduced long-term durability performance and properties for concrete which can be used to improve the future for design procedures with consideration on damages. More importantly, the developed monitoring system can also be

extended to apply in civil infrastructure with areas having limited accessibility, such as bridges, nuclear reactors, historical buildings, tunnels, powerplants, and dams. The capability of detecting hidden cracks in these concrete structures with low cost is also with high demand and significance. Moreover, since only point sensors are needed in the developed scenarios, the cost of the monitoring system is minimized and will be affordable for most concrete structures.

5.2. Limitations and Future work

The limitations of this work include:

1) The current work only considered two dimensions of the crack detection, however, in the real world, most of the cracks are in three dimensions;
2) The concrete properties used in this study was assumed to be linear and elastic material with no plasticity considered;
3) The sizes of the measurement samples were fixed and the size effect was ignored in this study;
4) The reinforcement may change the detection algorithm since the strain and stress distribution in reinforced concrete is significantly different when compared to unreinforced concrete as shown in Chapter 4, however, in the developed algorithm, reinforcement was not considered, which may yield significant measurement errors as indicated in Chapter 4.

With all the limitations mentioned above, in the future, more research work is needed to improve the measurement accuracy of the developed algorithm with considerations of three dimensions, plasticity in materials, sizes, and reinforcements in the concrete. In addition, potential field tests are also demanded in near future before any furthrt application of the crack detection in real world.

5.3. Publications

1- Alshandah, Mohanad, Ying Huang, Zhili Gao, and Pan Lu. “Internal crack detection in concrete pavement using discrete strain sensors.” *Journal of Civil Structural Health Monitoring* (2020): 1-12.

2- Alshandah, Mohanad, Ying Huang, Pan Lu, and Denver Tolliver. “Bottom-up crack detection in concrete pavements using in-pavement strain sensors.” In *Sensors and Smart Structures Technologies for Civil, Mechanical, and Aerospace Systems 2018*, vol. 10598, p. 105982I. International Society for Optics and Photonics, 2018.

3- Alshandah, Mohanad, Ying Huang, Jerry Gao, Pan Lu, and Denver Tolliver. “Experimental crack detection in concrete pavement using point strain sensors.” In *Sensors and Smart Structures Technologies for Civil, Mechanical, and Aerospace Systems 2019*, vol. 10970, p. 1097023. International Society for Optics and Photonics, 2019.

4- Detecting Cracks in Concrete Pavement Using Strain Sensor (Poster in ND EPSCoR 2018)

REFERENCES

[1] Mehta, Povindar Kumar. "Concrete. Structure, properties and materials." (1986).

[2] Setareh, Mehdi, and Robert Darvas. *Concrete structures*. Pearson/Prentice Hall, 2007

[3] Tang, Sheng Wen, Yan Yao, Carmen Andrade, and Z. J. Li. "Recent durability studies on concrete structure." *Cement and Concrete Research* 78 (2015): 143-154.

[4] Zhang, Jing-Kui, Weizhong Yan, and De-Mi Cui. "Concrete condition assessment using impact-echo method and extreme learning machines." *Sensors* 16, no. 4 (2016): 447.

[5] Broomfield, John P. Corrosion of steel in concrete: understanding, investigation and repair. CRC Press, 2003.

[6] Merritt, David K., B. Frank McCullough, and Ned Hamilton Burns. Construction and preliminary monitoring of the Georgetown, Texas precast prestressed concrete pavement. Center for Transportation Research, the University of Texas at Austin, 2001.

[7] Jamieson, N. J., and P. D. Cenek. "Effect of Pavement Construction on the Fuel Consumption of Trucks." In Proceedings of the Options for Post Millenium Pavements Symposium, Wairekei Resort, Taupo, New Zealand, pp. 17-19. 1999.

[8] Young, Steven B., Shannon Turnbull, and Andrea Russell. “Substudy 6: What LCA Can Tell Us about the Cement Industry.” (2002).

[9] Athena, I. “A Life Cycle Perspective on Concrete and Asphalt Roadways: Embodied Primary Energy and Global Warming Potential.” *Cement Association of Ottawa: Ottawa, ON, Canada* (2006).

[10] Kosmatka, Steven H., Beatrix Kerkhoff, and William C. Panarese. *Design and control of concrete mixtures*. Vol. 5420. Skokie, IL: Portland Cement Association, 2002.

[11] Hein, David, Shreenath Rao, Shiraz D. Tayabji, and Hyung Lee. Bases and Subbases for Concrete Pavements:[techbrief]. No. FHWA-HIF-16-005. United States. Federal Highway Administration, 2017.

[12] Houben, L. J. M. 2009. European Practice on Design and Construction of Concrete Pavements. 15th Argentine Congress on Road Safety and Traffic. Argentina.

[13] Delatte, Norbert. *Concrete pavement design, construction, and performance*. Crc Press, 2018.

[14] Guide, Roadside Design. "American Association of State Highway and Transportation Officials (AASHTO)." *Washington, DC* (2002).

[15] Taheri, Shima. "A review on five key sensors for monitoring of concrete structures." Construction and Building Materials 204 (2019): 492-509.

[16] Benedetto, Andrea. "A three dimensional approach for tracking cracks in bridges using GPR." Journal of Applied Geophysics 97 (2013): 37-44. DOI10.1016/j.jappgeo.2012.12.010

[17] Luburić, Ivan, Zvonimir Perić, and Silvestar Šesnić. "Electromagnetic modeling of the GPR response to the pipe system set in the concrete slab." In 2017 25th International Conference on Software, Telecommunications and Computer Networks (SoftCOM), pp. 1-5. IEEE, 2017. DOI: 10.23919/SOFTCOM.2017.8115531 .

[18] Scullion, Tom, and Timo Saarenketo. "Applications of Ground Penetrating Radar technology for network and project level pavement management systems." In Fourth International Conference on Managing Pavements, vol. 1. 1998.

[19] Khazanovich, L., Velasquez, R., and Nesvijski, E. G. “Evaluation of top-down cracks in asphalt pavements by using a self-calibrating ultrasonic technique.” Transportation research record 1940, no. 1 (2005): 63-68.

[20] Guo, E. H., L. Ricalde, and F. Petch. “Pavement strength measured by full scale test.” In *RILEM International Conference on Cracking in Pavements (6th: 2008: Chicago, Ill.)*. 2008.

[21] Hornych, Pierre, Jean Pierre Kerzreho, Armelle Chabot, Didier Bodin, Jean Maurice Balay, and Lydie Deloffre. “The LCPC’s ALT facility contribution to pavement cracking knowledge.” In *Proceding of the 6th International RILEM Conference*. 2008.

[22] Birtwisle, Alex, and Erica Utsi. “The use of ground penetrating radar to detect vertical subsurface cracking in airport runways.” In Proceedings of the 12th International Conference on Ground Penetrating Radar (GPR2008), Birmingham, UK. 2008.

[23] Choi, Pangil, Dong-Ho Kim, Bong-Hak Lee, and Moon C. Won. “Application of ultrasonic shear-wave tomography to identify horizontal crack or delamination in concrete pavement and bridge.” Construction and Building Materials 121 (2016): 81-91

[24] Khazanovich, Lev, Raul Velasquez, and Edouard G. Nesvijski. “Evaluation of top-down cracks in asphalt pavements by using a self-calibrating ultrasonic technique.” Transportation research record 1940, no. 1 (2005): 63-68.

[25] Tigdemir, Mesut, S. Figen Kalyoncuoglu, and U. Yalcin Kalyoncuoglu. “Application of ultrasonic method in asphalt concrete testing for fatigue life estimation.” NDT & E International 37, no. 8 (2004): 597-602.

[26] Khazanovich, Lev, Raul Velasquez, and Edouard G. Nesvijski. “Evaluation of top-down cracks in asphalt pavements by using a self-calibrating ultrasonic technique.” Transportation research record 1940, no. 1 (2005): 63-68.

[27] Qi, X., N. Gibson, and J. Youtcheff. “Fatigue cracking characteristics of accelerated testing pavements with modified binders.” In *Proceedings of the Sixth RILEM International Conference on Cracking in Pavements, June*, pp. 16-18. 2008.

[28] Patil, Pooja Krishnath, and S. R. Patil. “Structural health monitoring system using WSN for bridges.” In *2017 International Conference on Intelligent Computing and Control Systems (ICICCS)*, pp. 371-375. IEEE, 2017.

[29] Luo, Longxi, Maria Feng, Yoshio Fukuda, and Chao Zhang. “Micro displacement and strain detection for crack prediction on concrete surface using optical nondestructive evaluation methods.” *International Journal of Prognostics and Health Management* 6, no. SP3 (2015): 1-12.

[30] Bossi, Giulia, Luca Schenato, and Gianluca Marcato. “Structural health monitoring of a road tunnel intersecting a large and active landslide.” *Applied sciences* 7, no. 12 (2017): 1271.

[31] Cigada, A., L. Corradi Dell’Acqua, B. Mörlin Visconti Castiglione, M. Scaccabarozzi, M. Vanali, and E. Zappa. “Structural health monitoring of an historical building: The main spire of the Duomo di Milano.” *International Journal of Architectural Heritage* 11, no. 4 (2017): 501-518.

[32] Fraden, Jacob. Handbook of modern sensors: physics, designs, and applications. Springer Science & Business Media, 2004.

[33] Morris, Alan S. Principles of measurement and instrumentation. Prentice-Hall, Inc, 1994.

[34] Cook, Karissa, Navneet Garg, Amarjit Singh, and Murphy Flynn. “Detection of Delamination in the HMA Layer of Runway Pavement Structure Using Asphalt Strain Gauges.” Journal of Transportation Engineering 142, no. 11 (2016): 04016047.

[35] Bao, Yi, Fujian Tang, Yizheng Chen, Weina Meng, Ying Huang, and Genda Chen. “Concrete pavement monitoring with PPP-BOTDA distributed strain and crack sensors.” Smart Structures and Systems 18, no. 3 (2016): 405-423. DOI: http://dx.doi.org/10.12989/sss.2016.18.3.405.

Monitoring.” Structural Health Monitoring 14, no. 1 (2015): 110-123.

[36] Wu, Z. S., B. Xu, T. Takahashi, and T. Harada. “Performance of a BOTDR optical fibre sensing technique for crack detection in concrete structures.” Structures and Infrastructure Engineering 4, no. 4 (2008): 311-323.

[37] Chapeleau, Xavier, Juliette Blanc, Pierre Hornych, Jean-Luc Gautier, and Jean Carroget. “Assessment of cracks detection in pavement by a distributed fiber optic sensing technology.” Journal of Civil Structural Health Monitoring 7, no. 4 (2017): 459-470. DOI.https://link.springer.com/article/10.1007/s13349-017-0236-5#citeas

[38] Patil, P. K. and Patil, S. R. “Structural health monitoring system using WSN for bridges.” In *2017 International Conference on Intelligent Computing and Control Systems (ICICCS)*, pp. 371-375. IEEE, 2017.

[39] Maeijer, K. D., Patricia, G. L., Vuye, C., Voet, E., Vanlanduit, S., Braspenninckx, J., Stevens, N. and Wolf, J. D., “Fiber Optics Sensors in Asphalt Pavement: State-of-the-Art Review.” *Infrastructures* 4, no. 2 (2019): 36.

[40] Srinivasan, Amruthur V., and D. Michael McFarland. “Smart structures, analysis and design.” (2001): 1212-1212.

[41] Lele, S. P., and S. K. Maiti. “Modelling of transverse vibration of short beams for crack detection and measurement of crack extension.” *Journal of Sound and vibration* 257, no. 3 (2002): 559-583.

[42] Lee, Jinhee. “Identification of multiple cracks in a beam using vibration amplitudes.” *Journal of Sound and Vibration* 326, no. 1-2 (2009): 205-212.

[43] Maier, Giulio, Massimiliano Bocciarelli, Gabriella Bolzon, and Roberto Fedele. “Inverse analyses in fracture mechanics.” *International Journal of Fracture* 138, no. 1-4 (2006): 47-73.

[44] Abdul-Baqi, Adnan, and Erik Van der Giessen. “Numerical analysis of indentation-induced cracking of brittle coatings on ductile substrates.” International Journal of Solids and Structures 39, no. 6 (2002): 1427-1442.

[45] Ardito, Raffaele, P. Bartalotta, L. Ceriani, and Giulio Maier. “Diagnostic inverse analysis of concrete dams with statical excitation.” Journal of the mechanical behavior of materials15, no. 6 (2004): 381-390.

[46] Bassil, Antoine, Xin Wang, Xavier Chapeleau, Ernst Niederleithinger, Odile Abraham, and Dominique Leduc. “Distributed fiber optics sensing and coda wave interferometry techniques for damage monitoring in concrete structures.” *Sensors* 19, no. 2 (2019): 356.

[47] Song, N. N., and F. Wu. “Crack identification for reinforced concrete using PZT based smart rebar active sensing diagnostic network.” In *Nondestructive Characterization and Monitoring of Advanced Materials, Aerospace, and Civil Infrastructure 2016*, vol. 9804, p. 98041R. International Society for Optics and Photonics, 2016.

[48] Worley, Robert, Mandar M. Dewoolkar, Tian Xia, Robert Farrell, Daniel Orfeo, Dylan Burns, and Dryver R. Huston. “Acoustic Emission Sensing for Crack Monitoring in

Prefabricated and Prestressed Reinforced Concrete Bridge Girders." *Journal of Bridge Engineering* 24, no. 4 (2019): 04019018.

[49] Nahvi, H., and M. Jabbari. "Crack detection in beams using experimental modal data and finite element model." *International Journal of Mechanical Sciences* 47, no. 10 (2005): 1477-1497.

[50] Patil, D. P., and S. K. Maiti. "Detection of multiple cracks using frequency measurements." *Engineering Fracture Mechanics*70, no. 12 (2003): 1553-1572.

[51] Mungla, Mitesh J., Dharmendra S. Sharma, and Reena R. Trivedi. "Inverse method to identify crack parameters in multi-span beam using genetic algorithm." *Nondestructive Testing and Evaluation* 32, no. 3 (2017): 301-318.

[52] Moradi, Shapour, and Mohammad Hasan Kargozarfard. "On multiple crack detection in beam structures." *Journal of mechanical science and technology* 27, no. 1 (2013): 47-55.

[53] Wang, Chih-Shiung, and Lin-Tsang Lee. "Modified and simplified sectional flexibility of a cracked beam." *Journal of Applied Mathematics* 2012 (2012).

[54] Ostachowicz, W. M., and M. Krawczuk. "Analysis of the effect of cracks on the natural frequencies of a cantilever beam." *Journal of sound and vibration* 150, no. 2 (1991): 191-201.

[55] Bazant, Zdenek P. *Fracture Mechanics of Concrete Structures: Proceedings of the First International Conference on Fracture Mechanics of Concrete Structures (FraMCoS1), held at Beaver Run Resort, Breckenridge, Colorado, USA, 1-5 June 1992*. CRC Press, 2003.

[56] Bazant, Zdenek P. *Fracture and size effect in concrete and other quasibrittle materials*. Routledge, 2019.

[57] Rashid, Y. R. "Ultimate strength analysis of prestressed concrete pressure vessels." *Nuclear engineering and design* 7, no. 4 (1968): 334-344.

[58] Lotfi, Hamid Reza. "Finite element analysis of fracture of concrete and masonry structures." (1994): 0986-0986.

[59] Anderson, Ted L. *Fracture mechanics: fundamentals and applications*. CRC press, 2017.

[60] Shah, Surendra P., Stuart E. Swartz, and Chengsheng Ouyang. *Fracture mechanics of concrete: applications of fracture mechanics to concrete, rock and other quasi-brittle materials*. John Wiley & Sons, 1995.

[61] Mazzotti, Claudio, Antonio Bilotta, Christian Carloni, Francesca Ceroni, Tommaso D'Antino, Emidio Nigro, and Carlo Pellegrino. "Bond between EBR FRP and concrete." In *Design procedures for the use of composites in strengthening of reinforced concrete structures*, pp. 39-96. Springer, Dordrecht, 2016.

[62] Hillerborg, Arne, Mats Modéer, and P-E. Petersson. "Analysis of crack formation and crack growth in concrete by means of fracture mechanics and finite elements." *Cement and concrete research* 6, no. 6 (1976): 773-781.

[63] Otsuka, Koji, and Hidehumi Date. "Fracture process zone in concrete tension specimen." *Engineering Fracture Mechanics* 65, no. 2-3 (2000): 111-131.

[64] Isenberg, Jeremy. "Finite element analysis of reinforced concrete structures II." ASCE, 1993.

[65] Pook, Leslie Philip. *Linear elastic fracture mechanics for engineers: theory and applications*. WIT press, 2000.

[66] Roumaldi, J. P., and Gordon B. Batson. *Mechanics of crack arrest in concrete*. No. SP-249-12. 2008.

[67] Sih, George C., and A. Ditomasso, eds. *Fracture mechanics of concrete: Structural application and numerical calculation: Structural Application and Numerical Calculation*. Vol. 4. Springer Science & Business Media, 2012.

[62] ACI Committee 446, “Fracture Mechanics of Concrete: Concepts, Models and Determination of Material Properties,” ACI 446.1R-91, Reported by ACI Committee 446, Detroit, 1991.

[68] Bazant, Zdenek P. "Instability, ductility, and size effect in strain-softening concrete." *ASCE J Eng Mech Div* 102, no. 2 (1976): 331-344.

[69] Bažant, Zdeněk P. "Size effect on structural strength: a review." *Archive of applied Mechanics* 69, no. 9-10 (1999): 703-725.

[70] Alshandah, Mohanad, Ying Huang, Pan Lu, and Denver Tolliver. “Bottom-up crack detection in concrete pavements using in-pavement strain sensors.” In Sensors and Smart Structures Technologies for Civil, Mechanical, and Aerospace Systems 2018, vol. 10598, p. 105982I. International Society for Optics and Photonics, 2018.

[71] Theocaris, P. S., D. Pazis, and B. D. Konstantellos. "Elastic displacements along the flanks of internal cracks in rubber." Experimental mechanics 29, no. 1 (1989): 32-39.

[72] Sahoo, A. K., R. N. Dubey, and M. D. Pandey. “Crack Induced Stress and Deformation Field.” Transaction, SMiRT 19 (2007).

[73] Rice, JRf. “Elastic fracture mechanics concepts for interfacial cracks.” J. Appl. Mech.(Trans. ASME) 55, no. 1 (1988): 98-103.

[74] Raveendra, S. T., and P. K. Banerjee. “Computation of stress intensity factors for interfacial cracks.” *Engineering fracture mechanics* 40, no. 1 (1991): 89-103.

[75] Rooke, David Percy, and David John Cartwright. “Compendium of stress intensity factors.” Procurement Executive, Ministry of Defence. H. M. S. O. 1976, 330 p(Book). (1976).

[76] Anderson, Ted L. Fracture mechanics: fundamentals and applications. CRC press, 2017.

[77] Benarbia, Djamila, and Mohamed Benguediab. “Determination of stress intensity factor in concrete material under Brazilian disc and three-point bending tests using finite element method.” *Periodica Polytechnica Mechanical Engineering* 59, no. 4 (2015): 199-203.

[78] Seleem, M. H., Sallam, H. E. M., Attwa, A. J., Heiza, K. M., Shaheen, Y. B. “Fracture mechanics of self compacting concrete.” In: Mesomechanics-2008. Jan. 28- Feb. 01 2008, HBRC, Giza, Egypt, pp. 1-10. 2008.

[79] Lintz, Rosa Cristina Cecche, and Maria Rachel Russo Seydell. “Evaluation of tire rubber disposal in concrete for pavements.” *Journal of Urban and Environmental Engineering* 3, no. 2 (2009): 52-57.

[80] Wilson, Earl J. "Strain-gage instrumentation." *Harris’ Shock and Vibration Handbook, S* (1976): 17

[81] Fraden, Jacob. *Handbook of modern sensors: physics, designs, and applications*. Springer Science & Business Media, 2004.

[82] Zhang, Jun, and Qian Liu. “Determination of concrete fracture parameters from a three-point bending test.” Tsinghua Science and Technology 8, no. 6 (2003): 726-733.

[83] ASTM, C78. “Standard test method for flexural strength of concrete (using simple beam with third-point loading).” In American Society for Testing Materials. 2010.

[84] Bahraq, Ashraf Awadh, Mohammed Ali Al-Osta, Shamsad Ahmad, Mesfer Mohammad Al-Zahrani, Salah Othman Al-Dulaijan, and Muhammad Kalimur Rahman. "Experimental and Numerical Investigation of Shear Behavior of RC Beams Strengthened by Ultra-High Performance Concrete." *International Journal of Concrete Structures and Materials* 13, no. 1 (2019): 6.

[85] Crunarani, Cr I., and P. Saravanakumar. "Experimental Studies on RC Beams Strengthened with Epoxy and Polymer Grouting." *Asian Journal of Applied Sciences* 7, no. 2 (2014): 88-95.

[86] Ghazavy-Khorasgany, M., and V. Gopalaratnam. "Shear Strength of Concrete—Size and other influences." In *Proceedings of the JCI International Workshop on Size Effect in Concrete Structures, Sendai, Japan*, pp. 51-62. 1993.

[87] Riveros, Guillermo A., and Vellore Gopalaratnam. "Fracture response of reinforced concrete deep beams finite element investigation of strength and beam size." *Applied Mathematics* 4, no. 11 (2013): 1568.

[88] Daghash, Sherif M., and Osman E. Ozbulut. "Flexural performance evaluation of NSM basalt FRP-strengthened concrete beams using digital image correlation system." *Composite Structures* 176 (2017): 748-756.

[89] Kim, Hee Sun, and Yeong Soo Shin. "Flexural behavior of reinforced concrete (RC) beams retrofitted with hybrid fiber reinforced polymers (FRPs) under sustaining loads." *Composite structures* 93, no. 2 (2011): 802-811.

[90] Javaid, Syed Saad, Wade R. Lanning, and Christopher L. Muhlstein. "The development of zones of active plasticity during mode I steady-state crack growth in thin aluminum sheets." *Engineering Fracture Mechanics* 218 (2019): 106540.

[91] Bazant, Zdenek P., and Jaime Planas. *Fracture and size effect in concrete and other quasibrittle materials*. Vol. 16. CRC press, 1997.